Towards Bis-benzimidazole Near-Infrared Absorbing and Emitting Dyes

by

Tianyi Wang
BSc (Hons), University of Victoria, 2018

A Thesis Submitted in Partial Fulfillment
of the Requirements for the Degree of

MASTER OF SCIENCE

in the Department of Chemistry

We acknowledge with respect the Lekwungen peoples on whose traditional territory the university stands and the Songhees, Esquimalt and WSÁNEĆ peoples whose historical relationships with the land continue to this day.

Supervisory Committee

Towards Bis-benzimidazole Near-Infrared Absorbing and Emitting Dyes

by

Tianyi Wang
BSc (Hons), University of Victoria, 2018

Supervisory Committee

Dr. Robin G. Hicks (Department of Chemistry)
Supervisor

Dr. Neil Burford (Department of Chemistry)
Departmental Member

Abstract

Supervisory Committee

Dr. Robin G. Hicks (Department of Chemistry)
Supervisor

Dr. Neil Burford (Department of Chemistry)
Departmental Member

A conjugated bis-benzimidazole chromophore is predicted to show absorptions in the near-infrared (NIR) region of the electromagnetic spectrum. However, there are no reports to-date of any NIR absorbing and emitting dyes that are based on a bis-benzimidazole structural backbone. This thesis reports recent advancements in the discovery and study of this new class of dyes.

Following literature procedures, the syntheses of bis(benzimidazolyl)methane compounds are successful. An unexpected product isolated during the attempted oxidation of a bis(benzimidazolyl)methane compound using *p*-chloranil showed intense absorption in the NIR (λ_{max} = 712 nm, ε = 14600 $L \cdot mol^{-1} \cdot cm^{-1}$), solubilities in polar solvents like methanol and water, and electrochemical activities. X-ray crystallography, mass spectrometry, and NMR spectroscopy confirmed the connectivity and structure of the product to contain a combination of quinone and benzimidazole moieties, which later revealed to be the core chromophore by computational studies. This unprecedented combination of moieties gave a chromophore that is predicted to absorb in the far-red even without substitution.

Attempts to synthesize boron-based bis-imidazole dyes with *N*-methylation shed light on the feasibility of the design of such moiety. Considering the additional functionality that could be accessed through the methylation of the labile benzimidazole nitrogen atoms, N-methylated bis(benzimidazolyl)methane precursors were successfully synthesized and fully characterized. Attempts of the boron coordination showed promising signs, as the ^{1}H, ^{11}B, and ^{19}F NMR spectra showed solid evidence of the successful isolation of the boron chelate. Computational studies of methyl, phenyl, and triazole-substituted boron chelate derivatives projected absorptions in the NIR region. Intense transitions are found to be based on frontier molecular orbitals and differ significantly among the derivatives, predicting substantial tunability of this type of dyes.

Table of Contents

List of Figures

List of Schemes

List of Tables

List of Numbered Compounds

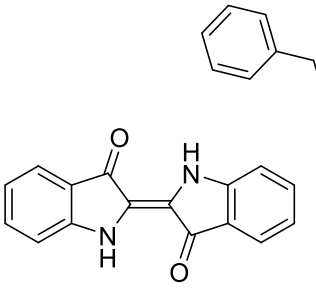

1.1

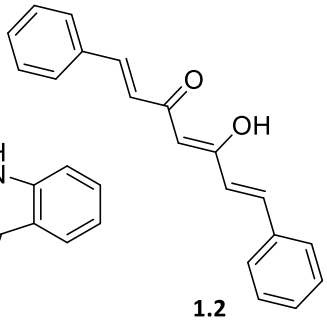

1.2

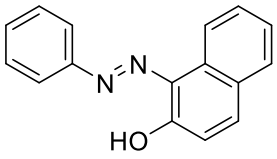

1.3

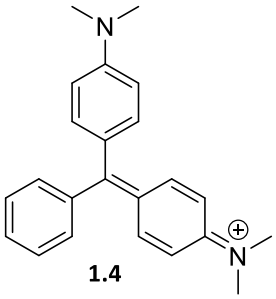

1.4

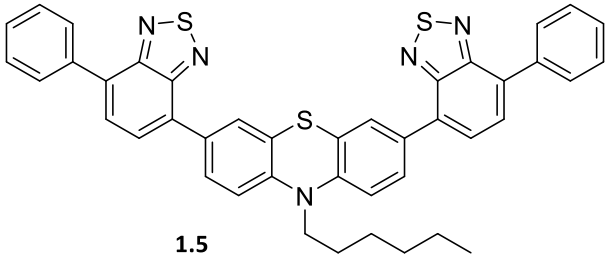

1.5

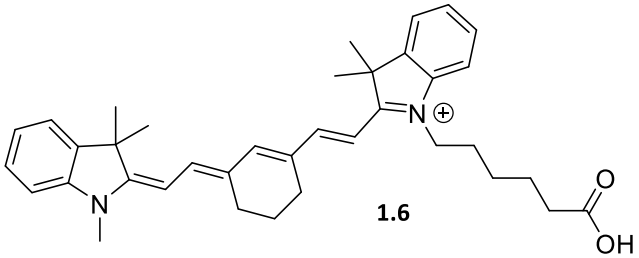

1.6

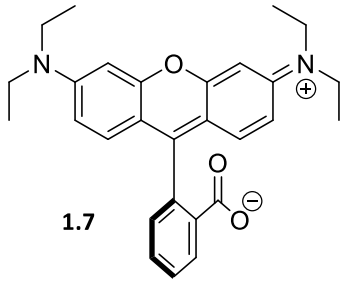

1.7

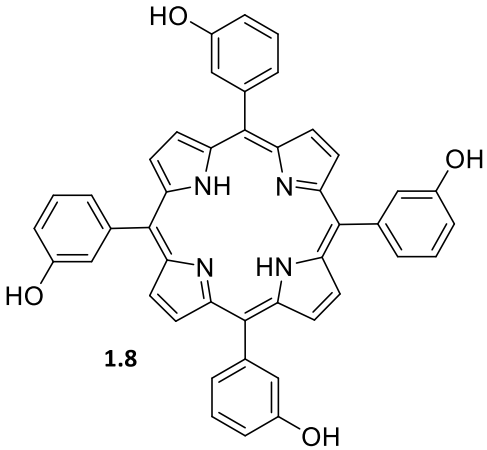

1.8

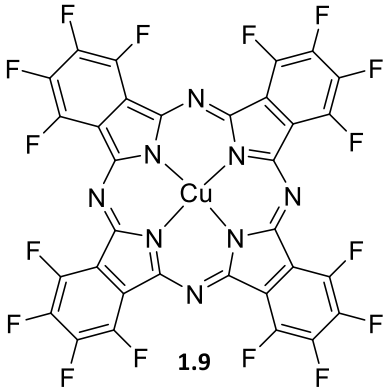

1.9

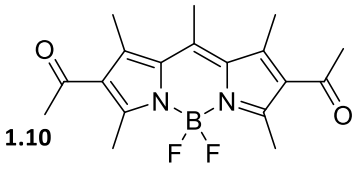

1.10

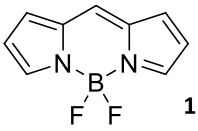

1.11

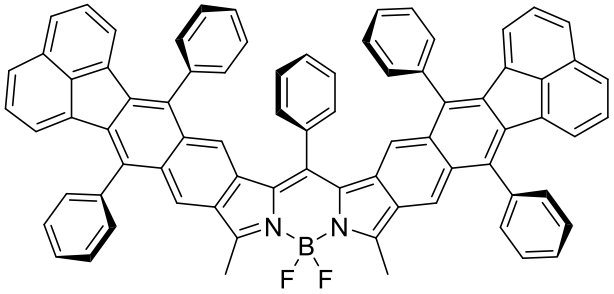

1.12

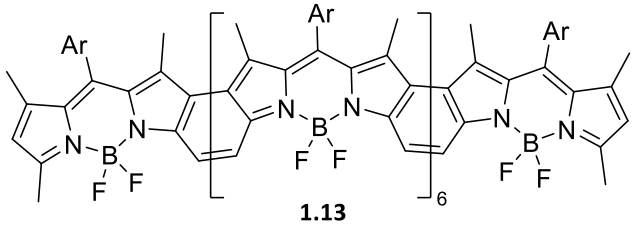

1.13

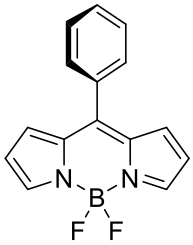

1.14

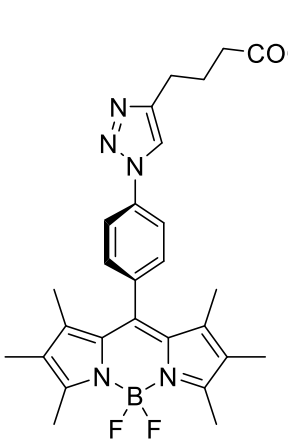

1.15

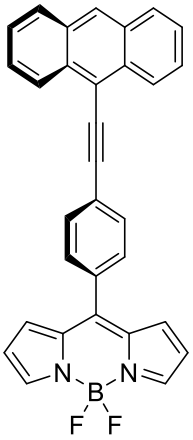

1.16

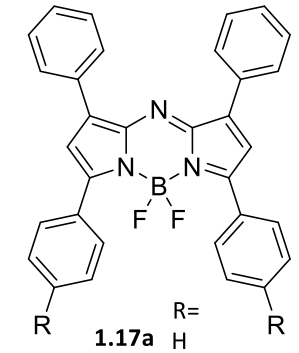

1.17a H
1.17b NMe_2

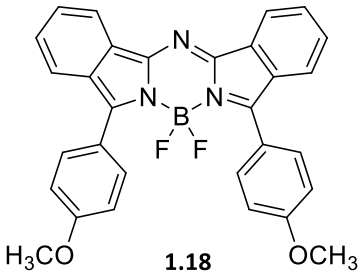

1.18

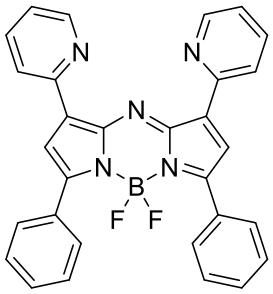

1.19

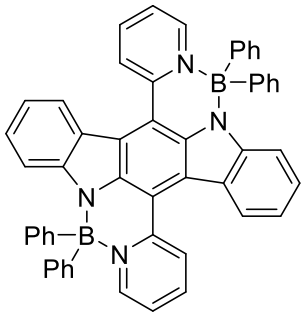

1.20

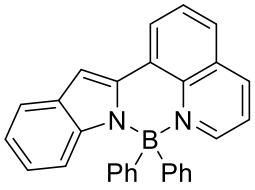

1.21

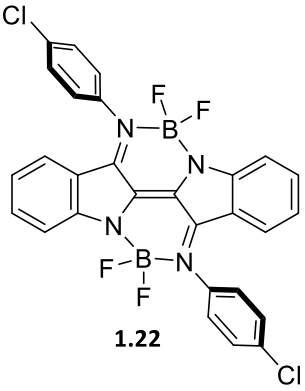

1.22

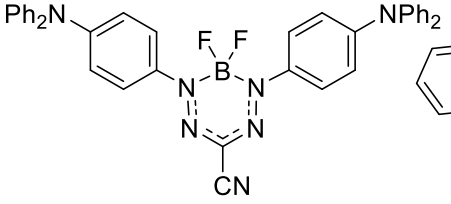

1.23

1.24 X=
a S
b O

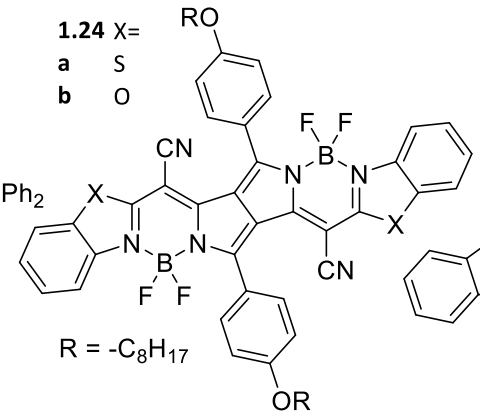

1.25 X=
a NMe
b NPh
c S
d O

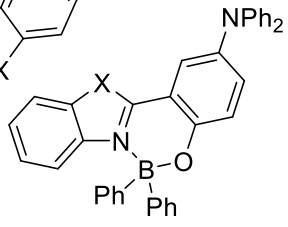

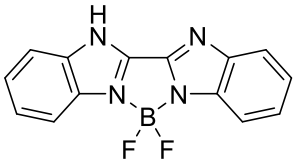

1.26

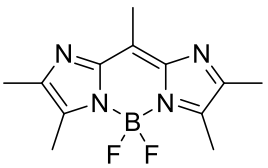

1.27

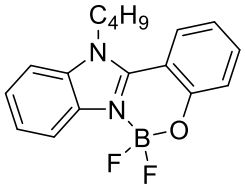

1.28

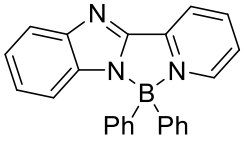

1.29

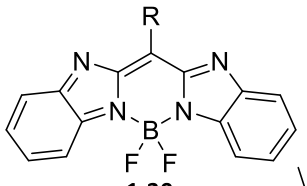

1.30

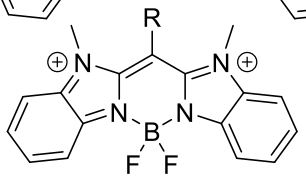

1.31

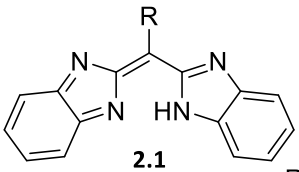

2.1

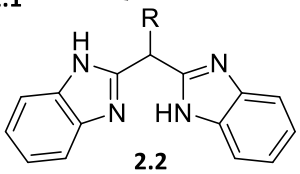

2.2

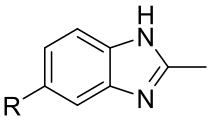

R=H **2.3a**
R=Me **2.3b**

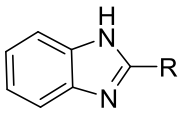

R=
H **2.4a**
Et **2.4b**
CH_2OH **2.4c**

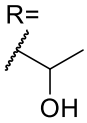

2.4d

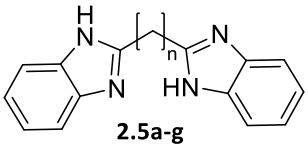

2.5a-g
n=2-8

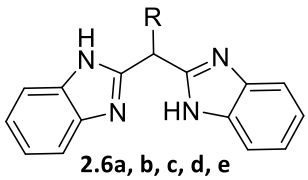

2.6a, b, c, d, e
R=H, Me, Et, nBu, iBu

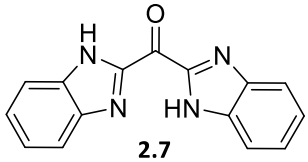

2.7

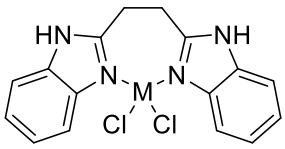

2.8a, b, c
M=Co, Ni, Cu

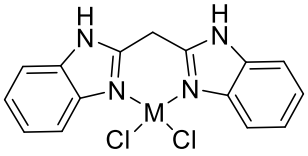

2.9a, b, c
M=Co, Ni, Cu

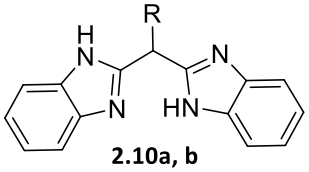

2.10a, b
R=Me, Ph

2.11

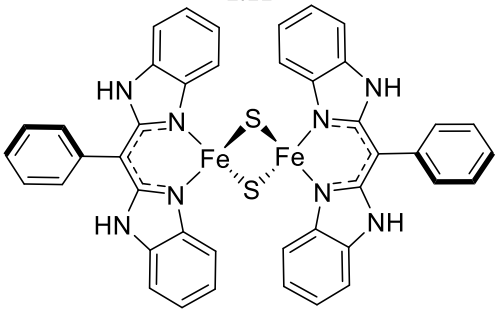

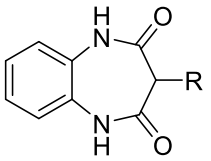

R=H **2.12a**
R=Me **2.12b**

2.13

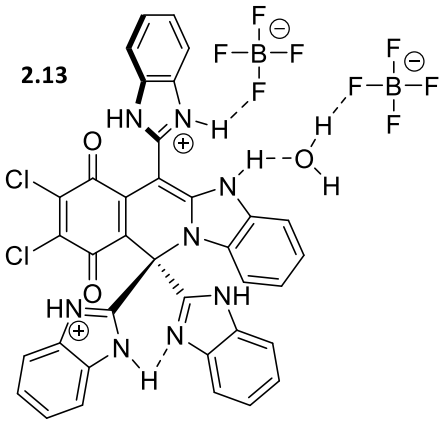

2.14

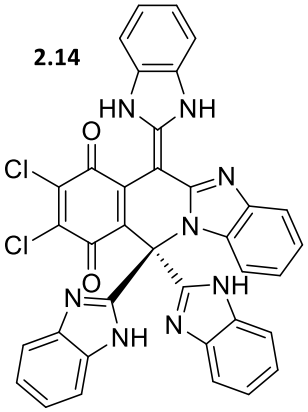

2.14t

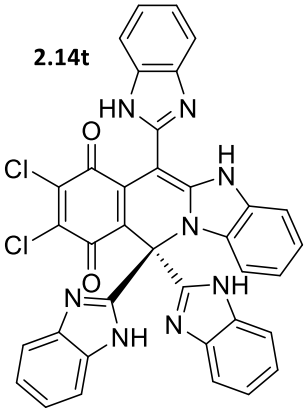

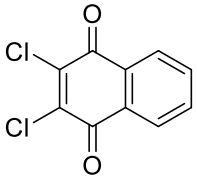

2.15

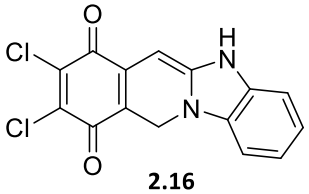

2.16

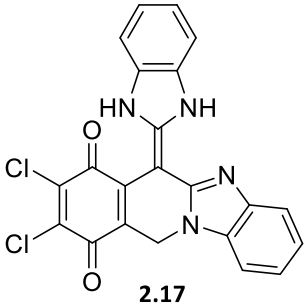

2.17

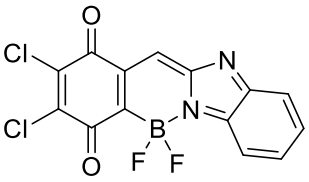

2.18

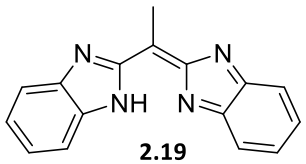

2.19

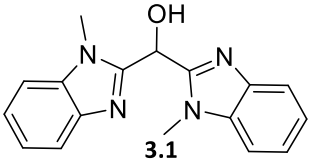

3.1

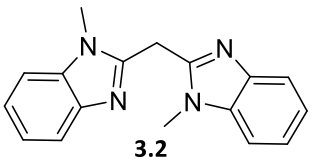

3.2

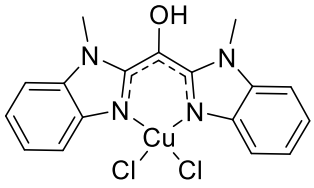

3.3

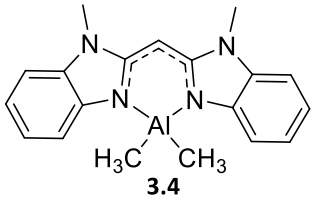

3.4

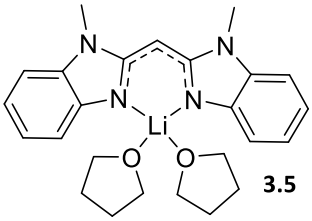

3.5

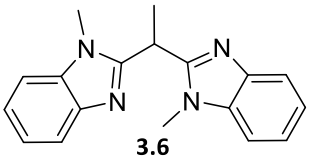

3.6

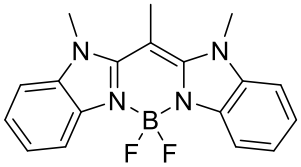

3.7

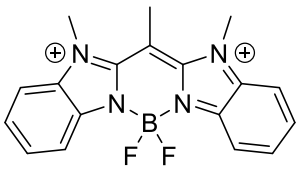

3.8

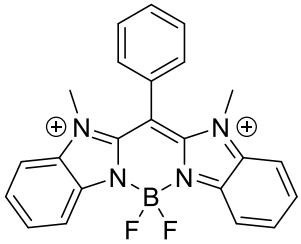

3.9

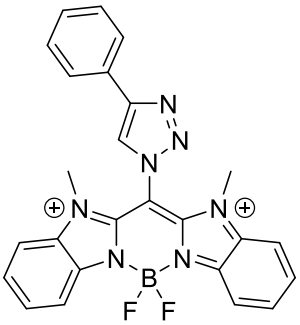

3.10

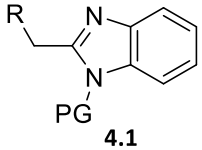

4.1

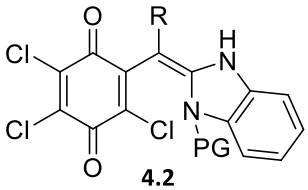

4.2

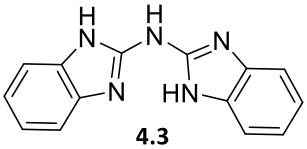

4.3

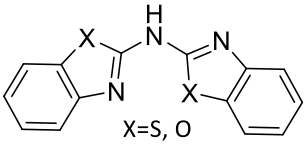

4.4

List of Abbreviations

Å	angstrom
Abs	absorbance
Ac	acetyl
B3LYP	Becke, 3 parameter, Lee-Yang-Parr (as a functional)
BODIPY	boron-dipyrrolemethene (4,4-difluoro-4-bora-3a,4a-diaza-*s*-indacene)
br	broad (as a spectral descriptor)
Bu	butyl
calc	calculated
CAM-B3LYP	Coulomb-attenuating method B3LYP (as a functional)
CPCM	Conductor-like Polarizable Continuum Model
D	Debye
d	doublet (as NMR multiplicity descriptor)
DCM	dichloromethane
decomp	decomposition
DEPT-135	Distortionless Enhancement by Polarization Transfer, 135°
DFT	Density Functional Theory
DIPEA	Diisopropylethylamine
DMSO	dimethyl sulphoxide
DSSC	dye-sensitized solar cell
E_o	redox potential
EM	electromagnetic
ESI	electrospray ionization
Et	ethyl
eq	equivalent
Fig	figure
FMO	frontier molecular orbital
FT	Fourier transformation
GGA	Generalized Gradient Approximation
H	hydrogen (as a unit for NMR integrations)
h	hour(s)
HMBC	Heteronuclear Multiple Bond Correlation
HOMO	highest occupied molecular orbital
HRMS	high-resolution mass spectrometry
HSQC	Heteronuclear Single Quantum Coherence
Hz	hertz
IR	infrared; infrared spectroscopy
λ	wavelength
lit	literature value
LUMO	lowest unoccupied molecular orbital
n	normal (as an indication for substitution pattern)

NHE	Normal Hydrogen Electrode
NIR	near-infrared
nm	nanometre
NMR	nuclear magnetic resonance
M	molarity
M06-L	Minnesota 2006 local (as a functional)
m	metre (as a SI unit); medium (as an IR peak height descriptor)
max	maximum
Me	methyl
min	minute(s)
MO	molecular orbital
mp	melting point
N	normality
NIR	near infrared
o	*ortho*-(substituted)
ODCB	*ortho*-dichlorobenzene
OLED	organic light-emitting diode
ORTEP	Oak Ridge Thermal-Ellipsoid Plot
p	*para*-(substituted)
PBE	Perdew-Burke-Ernzerhof (as a functional)
PCET	proton-coupled electron transfer
Ph	phenyl
ppm	parts per million
q	quartet (as NMR multiplicity descriptor)
s	singlet (as NMR multiplicity descriptor); strong (as IR peak descriptor)
sh	shoulder (as IR and UV-Vis-NIR spectral descriptor)
TDDFT	Time-dependent Density Functional Theory
UV	ultraviolet
Vis	visible
vs	against
w	weak (as IR peak descriptor)

Acknowledgement

For the mere five years I have passionately spent in the Hicks research group, first as an undergraduate novice and then a graduate but expensive novice, my great supervisor Dr. Robin G. Hicks have provided tremendous amount of academic, material, logistical, and mental support from the beginning at a cold winter day in the end of 2015 to the very week this thesis is finishing at a warmer winter day at the beginning of 2021. My academic life would look a lot more different without your help, and words cannot sufficiently describe all my thanks to you. Thank you, Robin.

I also want to send my great gratitude towards Dr. Neil Burford, our committee member and also a great leader of our Department and our Faculty. You are always up for a quick chat and provide feedback, and through small things like that you have been a fantastic supervisor in the committee. I also can still remember my first CHEM class at UVic and your passionate lectures that shed light on the ever new frontiers of chemistry. Thank you, Neil.

Research is always a team sport, and without my colleagues at UVic and across the continent I would not be able to complete the research. Thank you, Austin, for being a bro in lab and a great aid to the research described in this thesis; Dillon, for the nukes, copypastas, and providing very valuable advices during the process of solving the crystal structure; Nick, for all the gorgeous “what is a carbon” moments and running the VT NMR experiment for me; Shaun, for the random GeoGuessr and/or computational questions. Thank you, also, Chris Barr for all the help and training on NMR, and Dr. Tyler

Trefz for mass spectrometry. Thank you, Dr. Brian Patrick at UBC, for conducting the X-ray crystallography experiments that in tern becomes a solid pillar for the research described in this thesis.

It goes a long way from that kid in second year inorganic lab that forgot to close the separatory funnel and made quite a mess to the teacher that has to properly deal with those situations, and I definitely need to thank Dr. Dave Berry and Kelli Fawkes for their tireless training and mentorship along the way. I would not build up the interest and skills in instruction without you. Thank you, Dave, and Kelli.

In what one can only describe as the most tedious and crazy times, I would not survive THE 2020™ without all of you, my gorgeous friends outside Chemistry. Through your love, caring, intelligence, and resilience you have all showed, I became a much better and more normal human. You are my bubble, and you are all the best. Thank you all and forgive me that I cannot list all of you here.

Dedication

To all the scholars and students struggling for academic freedom and freedom of opinion, expression, belief, association, and movement.

"*So ein herrlicher sonniger Tag, und ich muss gehen.*"

"*And sunfire rained from the sky.*"

Chapter 1 Introduction

1.1 Near-Infrared Dyes

From 80-metre high frequency radio waves to deadly but life-saving gamma rays, the electromagnetic (EM) spectrum consists of waves with different energy levels, corresponding to different physical and chemical transitions and properties. Waves in the visible region, with wavelengths of approximately 400–700 nm[1] and energy levels corresponding to valence electron transitions of atoms and molecules, are the most illustrated in the daily lives and most accessible and relevant in chemistry, particularly in the field of dye chemistry. Natural dyes and pigments like indigo[2] (**1.1**), curcumin[3] (**1.2**) and titanium(IV) oxide,[4] alongside synthetic ones like azo dyes[5] (**1.3** as an example) and gentian violet[6] (**1.4**), are crucial to research, industry, and daily lives of ordinary peoples. Not only in traditional fields of textile dyeing[7] and food colouring[8] do those dyes play an important role, but their potential applications also extend way beyond their visible colour, for example in holographic imaging,[9] organic electronics,[10] and medicinal[11] uses. It is the current and future applications of dyes that lead to developments in their synthesis and functionalization by chemical means.

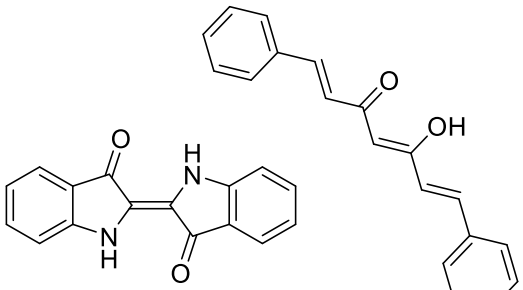

1.1

1.2

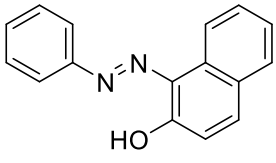

1.3

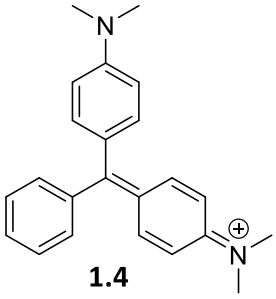

1.4

With the growing and diverse library of functional dyes available to the research communities, those capable of absorbing and emitting in the near-infrared (NIR) region, approximately[1] 700–2500 nm, promote similar electronic transitions as visible light. Many transition metal complexes inherently allow d-d transitions in the NIR.[12,13] More recent works focus on the use of lanthanide complexes as NIR absorbing and fluorescing dyes, utilizing their similar-principled d-f transitions.[14] Nanoparticles and polymer nanoparticles[15] absorb in the NIR are unique in their tunabilities and photophysical properties. By far the most diverse NIR dyes are based on small organic molecules, which is the focus of this section. The NIR dyes are particularly of interest due to their potential biological and material applications.

Bio-imaging uses of NIR dyes usually exploit the absorption and emission wavelengths and requires directed designs on the molecular moieties. The so-called first biological window, the part of the EM spectrum between 650 and 900 nm, is well established to be the benchmark for designing NIR dyes, due to the low absorption and autofluorescence from blood and tissue.[16] Naturally, those dyes can be used in the fields of biological imaging, fluorescent probing,[17] and photodynamic therapy.[18]

The advances in functionalized devices like dye-sensitized solar cells (DSSC) and organic light-emitting diode (OLED) saw an increase in the use of materials based of NIR dyes for the additional functionality provided by them. Among the whole EM spectrum, the low-energy visible region centred around 650 nm is highest in irradiance, making those dyes able to absorb and emit light up to the NIR region (~900 nm) suitable for efficient energy transfers that are required in DSSC.[19] As an example, Yella and

colleagues[20] in 2011 reported a *meso*-substituted Zn porphyrin that absorbs and emits around 700 nm to achieve a power conversion efficiency of 12.5%, the first dye to surpass the 12% threshold, showing comparable energy conversion capabilities to state-of-the-art Si-based and perovskite-based solar cells. They then further increased the efficiency to 13% on a similarly designed NIR-absorbing and emitting Zn porphyrin complex,[21] showing the striving potential. Similar to the recent development in the DSSC field, the increasing need of NIR-emitting OLED drives the incorporation of NIR dyes into OLED. In 2014, Yao and co-workers[22] reported a phenothiazine and benzothiadiazole-based dye **1.5**, which gave solid-state fluorescence in the NIR and incorporated it into a metal-free OLED. In addition, organic NIR dyes also show uses as panchromatic-absorbing materials,[23] proton-coupled electron transfer (PCET) agents,[24] and water-oxidation catalysts.[25]

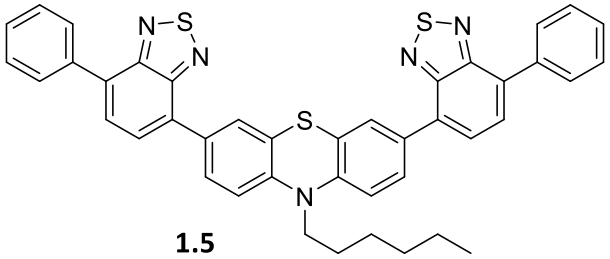

1.5

Some of the most common dyes, like the cyanine-type polymethine dyes, were synthesized and used long before the discoveries of their modern applications. The cyanine chromophore, illustrated by a commercially-available cyanine dye **1.6**, consists of a highly-conjugated π system. As the low-energy transitions of the dyes are usually based on π-π* transitions, those expanded π systems sufficiently promote lower energies in to the NIR region. Indeed, the tunability of cyanine dyes is mostly achieved

by modifying the length of the chromophore π system. Addition of each pair of π electrons equates to a bathochromic shift of 80–100 nm of absorption and fluorescence wavelengths.[17] In addition, incorporating different heterocycles at the terminal ends can sufficiently provide additional sources of tunability. Rather than indoline terminals, reports on cyanine dyes containing other heterocyclic terminals,[26,27] and they showed further redshifted wavelengths and other charming photophysical properties. Using both strategies, a recently reported cyanine dye[28] with 10 π electrons on the main chain and substituted xanthene showed an emission wavelength of 1140 nm and good quantum yield. A more recent report[29] on an intrinsically-designed heptamethine cyanine system fully exploited the cyanine dye chromophore and the effect of steric hinderance on photophysical properties to give absorbing and emitting wavelengths in the NIR region (~800 nm). However, elongation of the chain to further extend the bathochromic shifts of wavelengths prone to experimental and theoretical challenges. Although cyanine dyes are known to be challenging for computational studies, Jacquemin showed a theoretical limit of 17 carbons for the cyanine main chain,[30] meaning the extended conjugation observed for frontier molecular orbitals (FMOs) does not extent beyond this limit. Longer chains can also promote self-aggregations[26] and increase challenges in photostability.[31]

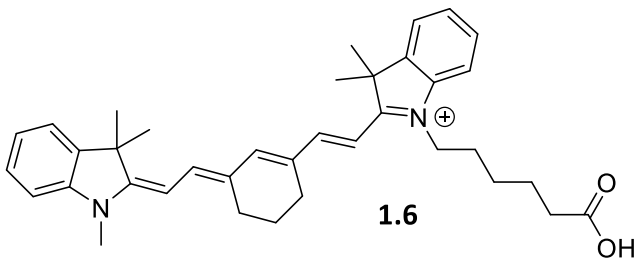

1.6

Similar to cyanine, many polyaromatic NIR dyes have an expanded conjugation system. The rhodamine dyes, a part of the xanthene dye family, are very commonly used due to their low price and tunability of photophysical properties. Although the most commonly-used dyes in this family, like Rho B (**1.7**), are not red- or NIR-absorbing (λ_{max}=564 nm)[32] the absorbing and fluorescent, rhodamine dyes still enjoy widespread uses due to their great quantum yields (Φ=0.916)[32] and unique on/off fluorescent responses that are originated from isomerization promoted by changes in conditions such as pH or UV-light.[33] In addition to diamino terminals and aryl groups, recent developments commonly modify the backbone by changing the heteroatom, and the resulting dye observed far-red or NIR absorbing abilities and swift responses to changes in electrochemical conditions.[34,35]

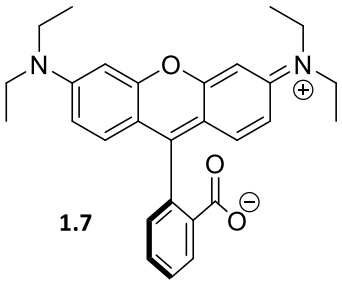

1.7

Porphyrins and phthalocyanines form another distinct class of dyes that absorb in the far-red and NIR, including the natural occurring chlorophyll compounds whose absorbing abilities. The *meso* position of the tetrapyrroles are particularly of interest as *meso*-substituents can effectively fine-tune the spectroscopic and electronic properties of the compounds.[19] The phorphyrin[18] (**1.8**) example exhibits far-red absorptions (λ_{max} = 648 nm), as the *meso*-substituents promote bathochromic shifts to their absorbing wavelengths. By contrast, with substitution on the *meso* positions not relatively feasible,

the modifications of properties are usually achieved by modifying the iso-indole backbone. In addition, the central coordination site can be filled with a number of metals and main group elements such as zinc and magnesium, yielding a wide range of spectroscopic, photophysical, and electrochemical properties. The commercially-available phthalocyanine example **1.9** exploits both modification strategies and has an absorption wavelength well in the NIR[36] (λ_{max}=790 nm).

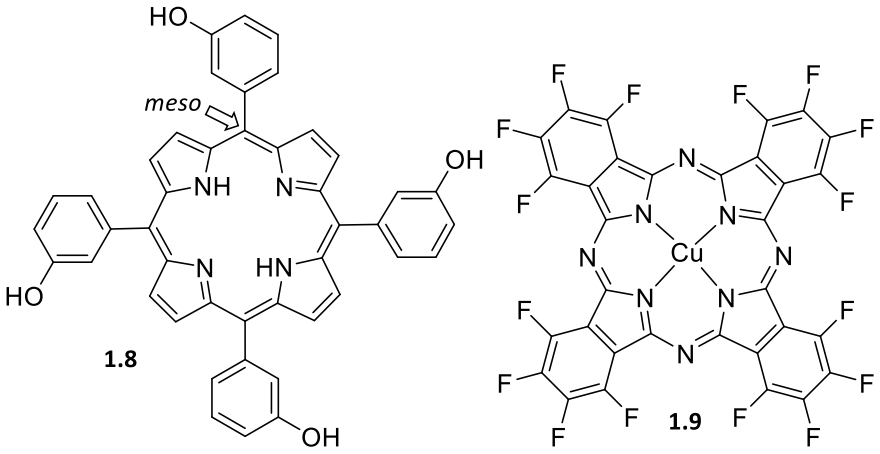

1.8 **1.9**

Alongside other highly conjugated, polyaromatic far-red/NIR dyes like rylene[37] and squaraine,[38] this large, diverse family of dyes provided state-of-the-art properties for synthetic and computational chemists for intrinsically designing new NIR dyes.

1.2 Boron-based Fluorescent Dyes

The boron-dipyrromethene compounds (BODIPY, formally 4,4-difluoro-4-bora-3a,4a-diaza-*s*-indacene) are among the most popular BF_2-based fluorescent dyes that are extensively studied for their syntheses and applications. From the first synthesized[39] BODIPY in 1968 (**1.10**), to the first synthesis of the "naked", fully unsubstituted

compound[40] 40 years after (**1.11**), to the recent NIR-absorbing and emitting examples,[41,42] the search for BODIPY derivatives with tunable and more preferable spectral, photochemical, and electronic properties continues, motivated by the current wide applications of BODIPY compounds. BODIPY compounds usually show small Stokes shifts and intensifies self-quenching,[43] which makes higher quantum yields, larger Stokes shifts, and bathochromic-shifted absorbing and emitting wavelengths main driving forces of the rapid expansion of this class of compounds.

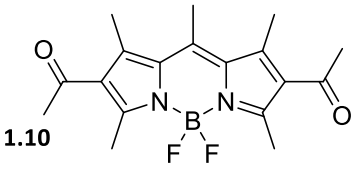

1.10

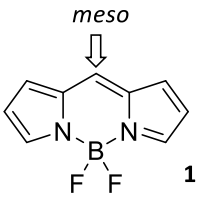

1.11

The most common synthetic strategy of designing NIR-absorbing is extending π-conjugation, as the extension, as explained in section 1.1, decreasing HOMO-LUMO gaps results in expanding scope for the NIR dyes. Aromatic substituents on the pyrrole backbone like phenyl and substituted phenyl groups and more exotic and property-oriented-designed heteroaromatic and metallocycles all gave examples of NIR dyes with ideal properties like extended Stoke shifts, improved solid state emissions, and higher quantum yields. Fused aromatic moieties can very efficiently extend the π-conjugation, lead to significantly red-shifted absorbing and emitting wavelengths, like the reported example[44] **1.12** that has the absorbance wavelength at 765 nm, however not stable in air. The recent work on BODIPY oligomers[45] further exploits the extension of π system, where the BODIPY octamer **1.13** absorbs well in the NIR region (λ_{max} = 957 nm).

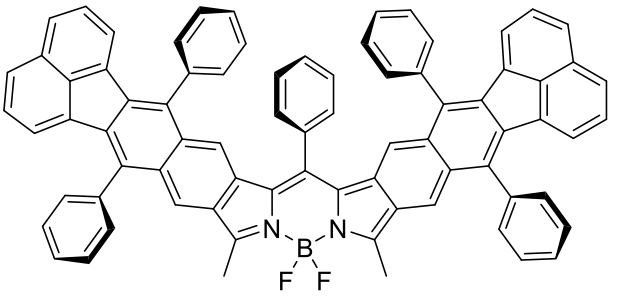

1.12

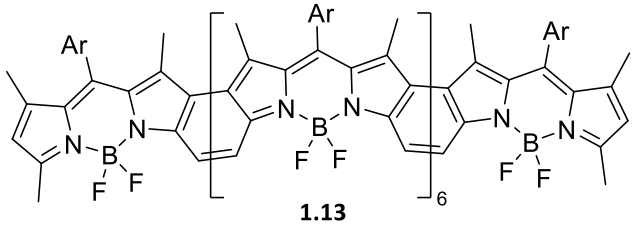

1.13

Modification of the substituents on the *meso* position (highlighted on structure of **1.11**) are the most commonly incorporated synthetic strategy to fine tune properties of BODIPY compounds. Calculated FMOs of a sample *meso*-aniline substituted BODIPY reported by de Jong and colleagues[46] showed extensive contributions from the *meso* substituents to the HOMO and LUMO, which opens pathways for the said tunability at the *meso* position. Furthermore, substituents on the *meso* substituent even showed extensive electron density on the HOMO, adding to the fine tunability needed. The *meso*-position also can be accessed synthetically at ease.[47] Hence, a vast majority of BODIPY compounds incorporate substitutions at the *meso* positions: from a simple phenyl substituent[48] (**1.14**), to triazole (**1.15**) linkers,[49] to polyaromatic groups like anthracene[50] (**1.16**) that drastically altered the photophysical and electronic properties of the chromophore.

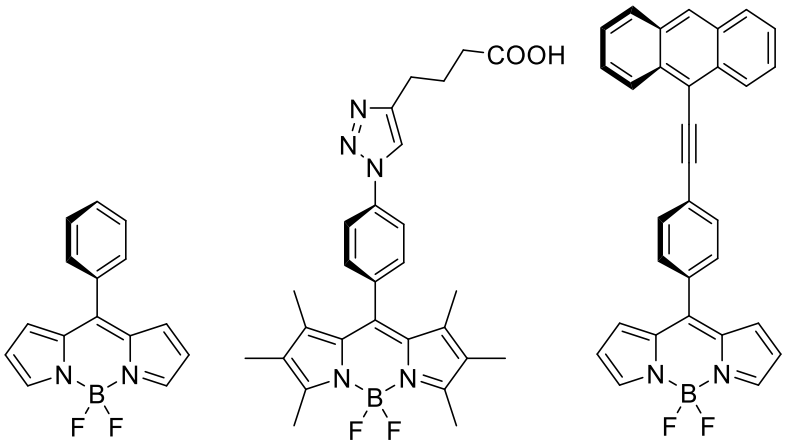

1.14 **1.15** **1.16**

Rapid expansion of BODIPY derivatives has led to other dipyrrole-based dyes, most notably the *aza*-BODIPY compounds. As substituents on the *meso* position have shown large participation in the LUMO of BODIPY, introducing a more electron-rich heteroatom to that position would lower the energy of LUMO and narrow the HOMO-LUMO gap for NIR transitions. Under those rationales, *aza*-BODIPY compounds are designed and synthesized, first in 1993 (**1.17a**) by Sathyamoorthi and colleagues, absorbs in far-red (λ_{max} = 653 nm) and is a significant bathochromic shift from that of the parent BODIPY compound.[51] First NIR-absorbing *aza*-BOPIDY **1.17b** was synthesized a decade after by substituting the phenyl substituents,[52] and exploiting this strategy can lead to further bathochromic shifts on the absorbing wavelength.[53] Extension of the π-system can also sufficiently drive the absorbing wavelength in the NIR region,[54,55] a phenomenon similar to BODIPY, as demonstrated by the benzannulated *aza*-BODIPY **1.18**. The NIR-absorbing *aza*-BODIPY compounds showed great versatility, and examples on property-directed modifications are many, such as a conformationally-restricted analogue for better photostability and photophysical properties,[56] or water-soluble

examples for bio-imaging and bioorganic labelling.[57] The *meso*-nitrogen also allows new applications, as demonstrated by **1.19** that has trace-metal detecting abilities based on tridentate coordination to late transition metals[58] as illustrated.

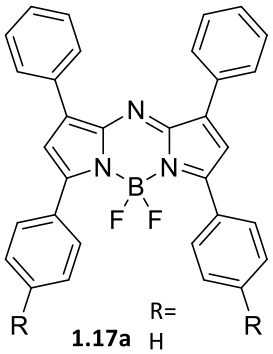

1.17a R= H
1.17b NMe_2

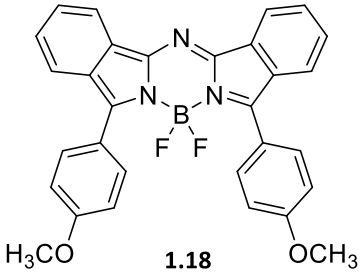

1.18

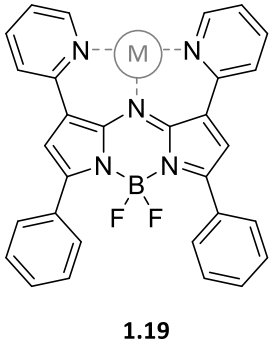

1.19

In addition to the advancements in BODIPY compounds, dyes based on heterocyclic groups and boron chelation is a diverse group of compounds that grows at a tremendous rate. Apart from 5-membered pyrrole, similar boron-based moieties have been tethered on 5, 6, and 7-membered heterocycles[59] through coordination with N, O, and C. Notable red absorbing examples include pyridine and indole-based[60] **1.20** (λ_{max} = 643 nm) and indole and quinoline-based **1.21** (λ_{max} = 611 nm). Attempts on tethering BF_2 moieties onto developed conjugated dye systems with low-energy transitions are also successful, affording NIR dyes like **1.22** (λ_{max} = 752 nm)[61] and **1.23** (λ_{max} = 760 nm). [62]

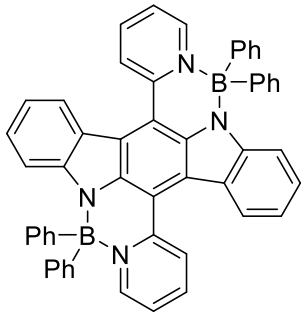

1.20

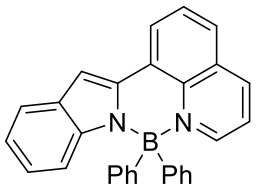

1.21

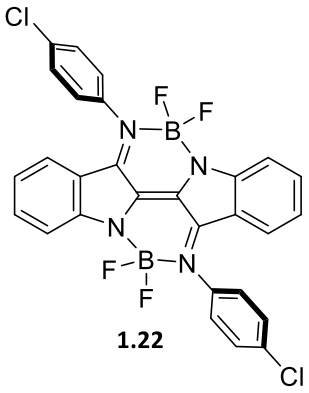

1.22

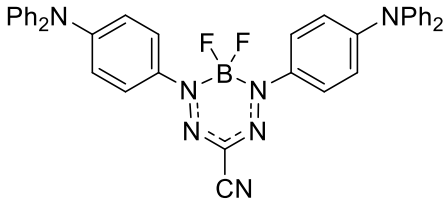

1.23

Among the few NIR-absorbing examples of heterocyclic boron-chelated dyes, the most notable are those containing benzimidazole, benzothiazole, and benzoxazole moieties. Similar to the rationale for substituting in the N at *meso* position of BODIPY, substitution of electronegative N, S, and O at the electron-rich 3-position allows low-energy transitions, giving bathochromic-shifted absorbing wavelengths. Such phenomenon is well demonstrated by the **1.24** and **1.25** compounds,[63,64] where all of them showed significant bathochromic shifts from their respective parent compounds.[65] Thanks to the push-pull system, **1.24** compounds absorb in the NIR, while **1.25** compounds do not absorb in red or NIR. Nevertheless, those compounds shed light on a new avenue of designing NIR dyes.

1.24 X=
a S
b O

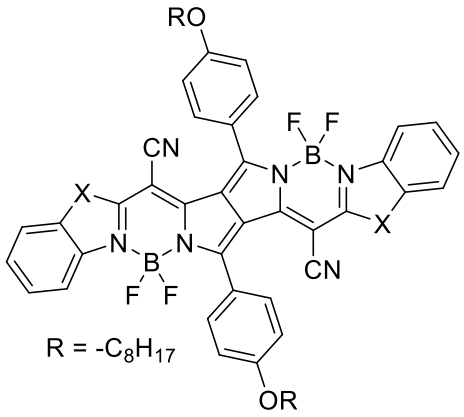

R = -C_8H_{17}

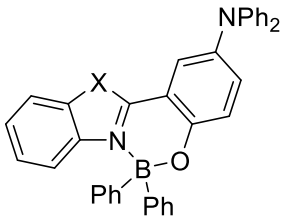

1.25 X=
a NMe
b NPh
c S
d O

1.3 Thesis Objectives

Among the many heteroaromatic boron-based dyes, those carrying methylene-bridged bis-benzimidazole as the core chromophore has yet to be synthesized. The closest examples[66] are the imidazole-based, directly-linked compound **1.26**, and within the same article the authors report failed attempts of synthesizing methinyl-bridged **1.27**. There are also those carrying a single benzimidazole unit, like aforementioned **1.25a–b**, and also **1.28** and **1.29**, none of which absorbs in the far-red or NIR regions.[67,68]

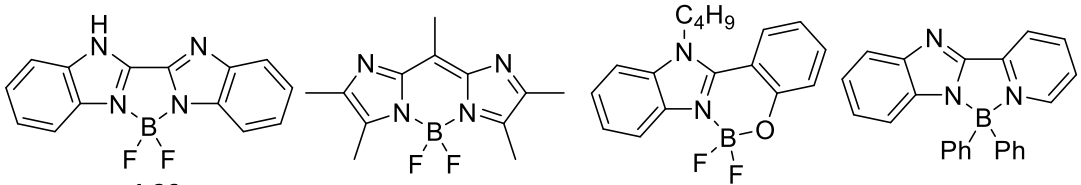

1.26 **1.27** **1.28** **1.29**

The methylene-bridged bis-benzimidazole dye **1.30** carries a fully-conjugated chromophore, and unlike reported benzimidazole-based dyes, could allow low energy transitions, plausibly in the far-red and NIR region. Hence, the main objective of the thesis is undoubtedly to discover reliable strategies to study bis-benzimidazole dyes like **1.30** using synthetic, analytical, and computational methods, whose progress is reported in Chapter 2. Such strategies can be extended to synthesize *N*-substituted derivatives like **1.31**, which was proposed to have far-red absorption[69] (without direct experimental data in a patent). Progress on those is reported in Chapter 3.

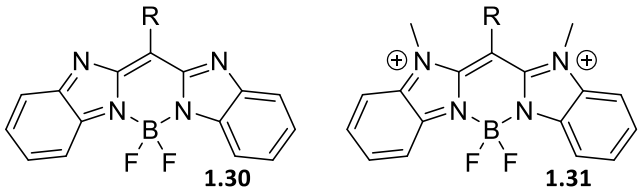

1.30 **1.31**

Chapter 2 Bis-benzimidazole Dyes

2.1 Introduction

As illustrated in Section 1.3, successful syntheses of compound **1.30** and its analogues are some of the ultimate goals of this thesis. Scheme 1 is a retrosynthetic analysis that illustrates a feasible pathway for the synthesis of this class of compound. The boron chelation step shows parallels to coordination chemistry and would rely heavily on the existing literature on BODIPY and other tetracoordinate boron compounds and will be discussed in greater detail in Chapter 3. The fully conjugated **2.1** can be synthesized by oxidation from **2.2**, a bis-benzimidazole compound that can be easily synthesized using traditional synthetic strategies from *o*-phenylenediamine and malonic acid and its derivatives that has been extensively studied.

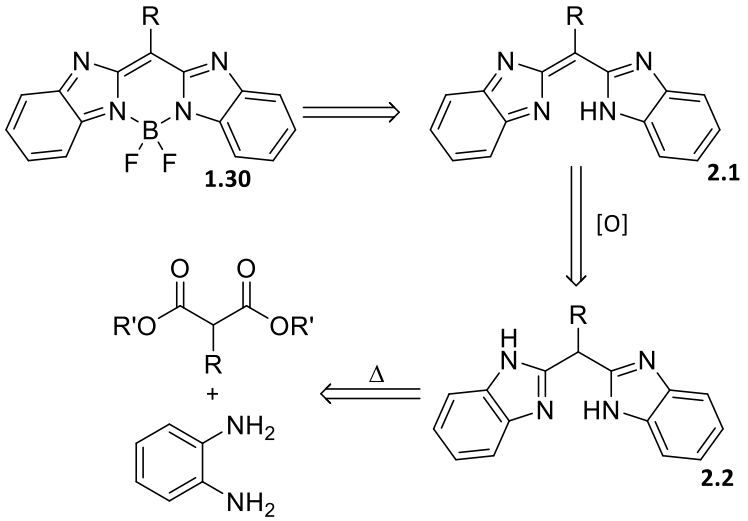

Scheme 1. Proposed pathway of the syntheses of 1.30.

The synthetic methodology of benzimidazoles described in Scheme 1, alongside most of examples of the benzimidazole syntheses, are based on the Phillips-Ladenburg

condensation, first reported[70] in 1875 where Ladenburg heated a mixture of *o*-phenylenediamine, or its substituted analogue, and glacial acetic acid to subsequently obtain 2-methyl benzimidazole compounds **2.3**. In 1928, Phillips[71] used the same methodology to synthesize otherwise substituted benzimidazole compounds **2.4** using respective carboxylic acids.

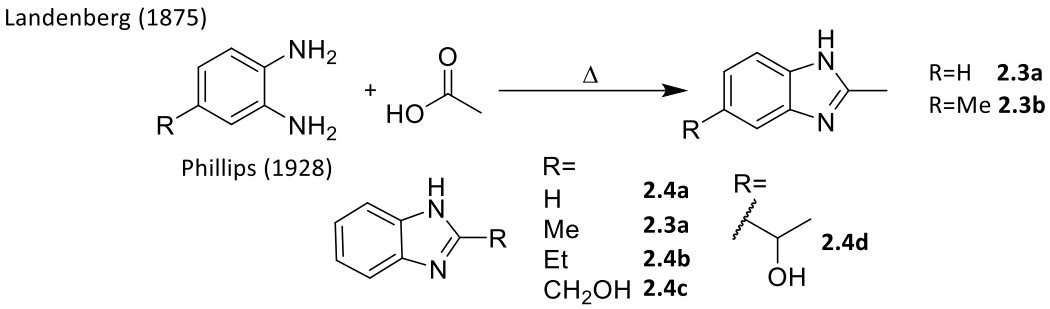

Scheme 2. Early syntheses of 2.3 and 2.4 derivatives.

A mere 150 years later of the first report, the methodology is very much still popular and evolving to synthesize a diverse library of compounds. Most of the optimizations of the methodology focused on the temperature of the reaction and searching for the most suitable carbonyl derivative, and both are crucial towards the syntheses of bis-benzimidazole compounds. In 1941, Shriner and Upson reported[72] the first examples of alkylidene-bridged bis-benzimidazole compounds (**2.5**), where the bridge ranged from two to 8 carbons, by heating the mixture of carboxylic acids and *o*-phenylenediamine with 5N HCl between 125–135 °C, giving mediocre yields (28–63%). The synthesis of methylene-bridged bis-benzimidazole **2.6** surprisingly requires much higher temperatures and more reactive carbonyl derivative precursors comparing to other bis-benzimidazole syntheses, as its first synthesis was reported in 1953 by Lane,[73] where malonamide and higher boiling point (197 °C) ethylene glycol were used. In 1966,

Vinot[74] reported the first syntheses of bis(benzimidazolyl)methane compounds with substituents on the methylene bridge (**2.6b–e**), by conducting the similar reaction at 180 °C and simultaneous distillation to remove water and ethanol by-products, giving medium yields (46–50%). More recent reports[75–79] of the syntheses of bridge-substituted bis(benzimidazole)methane compounds similarly used malonic acid, malonate, or malonamide to give medium to high yields, where the solvent used is usually various concentrations of $HCl_{(aq)}$. The characterization of those compounds are largely dependent on melting points and elemental analyses, where the first NMR data of **2.5a–b** and **2.6a** appeared[78] in 2007.

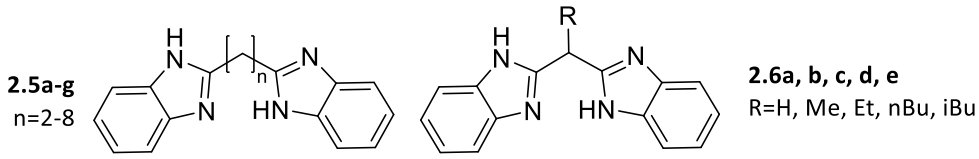

To synthesize the fully conjugated analogue of **2.1**, oxidation reactions of **2.6a** need to be selective, as the methylene bridge is reported to be susceptible towards oxidation to its ketone analogue **2.7**. In 1956, Efros and colleagues showed that metal-assisted oxidation, in their case Cr, does not decompose the benzimidazole core,[80] allowing further work on the oxidation of **2.6a**. The first of such oxidation reaction was reported in 1977, where Sprecher and Zuberbühler[81] stir a solution of **2.6a** with copper perchlorate under 1 atm of pure oxygen for 30 min and obtained **2.7**. They also reported that Co(II) complexes can serve as an alternative to the copper complex, which was confirmed by Yao and colleagues[82] in 2007. In 2009, da Silva Miranda and colleagues[77] reported the same oxidation reaction to **2.7** under similar conditions, using iron perchlorate or hydrogen peroxide solution, where both underwent proposed peroxide-

intermediated pathways.[77] Yang and colleagues[83] very recently reported that such oxidation reaction can take place in situ during the synthesis of **2.6a** at elevated temperatures in air, where they achieved appreciable yields (30%) of **2.7**.

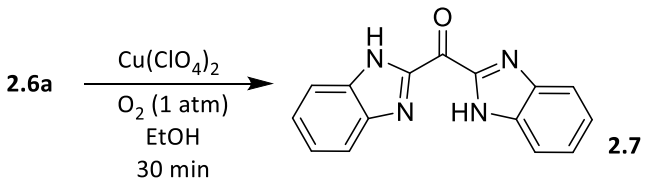

Scheme 3. Oxidation of 2.6a reported by Sprecher and Zuberbühler.

Largely driven by their spectroscopic properties and potential medicinal applications, transition metal complexes carrying bis-benzimidazole ligands have many reported examples. In 1988, Pujar and colleagues[84] reported the syntheses of cobalt, nickel, and copper complexes **2.8** and **2.9**, carrying **2.5a** or **2.6a** as ligands, respectively, where those complexes showed absorption λ_{max} in the visible red region of the EM spectrum (625 nm, **2.8b**). The **2.8** compounds also possess unusual seven-membered chelate rings that have sparked more interest in this class of compounds. This particular pattern of bis-imidazole being L_2-type ligands, i.e. two coordination sites in its neutral form, was confirmed by X-ray crystallography data reported by Yao and colleagues.[82]

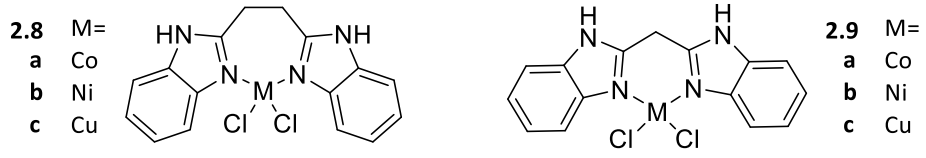

Expanding the scope of bis-benzimidazole ligands to other metals and main group elements requires the tuning of coordination pattern of the bis-benzimidazole ligands. In 2011 and 2013, Albers and colleagues[79,85] reported syntheses with revised methodology for bis-benzimidazole compounds **2.10**, where the authors used high

boiling point solvent 1,2,4-trichlorobenzene, controlled the system temperature at 180 °C, and obtained appreciable yields (40–60%). After the coordination with a [Fe_2-S_2] cluster, the proton on the *meso*-position of the ligand (highlighted showed on compound) on the binuclear complex **2.11** can be deprotonated through a PCET process, showing the tunability and versatility of this position of bis-benzimidazole ligands.

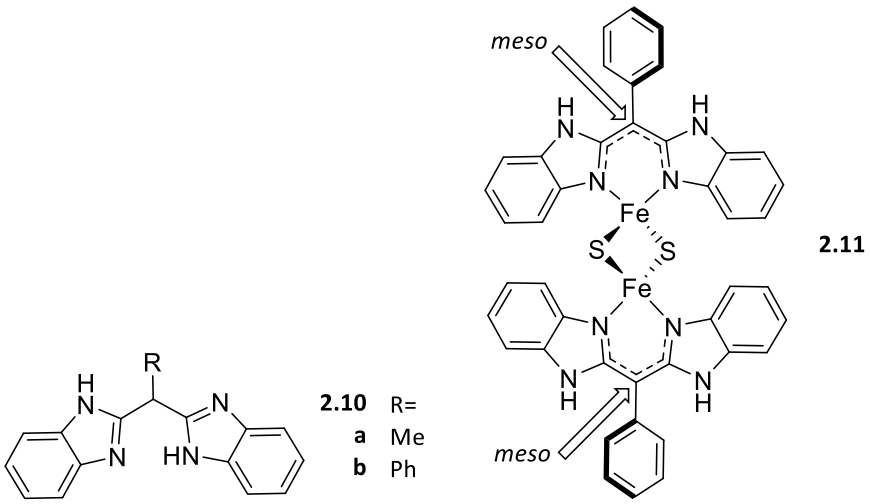

Despite the continuous effort made by researchers of all fields, examples of bis-benzimidazole coordinated main-group compounds, particularly boron, are few. The sole examples of main-group coordinated bis-benzimidazole complexes use an *N*-substituted bis-benzimidazole ligand, which are explained in detail in Section 3.1.

2.2 Bis(benzimidazolyl)methane

The synthetic arm of the project started with the attempts to synthesize bis(benzimidazolyl)methane compound **2.6a** according to modified literature procedures based on that of da Silva Miranda and collegues[77] and Albers and colleagues,[85] both of which invoked the traditional Phillips-Ladenburg reaction. Differ to the appreciable yields reported by precedented literature with an overnight reflux, low

yields were initially obtained, alongside side products like **2.12** and *o*-phenylenediamine starting material that revealed the incompleteness of the attempted reactions.

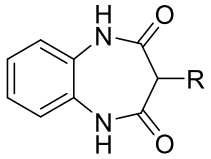

R=H **2.12a**
R=Me **2.12b**

The overnight reflux for the synthesis attempt of **2.6a** gave **2.12a** as the main product (Scheme 4), confirmed by its ^{1}H NMR spectrum (Figure 1). The spectrum shows few resemblances to the intended product but a sharp 2H singlet in the downfield region, corresponding to the N-H hydrogens, a 4H multiplet for the aromatic protons, and downfield shifted 2H singlet for the α-methylene hydrogens. This isolated compound was reported in literature before[86] as the main product after a 150 min reflux, revealing that longer time may be needed to allow the reaction to complete. Similarly, the first attempted synthesis of **2.6b** reveals a similar trend, giving **2.12b** as the by-product. Those results showed that the reaction conditions must be modified to achieve successful syntheses of the **2.6** derivatives.

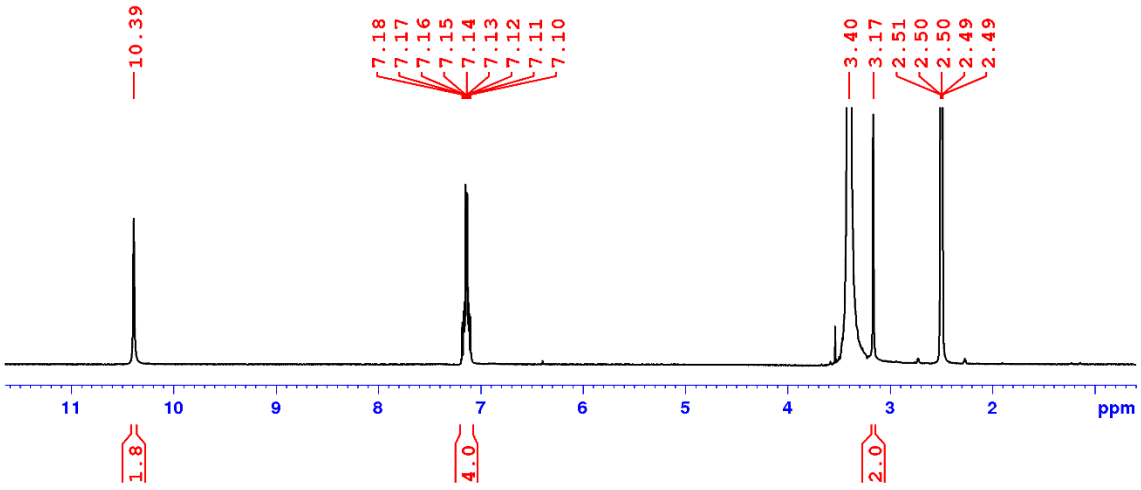

Figure 1. ^{1}H NMR spectrum of 2.12a in DMSO-d^{6} (300 MHz).

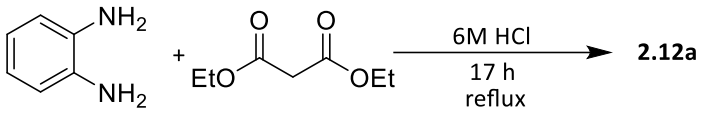

Scheme 4. Isolation of 2.12a.

Close-to-quantitative yields for **2.6a** derivatives were obtained using elevated temperature and significantly longer reaction times. The ^{1}H NMR spectrum of the isolated product matches those reported in literature,[76] and the compound was used without further purification.

Scheme 5. Synthesis of unsubstituted 2.6a

Similarly, a quantitative yield for **2.6b** compound was obtained with a change of solvent and longer reaction times. The use of ortho-dichlorobenzene (ODCB), a high-boiling point aromatic solvent, was inspired by the literature precedent of Albers and colleagues[85] that used 1,2,4-trichlorobenzene and controlled the temperature at 180 °C. With a boiling point of 180 °C, the cheaper solvent ODCB should suffice for these reactions, and indeed it did. The ^{1}H NMR of those compounds agree well with those reported in precedented literature.[79] For those requiring further purification, recrystallization from a mixture of ethanol and water was sufficient, and melting points are used as an additional tool to assess their purity.

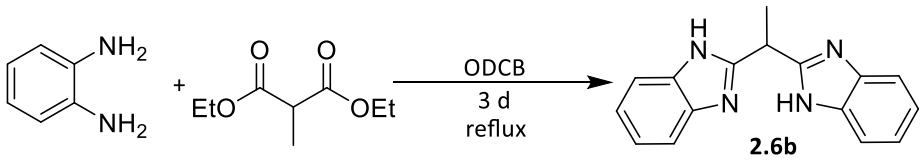

Scheme 6. Synthesis of substituted 2.6b.

The aforementioned experimental findings, particularly the isolation of by-products **2.12a–b** as major products, led to the proposed mechanism of the condensation reaction (Scheme 7). The longer required reaction time and temperature, and the reported uses of distillation, all demonstrate that the pathways lead to intended products **2.6a–b** are under larger kinetic control. Considering both cyclization reactions, 5-*exo*-*trig* and 7-*exo*-*trig*, respectively, are favoured under Baldwin's rules,[87] and 5- and 7-membered rings have comparative ring strain energies, such apparent difference in kinetics could be a result of the regional proximity between amino group and "amide" carbonyl that leads to non-ideal angles for the nucleophilic attack.

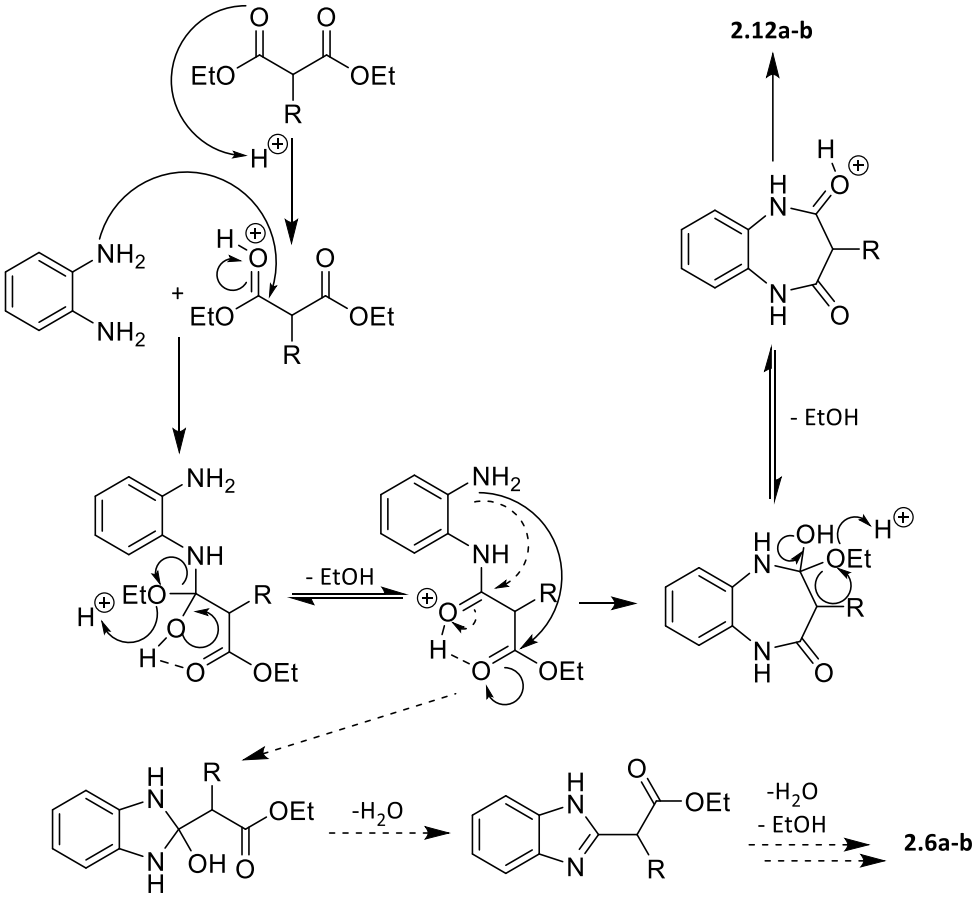

Scheme 7. Proposed mechanism of the condensation reaction during the synthesis of 2.6a–b. Solid arrows are the pathway leading to 2.12a–b, dashed ones are that of 2.6a–b.

2.3 Attempted Oxidation of **2.6a**

2.3.1 Synthesis and Structure

The first attempts of the **2.6a** oxidation were in polar solvents due to its solubility, where it only fully dissolves in DMSO and barely dissolves in acetone and alcohols. The oxidant chosen was *p*-chloranil, commonly used in oxidations of BODIPY chemistry.[88] Such reactions consistently led to an intense teal mixture, and upon isolation and purification, a dark green solid, colloquially named "Jade".

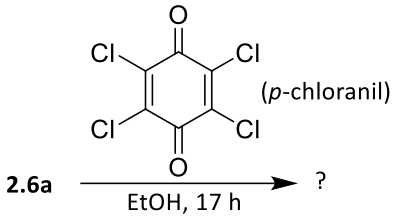

Scheme 8. Attempted oxidation of 2.6a leading to formation of Jade.

Jade shows rather unusual solubility, dissolving in only polar solvents like DMSO, methanol, and ethanol, and somewhat less so in acetone and acetonitrile. Its solubility in water is proportional to pH of the aqueous solution, where it dissolves well under basic conditions but only has modest solubility in neutral and acidic water solutions.

The mass spectrum of Jade (Figure 2) obtained through high-resolution mass spectrometry (HRMS) showed an exact mass of 667.11560. The spectrum also shows a clear isotopic pattern matching up nicely with any formula contains two Cl atoms. Accordingly, a molecular formula of $C_{36}H_{21}O_2N_8Cl_2$ (calc. 667.11590) was proposed for the singly protonated species and its calculated mass spectrum[89] (Figure 3) matches that experimentally obtained. In addition, 4 benzimidazole units are present, inferred by the number of N atoms, and precluding the possibility that Jade is the intended oxidation

product, which a calculated exact mass of 246.09. To add, the neutral form of Jade should have the molecular formula $C_{36}H_{21}O_2N_8Cl_2$, correlating to the mass of two bis(benzimidazolyl)methane units and a *p*-chloranil less two chlorides.

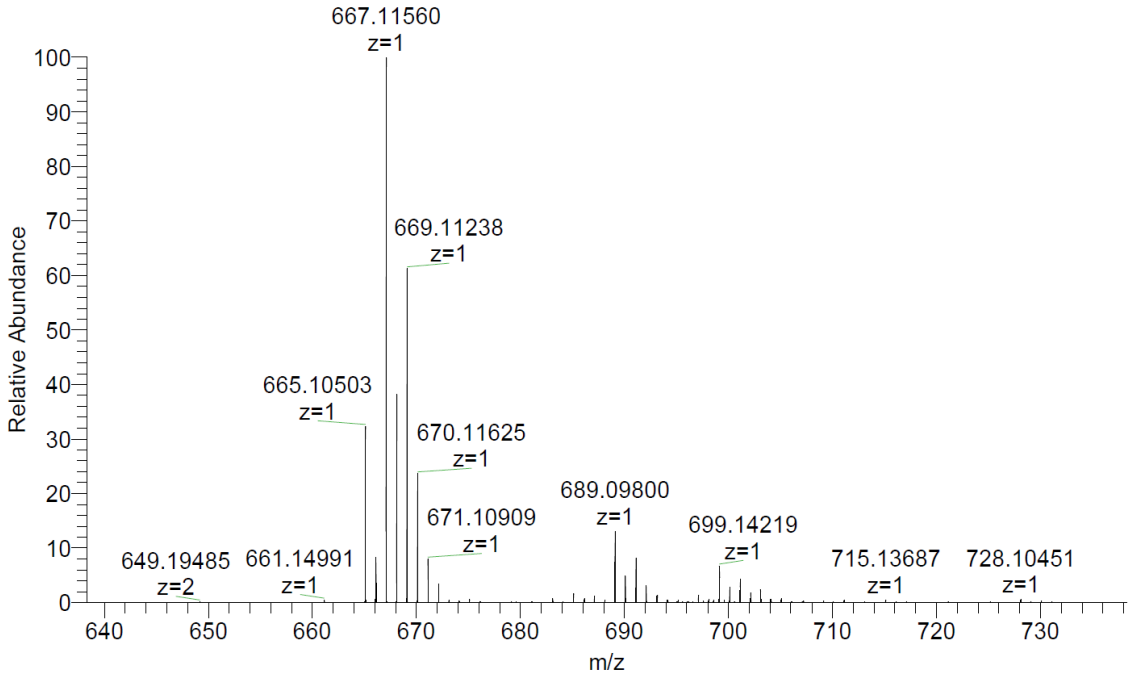

Figure 2. HRMS spectrum of Jade, localized view for [M+H$^+$].

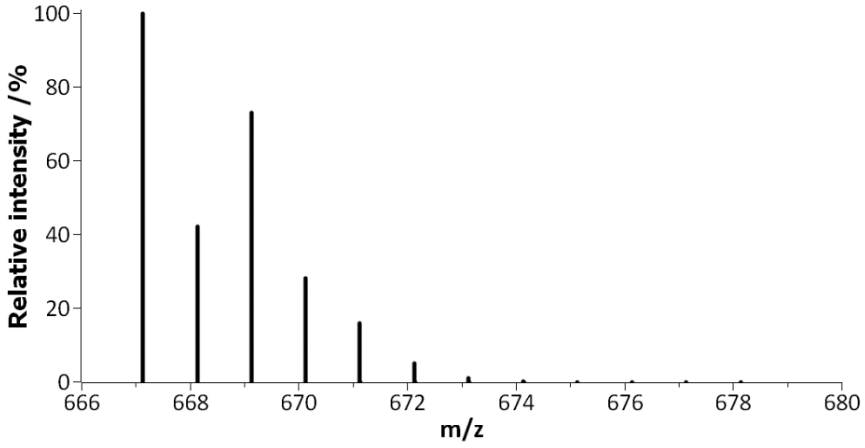

Figure 3. Calculated HRMS spectral pattern of Jade using its molecular formula.

Crystal structure obtained from X-ray crystallography (Figure 4) confirmed the molecular formula obtained by HRMS. The development of conditions and solvents to produce crystals suitable for X-ray crystallography was long and challenging, mainly due

to solubility and stability of Jade in various kinds of solvents. It was those attempts that allowed observations of the dependency of Jade's solubility on concentrations of H^+ in protic solvents, similar to its pH dependency observed in water. After many attempts, it was established that using methanol as the "good" solvent and acidified it with trace amount of an aqueous acid seems to give the most optimized results by yielding micro-crystalline solids. Indeed, very slowly evaporating a saturated methanol solution of Jade that was acidified with several drops of concentrated aqueous tetrafluoroboric acid solution in freezer and a flame tube gave suitable crystals, leading to a successfully solved crystal structure. The structure is determined to be the doubly-protonated derivative of Jade, **2.13**. An ORTEP diagram of its solved structure (Figure 4) and a list of selected bond lengths (Table 1) convey significant information about Jade's structure.

2.13

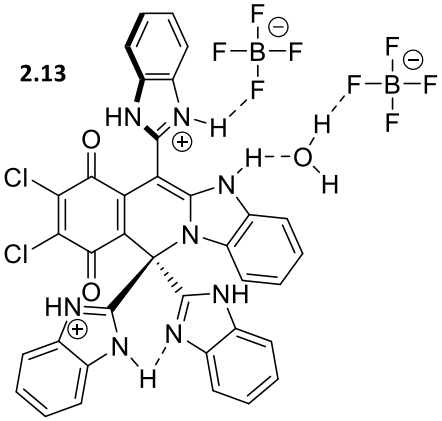

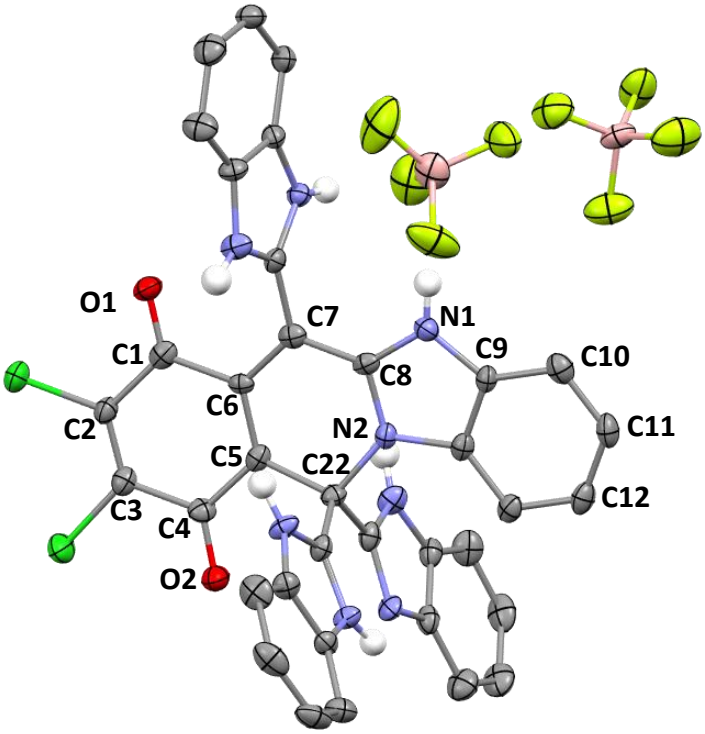

Figure 4. ORTEP diagram of compound 2.13. All hydrogen except those on nitrogen and solvent were removed for clarity. Thermal ellipsoids at the 50% probability level.

Table 1. Selected bond lengths for the crystal structure of 2.13.

Bond	Bond Length /Å
C1-O1	1.215(5)
C1-C2	1.492(6)
C2-C3	1.317(6)
C3-C4	1.497(6)
C4-O2	1.234(5)
C5-C6	1.389(6)
C6-C7	1.379(6)
C7-C8	1.413(6)
C8-N1	1.340(5)
C8-N2	1.366(5)
C9-C10	1.392(6)
C10-C11	1.391(7)
C11-C12	1.373(6)
C22-C5	1.534(6)
C22-N2	1.472(5)

The crystal structure of **2.13** showed a planar, fully delocalized moiety consists of quinone and benzimidazole, a structural combination that appears to have no literature precedent. The bond lengths of two CO bonds, 1.215 Å for C1-O1 and 1.234 Å for C4-O2, respectively, match with the average length[90] of C=O bonds at 1.197 Å and significantly shorter than C-O's average at 1.399 Å. Furthermore, from C1-C2, C2-C3, to C3-C4, the bond lengths showed a pattern of staggering single-double-single bonds, inferred by the average C-C and C=C bond lengths. Those are key pieces of evidence for the presence of a Cl-substituted quinone-like moiety. Through C7 to the co-planar benzimidazole unit, the CC and CN bonds showed intermediate bond lengths that in between those of single bonds and double bonds, illustrating the extended conjugation between the coplanar quinone and benzimidazole moieties. Bonds to the quaternary carbon C22 all correlate well with average bond lengths of C-C and C-O single bonds, for C5-C22 and C22-N2 bonds, respectively. Alongside the bond angles around C22, for example 108.2° of C5-C22-N2, those showed that C22 is indeed a proper sp^3-hybridized tetrahedral carbon and is unlikely that the conjugation would extend to the benzimidazole units on C22.

The proposed structure for neutral form of Jade is based on the crystal structure of **2.13** and computational data of the tautomers. Removing the protons on the positively-charged nitrogen atoms inferred for **2.13** give many possible tautomers with the most plausible being **2.14** and **2.14t**. Instead of being tilted, the benzimidazole unit in between the quinone and the N-substituted benzimidazole are coplanar with those moieties, according to their computational optimized structures. The existence of a hydrogen bond can sufficiently explain this change of conformation from **2.13**. The

calculated thermodynamics parameters using optimized geometries (Table 2) showed a small energy difference with **2.14** being the lower energy species, resulting in minor tautomerism in practical terms. Nevertheless, heating the sample to 380K showed no changes in the spectral pattern as the tautomerism only invokes the transfer of an exchangeable proton and other structural aspects of the compound are retained. Apart from confirming the structure of tautomers, dipole moment of **2.14** is calculated at 4.8 D. The number is even higher than that of DMSO and can explain the solubilities (or lacking thereof) of Jade.

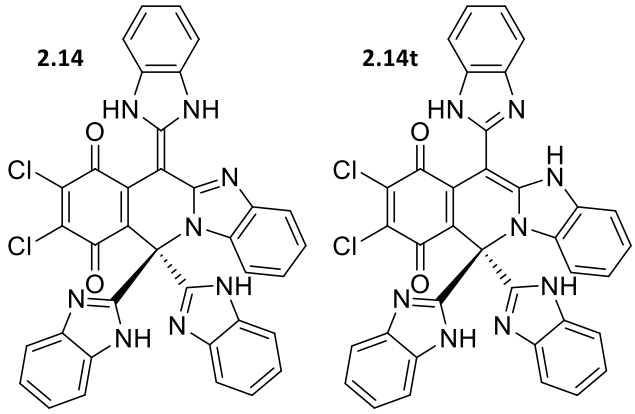

	2.14	⇌	***2.14t***
G^o /kJ·mol^{-1}	1138.97		1141.61
$\Delta_r G^o$ /kJ·mol^{-1}		2.64	
K_{eq}		0.34	

Table 2. Calculated thermodynamic parameters of 2.14 and 2.14t at 298.15K and 1 atm.

The NMR spectra of Jade is consistent with the structure of **2.14**. The ^{1}H NMR spectrum (Figure 5) showed three sets of multiplets in the aromatic region that could be grouped by their relative integrations and coupling constants and aligned well with the proposed structure. Due to the rapid exchanges of the N-H hydrogen, the two benzimidazole units connected by the tetrahedral carbon are chemically equivalent. The

two doublets of doublets (4H), at 7.72 and 7.33 ppm, correlate well with those interpretations. Similarly, the doublet of doublets at 7.88 and 7.62 ppm with 2H integrations correlate with the non-N-substituted benzimidazole unit next to the carbonyl with two pairs of chemically equivalent aromatic protons. Coupling constants of 3 and 6 Hz for those symmetrical benzimidazole units are in line with benzimidazole compounds reported in literature. All four remaining peaks in the aromatic region have a relative integration of 1H, corresponding to the four chemically-distinct protons on the *N*-substituted benzimidazole unit. The doublet-doublet-triplet-triplet multiplicity pattern correlates well with the proposed structure, and the coupling constants of 8 Hz also revealed the altered electronic structure of the substituted benzimidazole moiety.

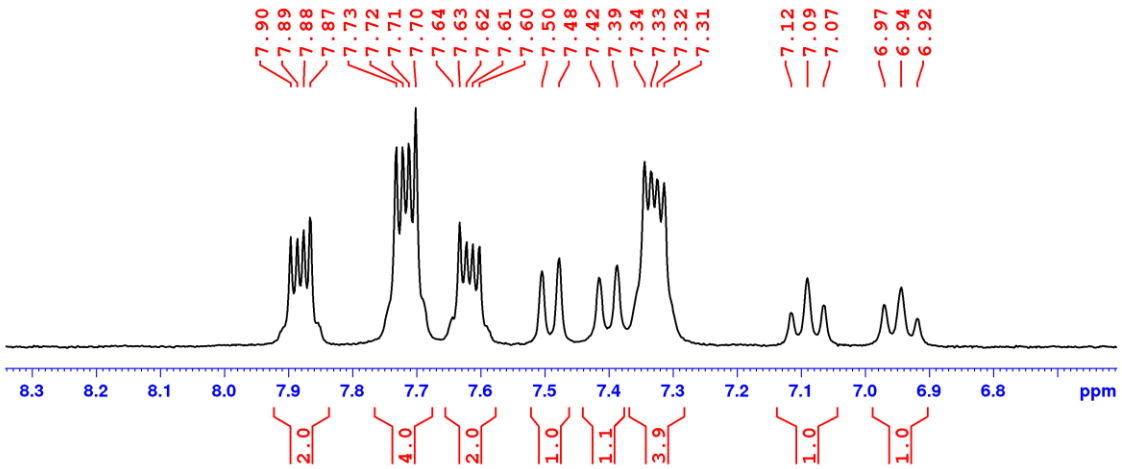

Figure 5. Aromatic region of ^{1}H NMR spectrum of 2.14 (Jade) in DMSO-d^{6} at 300 MHz.

The ^{13}C NMR spectrum (Figure 6) and 2D NMR experiments confirmed the aforementioned interpretations of distinct benzimidazole units. Most prominently, the singlets at 178 and 165 ppm reveals the presence of the carbonyl groups. Although the peaks are upfield-shifted from many carbonyl compounds, the chemical shift of the 178 ppm peak is in line with that of the similar conjugation-extended compound **2.15**,

reported[91] at 176.8 ppm. The further upfield-shifted 165 ppm may accredit to the fully substituted quaternary carbon two bonds away. Alongside the IR spectrum (Figure 7) that has a C=O stretching peak at 1747 cm^{-1}, those confirm the presence of carbonyl.

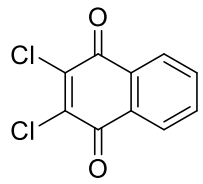

2.15

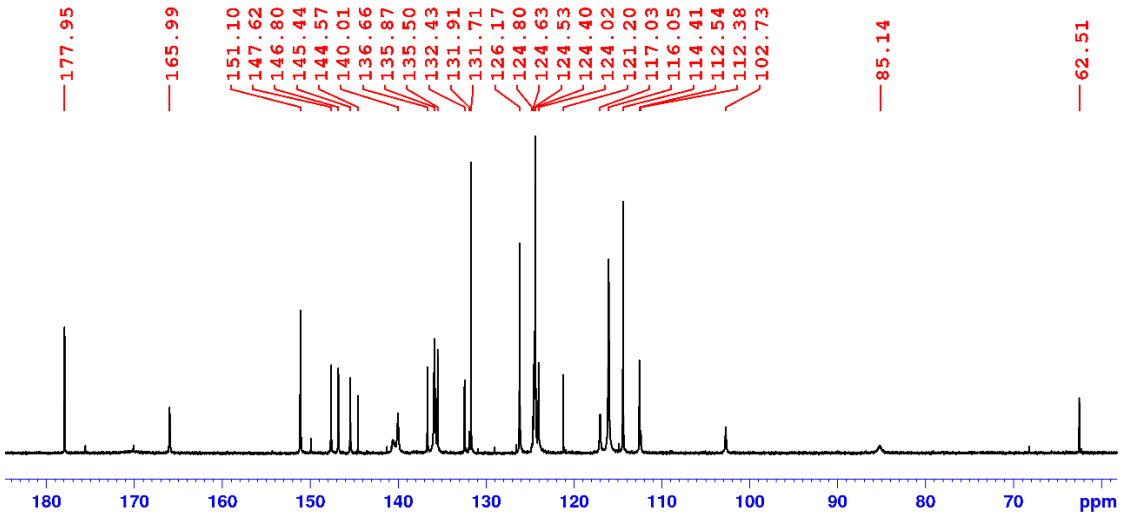

Figure 6. ^{13}C NMR spectrum of 2.14 in DMSO-d^6 at 125.8 MHz.

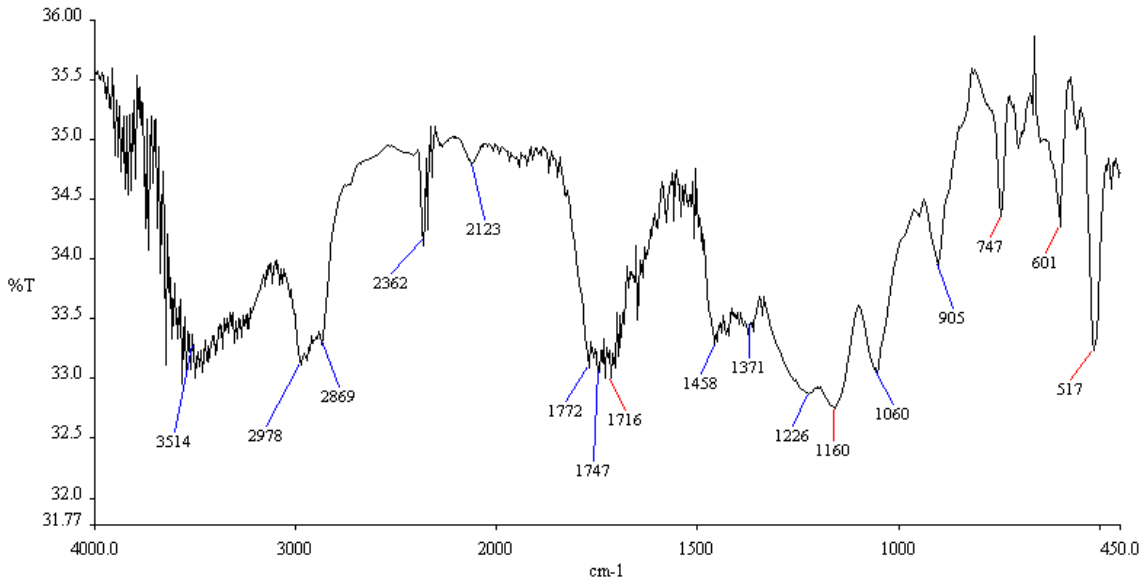

Figure 7. IR spectrum of 2.14 using KBr pellet.

DEPT-135, short-range HSQC, and long-range HMBC experiments assist the individual assignment of each ^{13}C NMR peaks. For the N-substituted benzimidazole unit, the most upfield-shifted proton peak is a triplet, hence assigned to the respective position showed in Scheme 9 under the chemical intuition that more electron-rich positions are more shielded. That peak shows long range interaction with the ^{13}C peak at 117 ppm, and in tern shows short-range interaction with the ^{1}H peak at 7.49 ppm. The rest of that benzimidazole unit can be assigned peaks in a similar fashion. The other "phase up" carbons can be easily divided into two groups based on the integrations of protons that they show short-rage interactions with, and then those who "disappears" using long-range interactions. The ^{13}C peak at 62.5 ppm is the quaternary tetrahedral carbon as shown, and the aforementioned carbonyl peaks are assigned according to intuitions on shielding affects. There are 9 carbon peaks that cannot be accurately assigned, and 8 carbons have not been assigned a peak (circled in Scheme 9). For all those 8 carbons, accurate assignments may not be possible due to their similarities in

chemical environments and expected chemical shifts, but more importantly the lack of nearby protons to probe experimentally with long-range interactions. There is also an extra peak and is most likely from an unknown impurity, as ^{13}C spectrum of possible impurities like *p*-chloranil and *o*-phenylenediamine did not have any peaks that match with those unassigned.

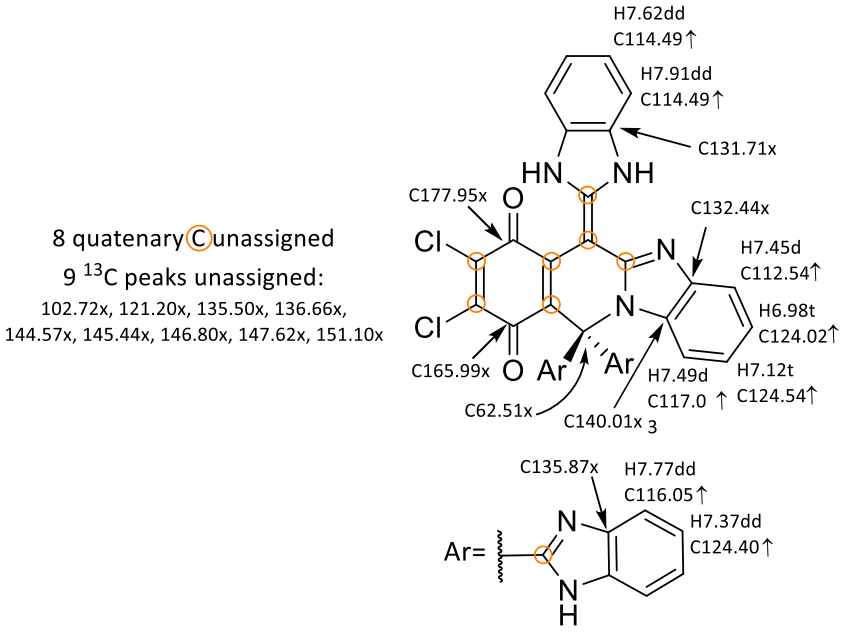

Scheme 9. Structural interpretation of NMR spectral data of 2.14.

2.3.2 Energy Properties

The electronic spectrum of **2.14** (Figure 8) confirmed the existence of board, intense absorptions in the far-red and NIR region. The maximum absorption wavelengths are 321 and 712 nm, with molar extinction coefficients 31000 and 14600 $L \cdot mol^{-1} \cdot cm^{-1}$, respectively. There is also a weak shoulder observed at approximately 430 nm. Absorption of Jade behaves well in accordance with the Beers–Lambert law, as illustrated by Figure 9. Those findings correlate well with the intense teal colour (inset of Fig. 8) observed for Jade as a solid and in solution.

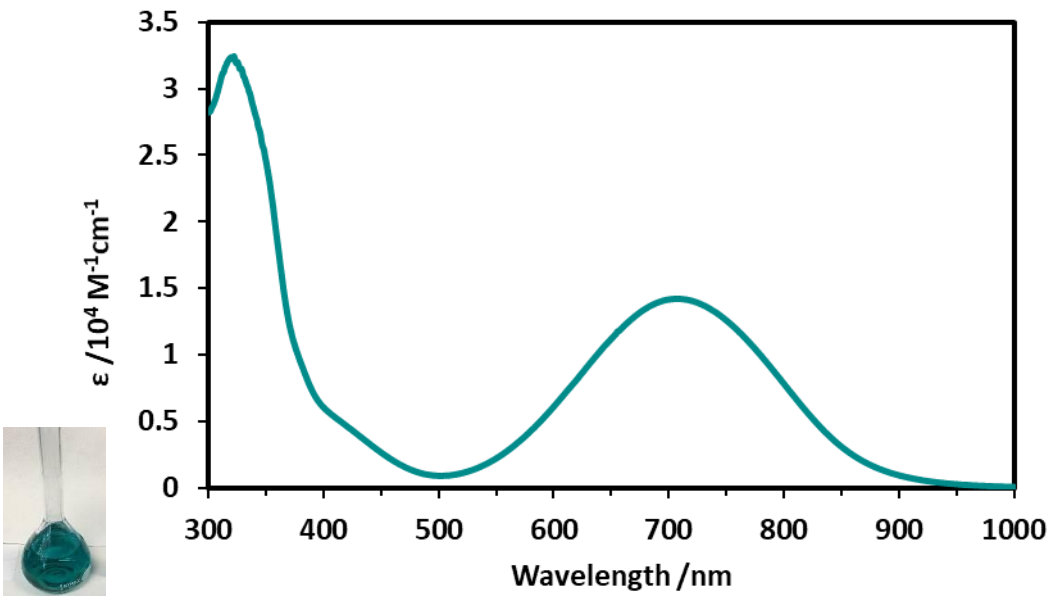

Figure 8. UV-Vis-NIR spectrum of 2.14 in methanol (74 μM); photo of this solution on the left.

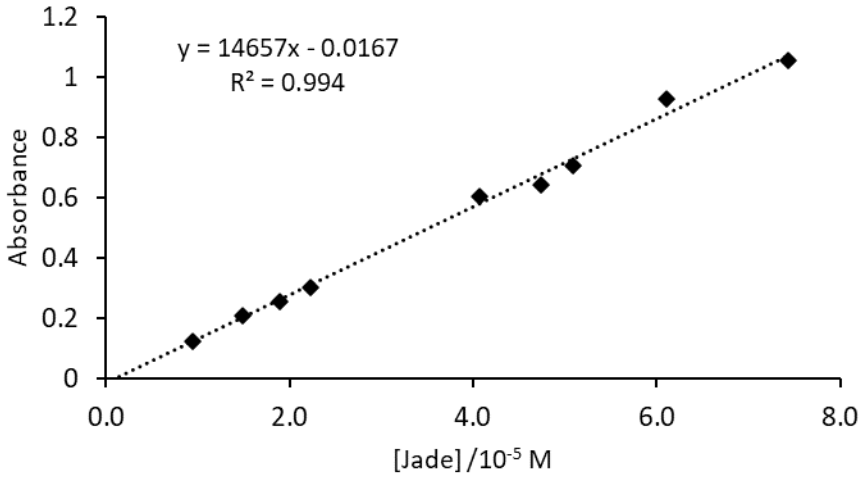

Figure 9. Beer–Lambert law plot of absorbance of 2.14 at 712 nm using three independently-prepared triplicate solutions.

Extensive benchmark of TDDFT studies on **2.14** yield computational transitions and spectra that are in agreement with the experimental UV-Vis-NIR spectrum. In computational chemistry, functionals are crucial to the accuracy of the computational results, especially so for TDDFT[92]. Popular functionals are divided into different categories based on their mathematical infrastructures, namely GGA (PBE), meta-GGA

(M06-L), hybrid-GGA (B3LYP, PBE0), and range-separated hybrid-GGA (CAM-B3LYP). Results among those categories of functionals can be drastically different and needs to be individually conducted and carefully compared against experimental data, i.e. *benchmark*. Using the optimized structure of **2.14**, benchmarking using the said functionals showed CAM-B3LYP being the most suitable functional for further analyses (Figure 10). After correcting the data for methanol solvent environment, the calculated transitions match with the experimental UV-Vis-NIR spectral pattern of **2.14** in methanol (Figure 11), capturing the intense transitions with small errors and correctly demonstrating the shoulder at approximately 420 nm.

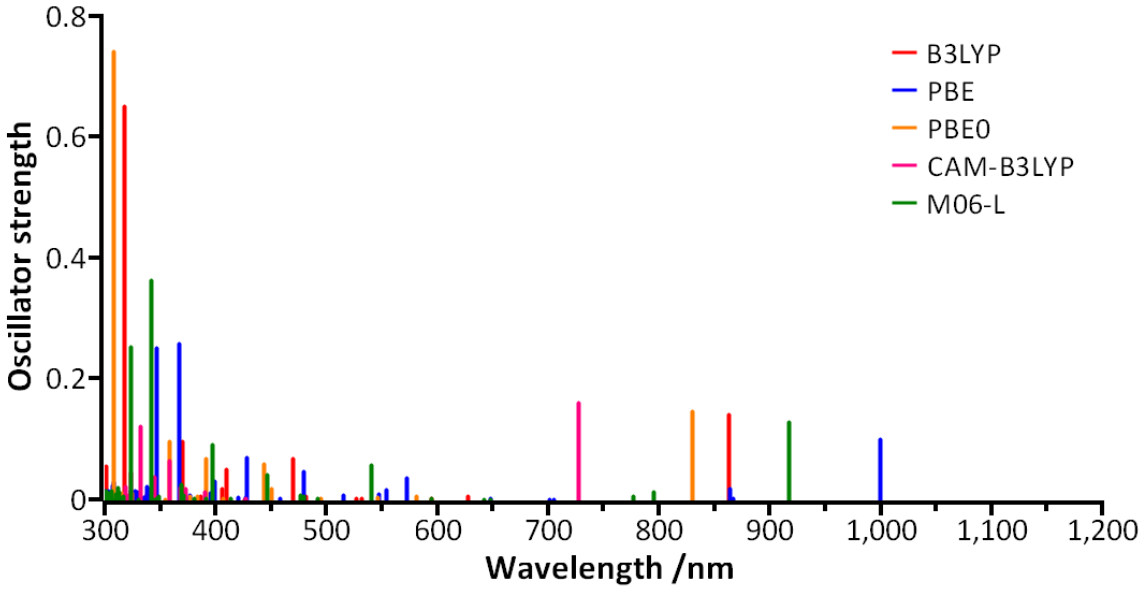

Figure 10. Benchmark of TDDFT results of 2.14 using the listed functionals.

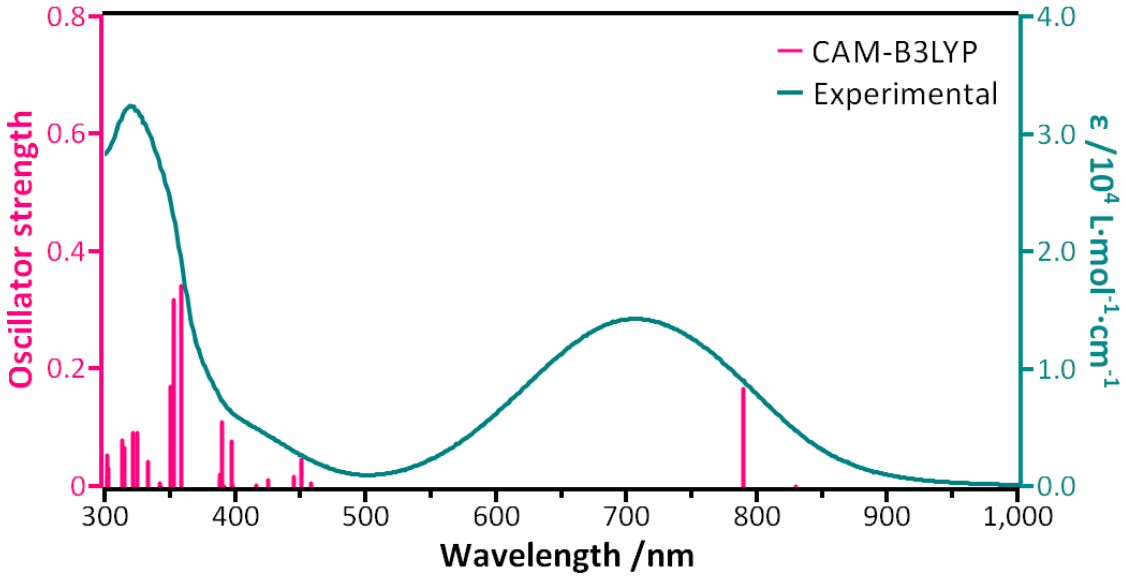

Figure 11. Comparison of experimental UV-Vis-NIR spectrum of 2.14 in methanol (curve) and TDDFT calculated transitions (bars) using methanol parameters and the listed functional.

The low-energy HOMO-LUMO transition showed exclusive participation from the heavily delocalized FMOs. Further analyses on the lowest energy transition showed that it has exclusive HOMO-LUMO characteristics (93.4%). The plotted HOMO (Figure 12, left) showed extensive delocalization among the two benzimidazole units that are coplanar to the quinone unit, where the LUMO (Figure 12, right) is more localized at the said quinone unit. As demonstrated, a push-pull system is clearly present, with relatively electron-rich benzimidazoles acting as donors and highly electro-poor quinone acting as acceptors. Explained in Chapter 1, such systems are known to generate NIR dyes.

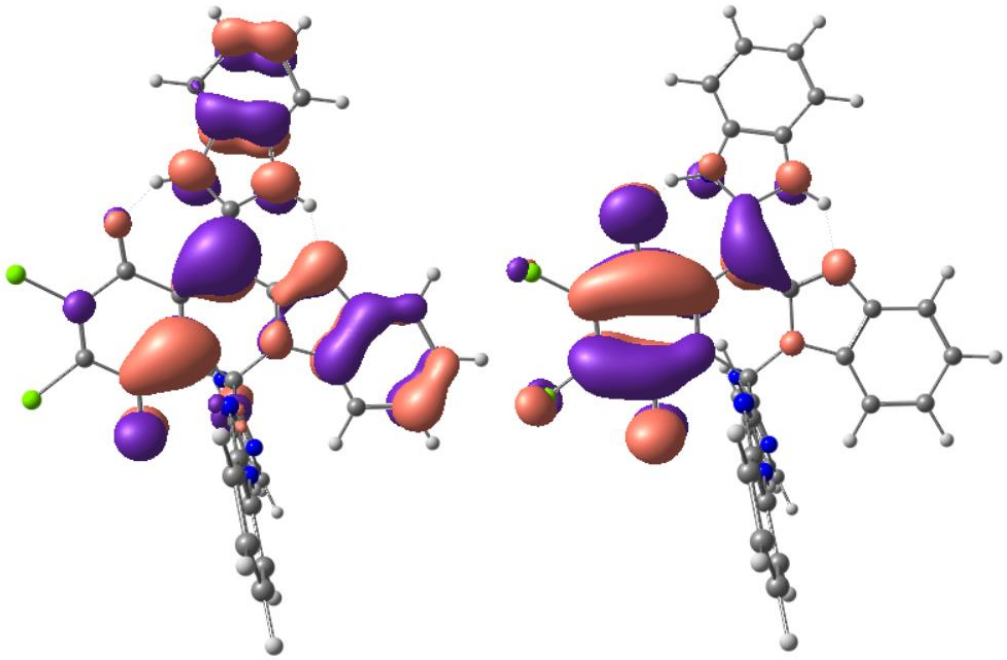

Figure 12. Calculated HOMO (left) and LUMO (right) of 2.14 using CAM-B3LYP functional and methanol parameters. Contour level for illustration set at 0.03.

Cyclic voltammetry (CV) experiments of **2.14** showed a reversible redox event at 0.23 V (vs. NHE) and several non-reversible redox events at -0.13 V and 0.76 V (Figure 13). The structure of **2.14** contains a quinone unit that can be reduced, and indeed the reversible event at 0.23 V can attribute to a two-electron, two-proton reduction, as demonstrated by its larger current flow. The interpretation is supported by literature findings[93] of sterically bulky quinones. Estimated by the computational HOMO-LUMO gap (3.93 eV) using literature correlations[94] between computational energy gaps and reduction potentials, an one-electron reduction potential for **2.14** is expected to be at around -0.7V. That estimation is also in line with literature predictions.[93] Nevertheless, the narrow electrochemical measurement window of water and solubility hinders the ability to obtain more information on the electrochemical properties of **2.14**.

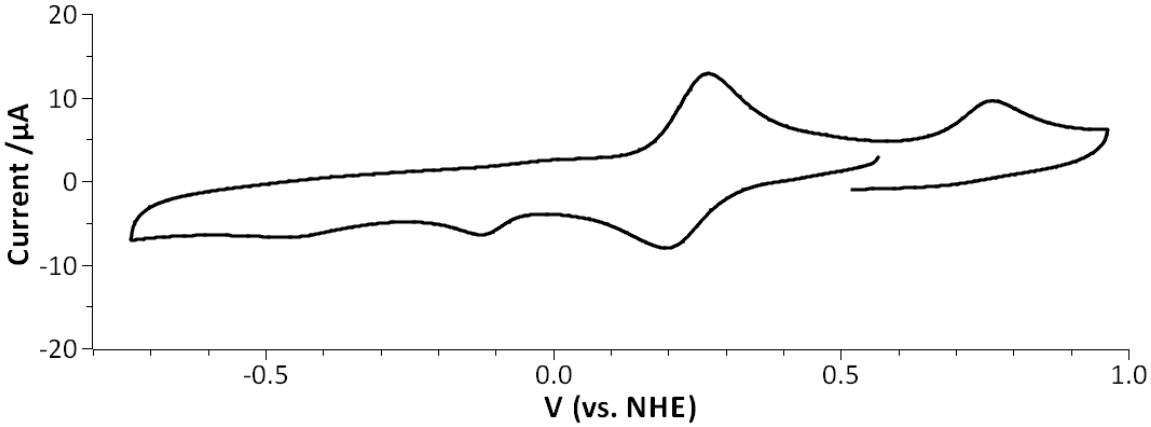

Figure 13. Cyclic Voltammogram of 2.14 in pH = 7.8 aqueous phosphate buffer solution.

2.3.3 Computational Studies of the Core Chromophore

Credible computational results of Jade regarding its electronic structure showed that the benzimidazole-quinone pair is the main chromophore that allows low-energy transitions. Calculated transitions and FMOs of analogues **2.16** and **2.17** gave further insight of this unprecedented pair of moieties.

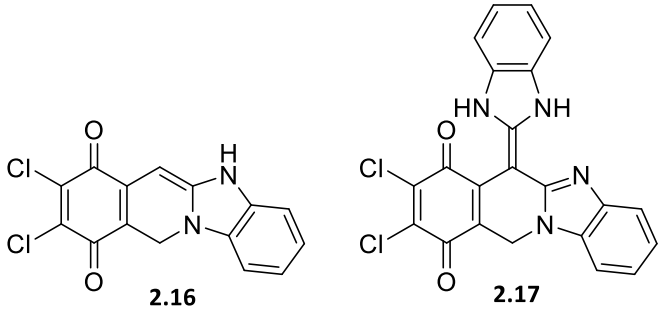

Surprisingly, calculated transitions **2.16** by TDDFT consists low energy transitions that projects to be in the far-red region. Thanks to the coplanar geometry and push-pull system that still presents in **2.16**, as demonstrated by its geometry and FMOs (Figure 14), the low energy transition that is similarly HOMO-LUMO in characteristics is well in the far-red region, at 630 nm. These results confirm that the benzimidazole units connected via the tetrahedral carbon on **2.14** is not part of the key chromophore, where both

benzimidazole units that are coplanar to the quinone moiety are crucial to obtain transitions in the NIR region. Such conclusions are undoubtedly confirmed by the calculated transitions of **2.17**, where it is projected to show transitions in the NIR region, at 767 nm. While this wavelength is even longer than those from experimental studies of **2.14**, it is unclear whether such shift conveys a chemical message or an artifact of computational methods similar to that observed for the results of **2.14**. Nevertheless, through those computational studies, the core chromophore of **2.14** is undoubtedly the quinone-benzimidazole dyad, where the additional benzimidazole unit pushes the transition energy into the NIR region.

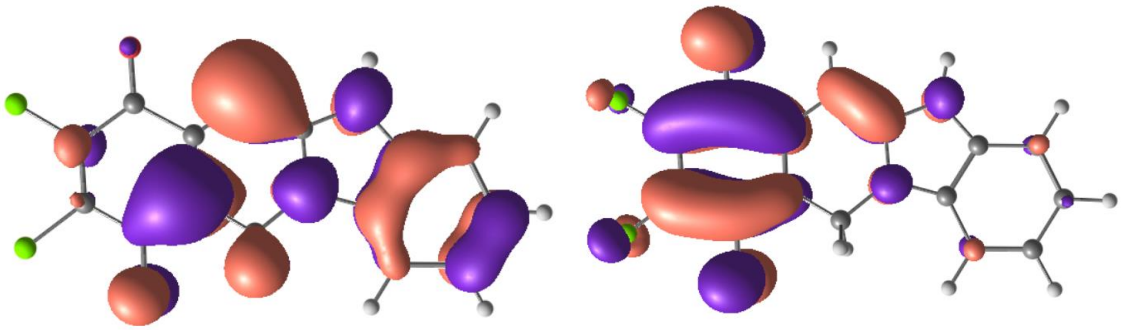

Figure 14. HOMO (left) and LUMO (right) of 2.16 using CAM-B3LYP. Contour level set at 0.03.

The tetrahedral carbon of **2.16** showed great resemblance to a four-coordinate boron with respect to its geometry, hence computational work on the BF_2-based analogue **2.18** can shed light on the versatility of this chromophore. To have a neutral compound, the organic bulk part of **2.18** is one hydrogen less at the benzimidazole nitrogen to give a fully conjugated structure. Calculated transitions showed an intense, similarly low energy transition at 711 nm, and the orbitals responsible for that transition, namely HOMO-2 and LUMO (Figure 15), are delocalized among atoms of the full molecule as expected.

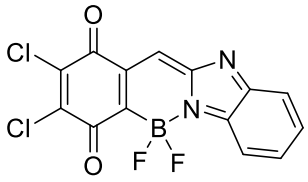

2.18

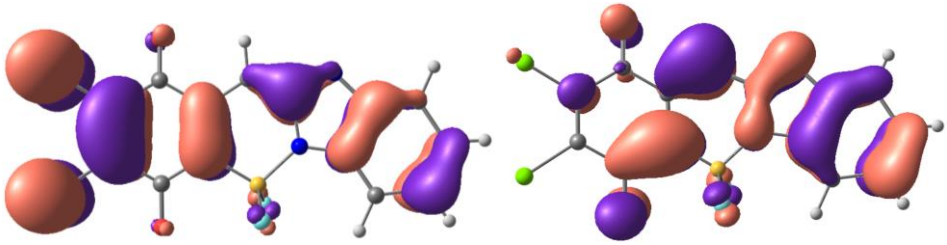

Figure 15. HOMO-2 (left) and LUMO (right) of 2.18 using PBE. Contour level 0.03.

2.3.4 Derivatives of **2.14**

Preliminary coordination chemistry of **2.14** using zinc and boron gave inconclusive results. Boron coordination chemistry with **2.14** is challenging due to its poor solubility in aprotic, non-polar solvents that are commonly used for boron coordination reactions. The sole attempt of such reaction in toluene at elevated temperature yielded a black mixture with non-interpretable ^{1}H NMR spectrum and no chance of purification. As explained by Sakamoto[95] and colleagues in 2012, Zn coordination can act as an effective substitution to study dye systems that would not allow boron coordination, and that inspired some attempts on Zn coordination with **2.14**. Following modified literature procedure of Zn coordination,[95,96] addition of zinc(II) acetate to a methanol solution of **2.14** showed an apparent colour change from teal to green, in line with commonly-observed redshifted absorbance wavelengths observed in Zn complexes.[95,96] Although the ^{1}H NMR spectrum of the crude complex is too complex to give conclusive information about the formation of the complex, low-resolution mass

spectrum of the crude solid gave masses that roughly correlate to the coordination of one and two Zn atoms. Differ to the parent compound **2.14**, the crude solid showed extraordinary solubilities among different solvents, which in tern makes purification by recrystallization very challenging. Attempts to purify the solid by chromatography under various conditions also failed.

2.4 Attempted Oxidation of **2.6b**

As explained in previous sections, attempts to oxidize **2.6b** lead to unexpected results. As **2.6a** showed significantly different reactivity thanks to both hydrogens on the methylene group, it was expected that **2.6b**, with only one hydrogen available at the methylene position, should be oxidized to the intended product **2.19**. Both attempted syntheses (Scheme 10) in ethanol and THF gave dark brown mixtures that cannot be purified. UV-Vis spectrum of the mixture showed a shoulder at approximately 420 nm. Multiple attempts to purify by chromatography or recrystallization has failed.

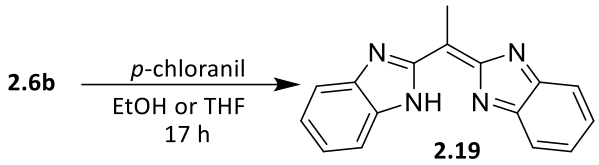

Scheme 10. Attempted synthesis of 2.19 using 2.6b.

Computational results of **2.19** revealed that the fully oxidized compound would not be NIR-absorbing. TDDFT calculated transitions using B3LYP functional only showed an intense transition at 453 nm, which resembles the experimental UV-Vis spectrum obtained on the reaction mixture, and the FMOs responsible for the intense transition (Figure 16) showed a fully delocalized electronic structure.

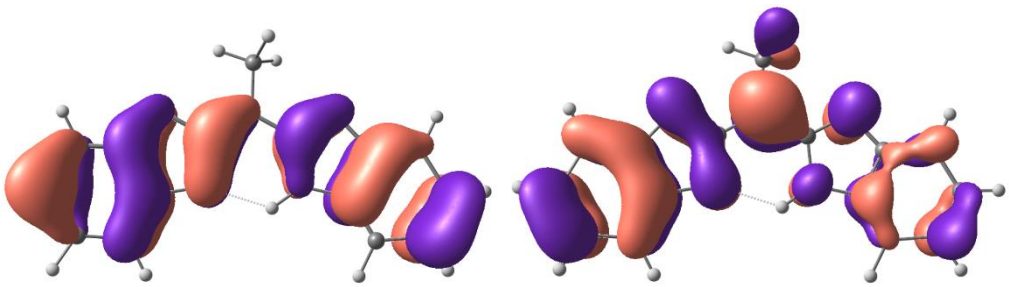

Figure 16. HOMO (left) and LUMO (right) of 2.19 using B3LYP functional.

2.5 Summary

Bis(benzimidazolyl)methane compounds (**2.6a–b**) were synthesized with good yields using experimental procedures. Dilactam by-products **2.12** were isolated, giving an insight on the mechanism of the long-known Phillip-Ladenburg reaction to synthesis benzimidazoles and confirming experimental findings of literature precedents.

Jade (**2.14**) was obtained by a reaction of **2.6a** and *p*-chloranil and is a bis-benzimidazole NIR dye, showing intense absorption at 712 nm. Molecular structure of Jade consists two bis-benzimidazole units and a Cl-substituted quinone, confirmed by HRMS, X-ray crystallography, NMR, and IR. Computational studies of **2.14** and its simpler analogues showed a coplanar quinone-benzimidazole chromophore, an unprecedented combination of moieties.

2.6 Experimental

2.6.1 Materials and General Procedures

Reagents and solvents were purchased from commercial sources and used without purification. NMR experiments were conducted at 300 K (unless otherwise noted) on Bruker AV300 (300 MHz) / NEO500 (500 MHz) NMR spectrometers and locked

using the deuterium signals of the respective solvents. ^{1}H / ^{13}C NMR spectra were manually calibrated according to literature values of residue solvents[97] (ppm): DMSO-d^6, 2.50 / 39.52; CD_3OD, 3.31 / 49.00; $CDCl_3$, 7.26 / 77.16. Low resolution mass spectra were obtained using Thermo Scientific MSQ Plus mass spectrometer. Accurate mass determination through high resolution mass spectrometry were obtained using by electrospray ionization using a Thermo Scientific Exactive Plus Orbitrap Ultimate 3000 LC-MS system. The eluent used was a 10:90 mix of Mili-Q water and Optima Methanol. IR spectra were obtained using PerkinElmer SpetrumOne FT-IR spectrometer. UV-Vis-NIR absorbance spectra were obtained using Agilent 8453 UV-Vis-NIR spectrometer in a 10 cm quartz cell in respective solvents. Melting points were obtained using a mercury thermometer reading to 400 °C and are uncalibrated.

Cyclic voltammograms were obtained using Bioanalytical Systems E2 Epsilon Electrochemical Analyzer with a cell consisting of a glassy carbon working electrode, platinum wire counter electrode, and a silver wire quasi-reference electrode. Experiments are performed in pH=7.8 aqueous phosphate buffer solution, which was prepared according to modified literature procedure[98] and degassed by Ar gas, at 100 mV/s, and calibrated using ferricyanide as an internal standard[99] (E_o= 0.4263 V vs. NHE). Sample was introduced with minimal amount of DMSO due to solubility.

X-ray crystallography data was obtained at Structural Analysis Laboratory, Department of Chemistry, University of British Columbia, Vancouver, BC. A suitable crystal was selected, and X-ray refraction data was collected on a Bruker APEX-II CCD diffractometer with CuKα (λ = 1.54178 Å) radiation. The crystal was kept at 296.15 K

during data collection. The structure was solved using Olex2 software[100] with the ShelXT structure solution program[101] using Intrinsic Phasing and refined with the ShelXL refinement package[102] using Least Squares minimisation. The structure was solved by the author and treatment of the solvent mask was recommended by Dr. Dillon T. Hofsommer at the University of Louisville, KY, USA.

2.6.2 Synthetic Details

Bis(1H-benzimidazol-2-yl)methane (**2.6a**)

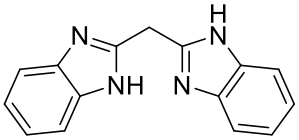

A 100 mL round bottom flask was charged with a stir bar, 5.1952 g o-phenylenediamine (0.04804 mol), 3.7 mL diethyl malonate (3.86 g, 0.0241 mol, 0.5 eq.) and 30 mL 6M $HCl_{(aq)}$. The suspension was heated and kept at 155 °C using an oil bath and turned to a clear, orange solution. The boiling solution was heated for 6 days on which the colour turned light blue and white precipitates formed. The mixture was then cooled to rt and in an ice bath, and the resulting white crystals was filtered and washed with cold 1M $HCl_{(aq)}$. The crystals were then dissolved in approx. 100 mL of 88 °C hot water and neutralized using approximately 20 mL of concentrated $NH_3 \cdot H_2O$. The resulting white precipitate was filtered and dried overnight, affording the title compound (3.7003 g, 0.01484 mol, 61.8%). ^{1}H NMR (DMSO-d^6, 300 MHz; δ /ppm): 12.42 (s, br, 2H), 7.50 (dd, *J*=3 and 6 Hz, 4H), 7.14 (dd, *J*=3 and 6 Hz, 4H), 4.48 (s, 2H). Mp: 266 °C (decomp.) (lit.[86] >300 °C).

1,1-bis(1H-benzimidazol-2-yl)ethane (**2.6b**)

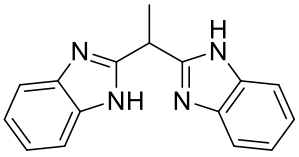

A 100 mL 3-neck round bottom flask was charged with a stir bar, 2.0917 g *o*-phenylenediamine (19.289 mmol), and 3.0 mL *o*-dichlorobenzene. The slurry was heated to boil and became an orange solution. To the solution, 1.70 mL of methyl diethylmalonate (9.97 mol, 0.52 eq.) was added dropwise using an addition funnel. The mixture was refluxed overnight for 19 h. Beige-coloured precipitation formed upon cooling the mixture to rt. The mixture was filtered and washed with hexanes, isolating the crude solid. It was then dissolved in 3M $HCl_{(aq)}$ and filtered. The resulting dark brown solution was neutralized using sat. $NaOH_{(aq)}$ solution to basic pH, giving beige-coloured precipitates. Filtration and washing with $NaOH_{(aq)}$ yielded the title compound (2.7042 g, 0.01031 mmol, quantitative) as a beige-coloured solid. ^{1}H NMR (DMSO-d^{6}, 300 MHz; δ /ppm): 7.36 (dd, *J*=3 and 6 Hz, 4H), 6.85 (dd, *J*=3 and 6 Hz, 4H), 4.52 (q, *J*=7 Hz, 1H), 1.74 (d, *J*=7 Hz, 3H). Mp: 262-264 °C (lit.[85] 265 °C).

2,9,9-tris(1H-1,3-benzodiazol-2-yl)-5,6-dichloro-10,17-diazatetracyclo[8.7.0.0^{3},^{8}.0^{11},^{16}]heptadeca-1,3(8),5,11(16),12,14-hexaene-4,7-dione ("Jade", **2.14**)

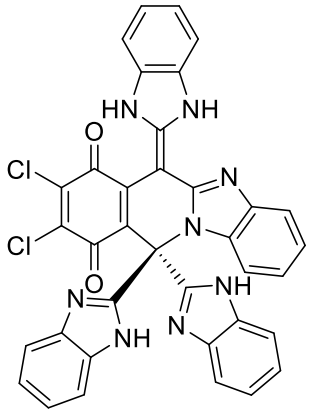

A 100 mL Erlenmeyer flask was charged with stir bar, 485.5 mg bbim (1.955 mmol), 485.1 mg *p*-chloranil (1.973 mmol, 1.0 eq.), and 10.0 mL anhydrous ethanol. The dark green mixture was stirred overnight for 21 h, filtered, and washed with minimal cold ethanol and rt acetone. The solid was redissolved fully in minimal methanol (~200 mL), stirred, filtered, and evaporated to dryness. The title compound was isolated (114.6 mg, 0.1717 mmol, 8.783%) as dark teal solid. ^{1}H NMR (DMSO-d^{6}, 500 MHz; δ /ppm): 13.68 (s, br), 7.88 (dd, 2H, *J*=3 and 6 Hz), 7.72 (dd, 4H, *J*=3 and 6 Hz), 7.61 (dd, 3H, *J*=3 and 6 Hz), 7.49 (1H, d, *J*=8 Hz), 7.40 (1H, d, *J*=8 Hz), 7.33 (4H, dd, *J*=3 and 6 Hz), 7.09 (t, 1H, *J*=8 Hz), 6.94 (t, 1H, *J*=8 Hz). ^{13}C{^{1}H} NMR (DMSO-d^{6}, 125.8 MHz; δ /ppm; DEPT-135 phases): 177.95x, 165.99x, 151.10x, 147.62x, 146.80x, 145.44x, 144.57x, 140.01x, 136.66x, 135.87x, 135.50x, 132.43x, 131.91x, 131.71x, 126.17↑, 124.54↑, 124.40↑, 124.02↑, 121.20x, 117.03↑, 116.05↑, 114.40↑, 112.54↑, 102.72x, 62.51x. UV-Vis-NIR (λ_{max} /nm, ε /L·mol^{-1}·cm^{-1}): 321 (31000), 430sh, 712 (14600). HRMS (ESI+): calc. [M+H^{+}]: 667.11590; found: 667.11560. Mp: >350 °C. FT-IR (ν /cm^{-1}): 517s, 601m, 747m, 905m,

1060m, 1160m, 1226sh, 1371w, 1458w, 1747s (C=O), 2123w, 2362s, 2869sh, 2978s, 3514s,br (N-H).

2.6.3 Computational Methods

All calculations were conducted using ORCA 4.0.1.2 software[103] on Compute Canada clusters, with tight self-consistent field convergence thresholds and tight geometry optimization convergence thresholds. Calculations use B3LYP,[104,105] CAM-B3LYP,[106] PBE,[107] PBE0,[108] or M06-L[109] functionals, def2-TZVP[110] basis set, def2/J[111] auxiliary basis set, RIJCOSX[112] approximation, and D3BJ[113] corrections. CPCM[114] models are used for calculations using methanol parameters.

Chapter 3 *N*-Methylated Bis-benzimidazole dyes

3.1 Introduction

In addition to modifications made at *meso* position explained in the last chapter, another modification to the bis-benzimidazole scaffold is alkylation at the nitrogen atoms. The methylation is beneficial in its ability to prevent unwanted reactions with the chemically labile benzimidazole N-H and provide an alternative strategy that, as illustrated in Scheme 3.2, avoids handling an unstable, electron-poor precursor, as is the case for many BOIDPY compounds.[47,88] Conducting the methylation after boron chelation also would be prone to the limitation of the stability of the boron complex and unwanted reactions involving the labile BF_2 moiety under those conditions.

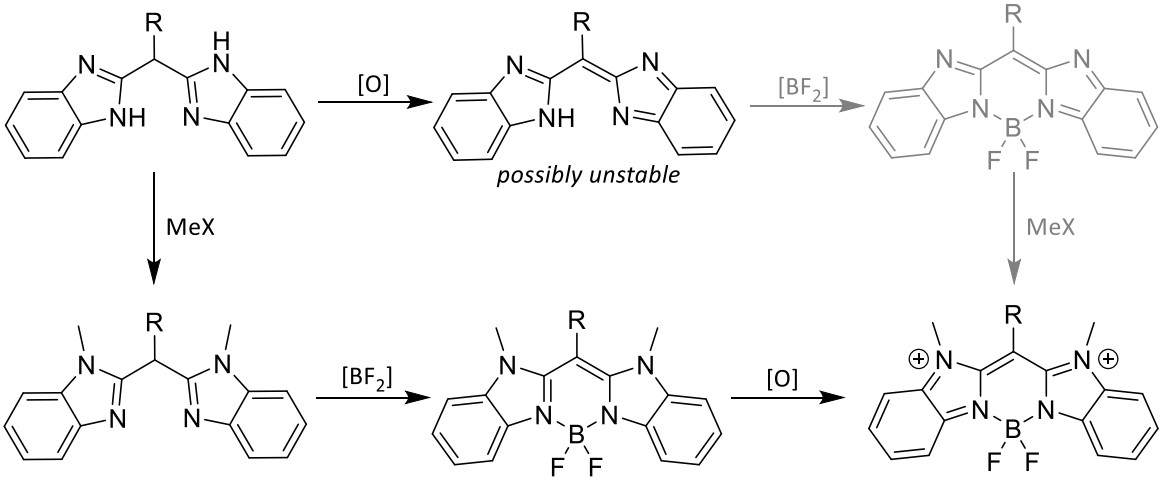

Scheme 11. Roadmap to a fully-conjugated chromophore allowed by N-methylation.

Boron chelation of a mono-anionic ligand is a preferred binding mode for boron and literature precedence shows homogeneity for its experimental conditions. This work has been pioneered by reported methods[115] (Scheme 12) and used to make boron

complex of 1,3-diketimines, where the C3N2 binding motif (highlighted) is similar to that of the proposed bis-benzimidazole ligands. The use of trifluoro diethyl etherate and a medium-strength base, like triethylamine or more commonly Hünig's base (DIPEA), is universal among the published literature[40,88,116–118] of boron complex syntheses.

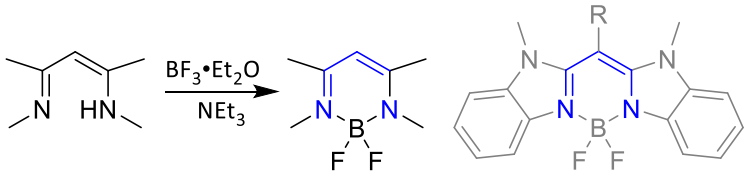

Scheme 12. Boron complex synthesis of 1,3-diketimine, with C3N2 bonding motif highlighted.

Experimentally, the alkylation needs to be selective to keep the pocket available for boron coordination (Scheme 13), requiring design and careful stoichiometric control.

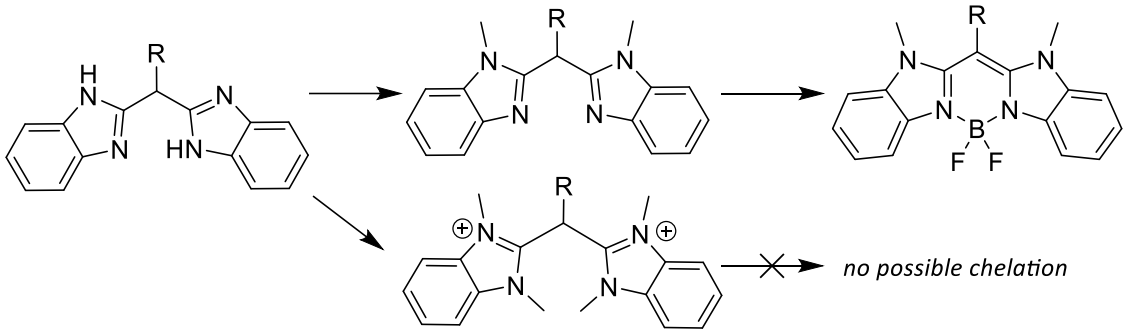

Scheme 13. Designing the synthesis of N-methylated bis-benzimidazole boron complex.

Synthetic strategies of *N*-substituted benzimidazoles are rich in literature precedent. A common method is to synthesize the benzimidazole with N-substituted *o*-phenylenediamine, as demonstrated by Liu and colleagues[119] in 2019 (Scheme 14) among other examples[120,121]. The price of the mono-substituted phenylenediamine (8–10 times higher than unsubstituted) and particular lower yields hinders applicability of this method.

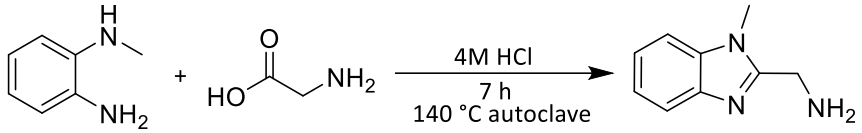

Scheme 14. Synthesis of N-methylated benzimidazole reported by Liu and colleagues.

The direct methylation of benzimidazole compounds using an electrophilic methyl source is comparatively more popular. Early reported examples, like the earliest one by Quast and Schmitt[122] in 1968 showed that the methylation of benzimidazole compounds can proceed with very mild conditions. Dubey and colleagues[123] in 2000 confirmed this conclusion with a number of alkyl groups under similar conditions.

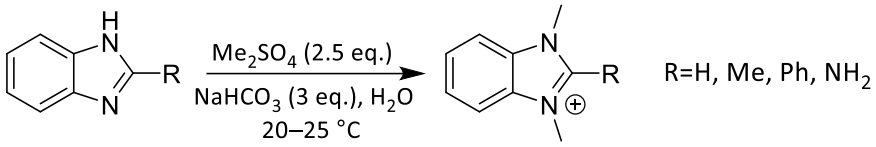

Scheme 15. Methylation of benzimidazole reported by Quast and Schmitt.

Selective methylation of benzimidazole compounds similarly requires mild conditions. In 2008, Chen and colleagues[124] reported mono-alkylation of benzimidazole using butyl bromide at 30–40 °C, which are comparatively slightly elevated due to solubility. Zhou and colleagues in 2011 reported the first mono-methylation of benzimidazole compounds using sodium hydride as base and THF as solvent at 0 °C. In 2003, Stibrany and colleagues[125] reported one of the few direct alkylation of bis-benzimidazole compounds, using DMSO or THF as solvent and excess NaH (Scheme 16, **3.1** as an example) at room temperature.

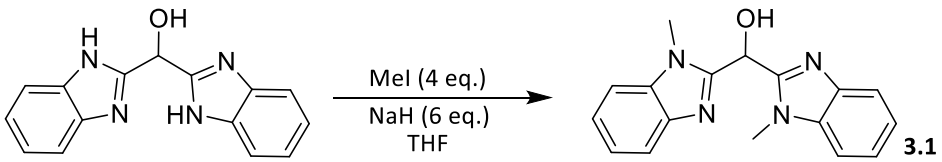

Scheme 16. Methylation of 3.1 reported by Stibrany and colleagues.

Reported examples of the *N*-substituted ligands involves transition metal complexes and main-group compounds, but notably without any boron chelates. The first attempted at the metal coordination of any N-methylated bis-benzimidazole ligand like **3.2** was made using manganese(II) acetate, though led to an oxidative dimerization, and reported by Bradamante and colleagues[126] in 1996. The first successful metal complex syntheses were by Abbotto and colleagues[127] in 1998, where Zn, Cu, Co complexes that each carries two bis-benzimidazole ligands were reported, and the corresponding mono-ligand Zn, Cu, Ni, and Co complexes later[128] in 2002.

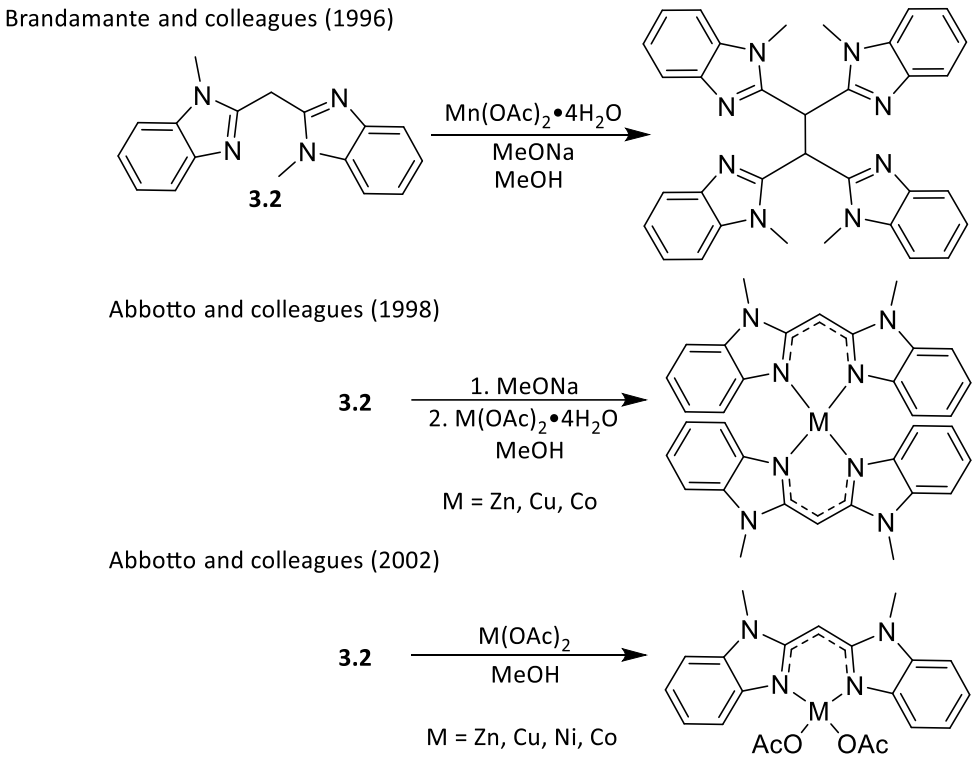

Scheme 17. Precedented attempts to synthesize transition metal complexes of 3.2.

In 2003, Stibrany and colleagues[125] reported the mono-ligand Cu complex (**3.3**) using a *meso*-substituted bis-imidazole ligand among others and showed that the complexes are good homopolymerization catalysts for *tert*-butyl acrylate. Main group complexes of N-substituted bis-benzimidazole ligands was first reported in 2017 by

Dauer and colleagues[120] where Al and Li complexes, **3.4** and **3.5**, respectively, were synthesized under rigorous air-free conditions.

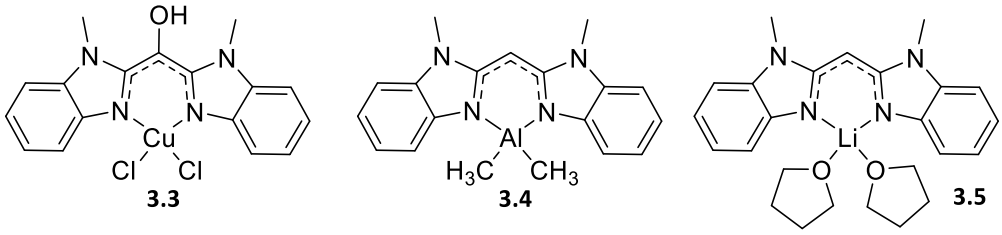

3.2 Synthesis of N-substituted Ligand

The synthetic procedure used is modified from that of Stibrany and colleagues.[125] *N*-methyl bis(benzimidazolyl)methane **3.6** was synthesized from its corresponding non-substituted parent compound **2.6b** in good yields. This is the first reported synthesis of **3.6**, and the product was characterized with NMR spectroscopy.

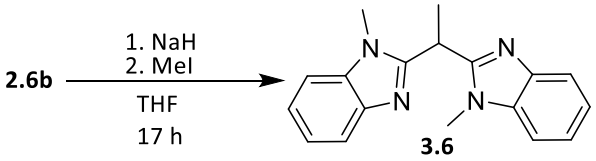

Scheme 18. Synthesis of 3.6

The ^{1}H NMR of **3.6** (Figure 17) showed heavily downfield-shifted methyl groups at 3.65 ppm, in line with reported examples of N-substituted methyl groups on heterocycles. Differ to the 4H-4H integration patterns of the parent compound **2.6b**, a 2H-6H pattern was showed. The 2H multiplet at 7.78 ppm correspond to the aromatic hydrogens closest to the substituted nitrogen atoms, and the shifts can be explained by the significant alternation of electronic environment by the methyl substituent. These interpretations can be confirmed by the literature values of similarly substituted benzimidazole[129] and bis-benzimidazole[125] compounds.

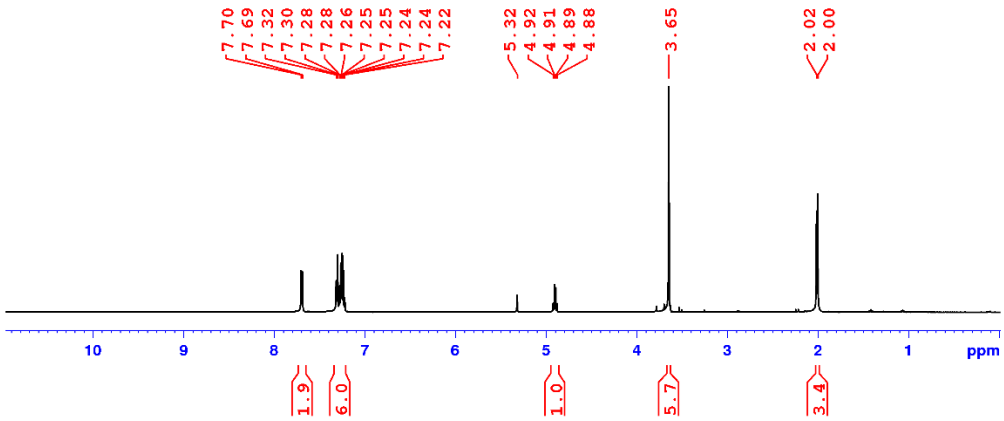

Figure 17. ^{1}H NMR spectrum of 3.6 in CD_2Cl_2 at 500 MHz.

^{13}C NMR spectra confirmed the structural assignment of **3.6**. The quaternary carbons that disappears on DEPT-135, namely the three peaks in 135–155 ppm, corresponding to the three quaternary aromatic carbons of benzimidazole. The four other aromatic peaks are all present and in the expected chemical shift range. NOE applied during acquisition of ^{13}C NMR spectra dictates that the peak height linearly correlates with the number of protons, hence the peak at 34 ppm was assigned to the carbon in between benzimidazole units that attached to only one proton. The 30 ppm peak has a chemical shift correlate to electronic-withdrawing environment, hence assigned to the methyl groups substituted to the nitrogen atoms. The 17 ppm peak is assigned to the methyl group submitted to the methylene bridge. Similar to the ^{1}H NMR spectrum, the ^{13}C spectrum (Figure 18) shows that two benzimidazole units are chemically equivalent.

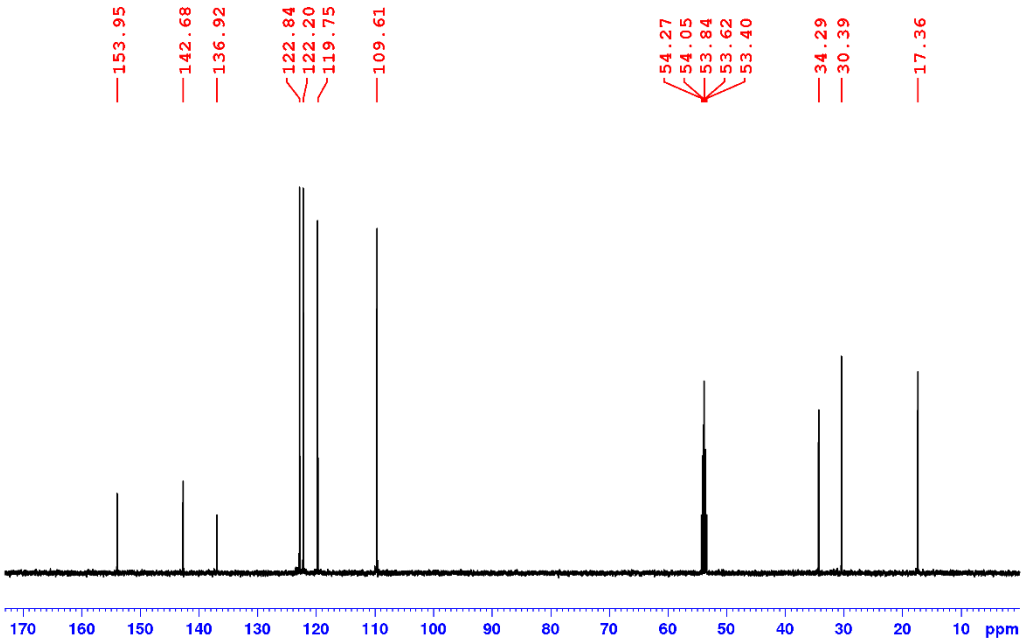

Figure 18. ^{13}C NMR spectrum of 3.6 at 125.8 MHz in CD_2Cl_2.

3.3 Attempted Synthesis of Boron Chelate

The coordination of difluoroborate moiety was attempted multiple times according to literature precedent for BODIPY compounds. Those attempts follow literature procedures[88,118] of boron chelation using stable ligands. Under irradiance of near-UV light, the crude compound showed bright, purple-coloured fluorescence (Figure 19). The compound is not stable on silica, though attempts to purify by filtration on alumina has made sufficient progress to obtain informative spectra.

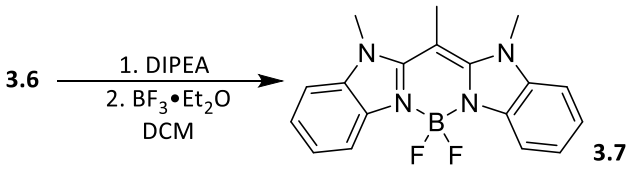

Scheme 19. Synthesis of 3.7

Figure 19. A DCM solution of Crude 3.7 irradiated with near-UV in darkness.

The proton-decoupled ^{11}B and ^{19}F NMR spectra (Figure 20 and 21, respectively) gave promising signs of the successful addition. The ^{11}B spectrum showed a clear triplet against the broad baseline peak caused by borate glass, whose coupling constant (J = 29.3 Hz) matches exactly to the quartet observed in the ^{19}F NMR spectrum. The multiplicities of both spectra agrees with those expected for a difluoroborate moiety, considering the number of fluoride nuclei for the 1:2:1 triplet for the boron spectrum and nuclei spin of ^{11}B (I = $^{5}/_{2}$) for the 1:1:1:1 quartet of the fluorine spectrum. Those spectra also differ significantly from the singlets on the spectra of highly symmetrical starting materials and by-products like $BF_3{\cdot}Et_2O$[130] or BF_4^- anion (Appendix III–12). The chemical shifts are also in the range of those reported[117] for BODIPY compounds.

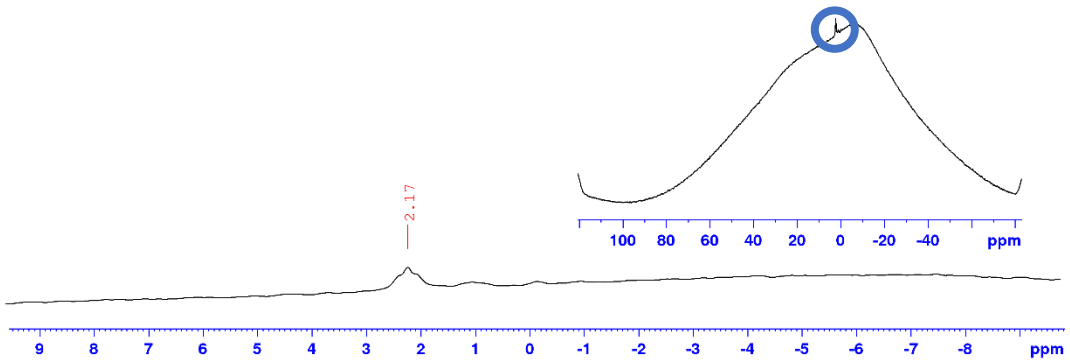

Figure 20. $^{11}B\{^1H\}$ NMR spectrum of crude 3.7 in $CDCl_3$ at 160.5 MHz, focused on main peak. Full spectrum showed in inset.

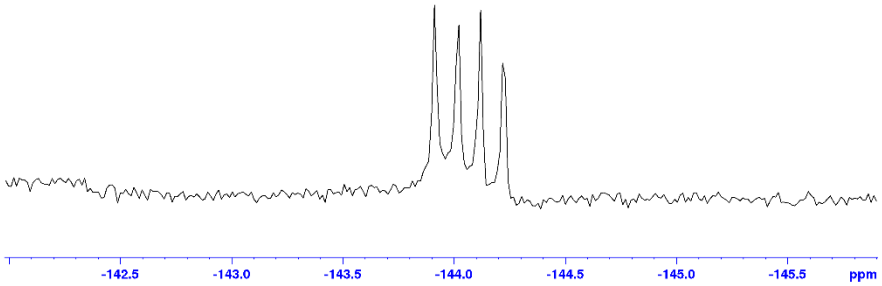

Figure 21. $^{19}F\{^1H\}$ NMR spectrum of crude 3.7 in $CDCl_3$ at 282.5 MHz, focused on main peak.

The ^1H NMR spectrum of crude **3.7** (Figure 22) showed significant changes relative to the spectrum ligand **3.6**. The aromatic peaks showed a doublet-triplet-triplet-doublet pattern that deviates significantly from that of **3.6**, showing the electronic environment of the benzimidazoles have been significantly changed, adding the credibility of successful boron chelation. In addition, the 1H quartet disappears, while the 3H doublet changed to a singlet; both are evidence of a successful deprotonation at the methylene bridge. Attempts to further purify the compound by chromatography or recrystallization consistently led to decomposition of the compound.

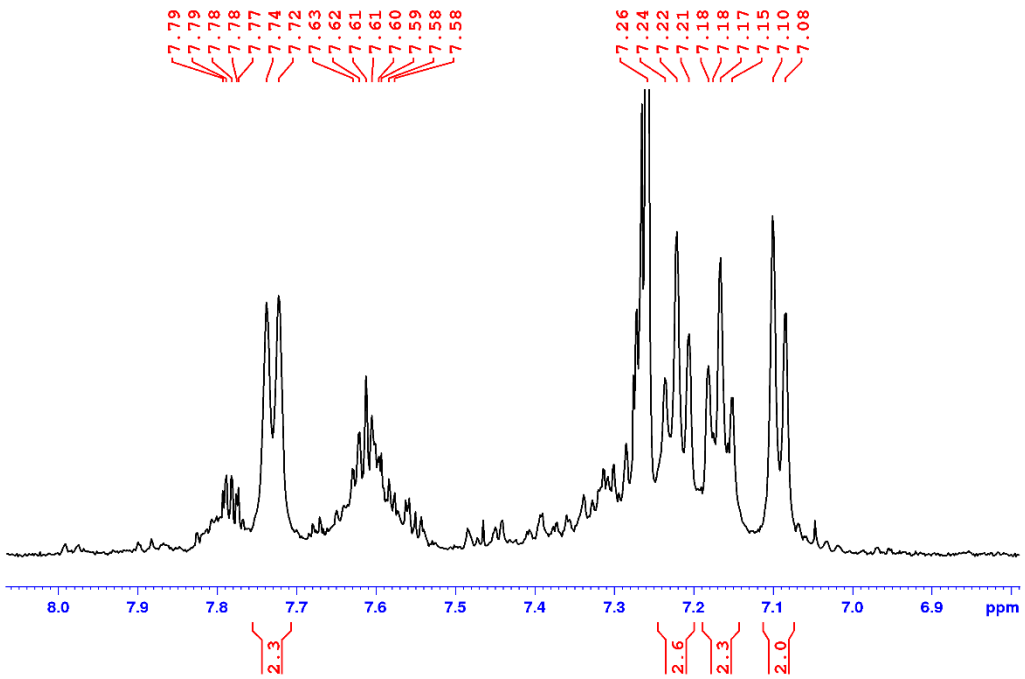

Figure 22. Aromatic region of the ^{1}H NMR spectrum of crude 2.13 in $CDCl_3$ at 500 MHz.

3.4 Computational Studies of Boron Chelate

Computational studies showed that neutral boron chelates only absorbs in the visible region while its the oxidized, positively charged derivatives are predicted to be NIR-absorbing dye. TDDFT calculations of **3.7**, though showed fully conjugated FMOs (Fig. 23), showing a blue-absorbing spectrum with the most intense transition at 354 nm.

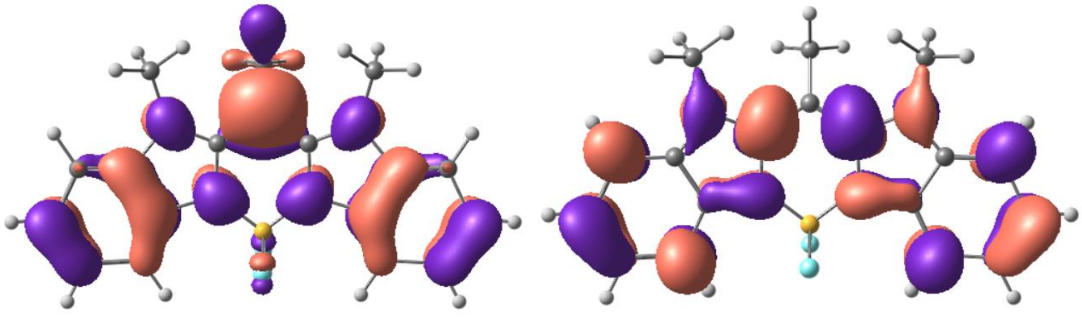

Figure 23. HOMO (left) and LUMO (right) of 3.7 using B3LYP functional. Contour level at 0.03.

Similarly using B3LYP, the oxidized species **3.8** showed redshifted intense transition at 547 nm, with additional transitions predicted in the NIR at 799 and 838 nm.

Comparing its FMOs (Figure 24) to those of **3.7** showed an inverted pattern, proving the oxidized species showed similar electronic structure to its precursor but a narrowed HOMO-LUMO gap, allowing lower-energy transitions predicted.

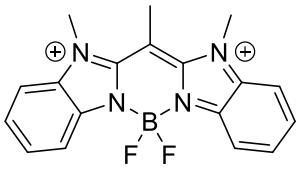

3.8

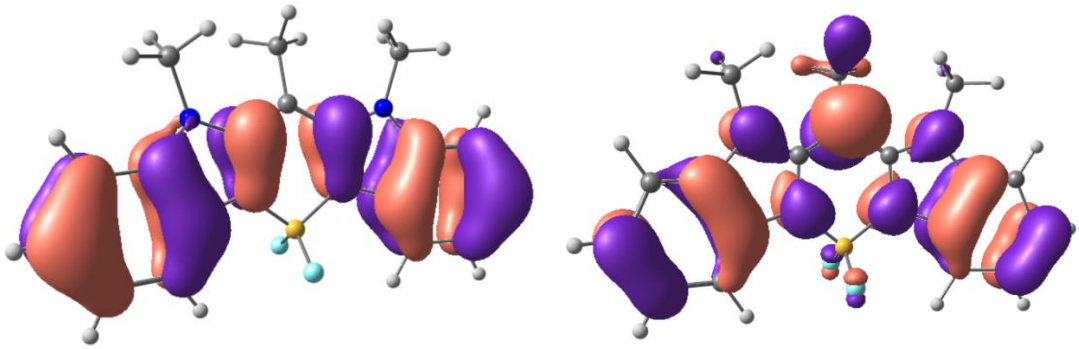

Figure 24. HOMO (left) and LUMO (right) of 3.8 using B3LYP. Contour level 0.03.

Computational studies on derivatives **3.9** and **3.10** showed altered transitions comparing to that of **3.8** and in the case of **3.10**, an intense transition well in the NIR region. Unlike *meso*-methyl **3.8** where the most intense transition is primarily HOMO-LUMO in nature (76.2%), the *meso*-phenyl **3.9** has the intense transitions at 587.7 and 545.5 nm. Both transitions are drastically different in nature comparing to that of **3.8**: the donor orbital responsible to the 587.7 nm transition is HOMO-3 rather than HOMO, an orbital, while the 545.5 nm transition is mainly based on the HOMO-LUMO transition (65.8%) but have mixed contribution from all other occupied FMOs. The *meso*-triazole substituted **3.10** showed a similar trend with its predicted intense transitions (Figure 25) at 1109 and 1019 nm corresponding primarily to HOMO-1 to LUMO (87.1%) and HOMO to LUMO transitions (84.8%), respectively. The occupied FMOs are mainly localized in

the *meso*-substituent, while the LUMO delocalized throughout the molecule, illustrating a push-pull system that could explain the low-energy transitions. The significant differences in the nature of transitions, mainly the mixed contributions from occupied FMOs other than HOMO, also showed that the oxidized bis-benzimidazole boron species are very prone to substitution effects, especially for substituents on the *meso*-position.

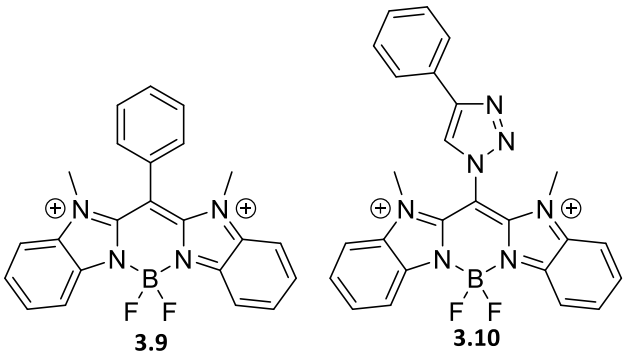

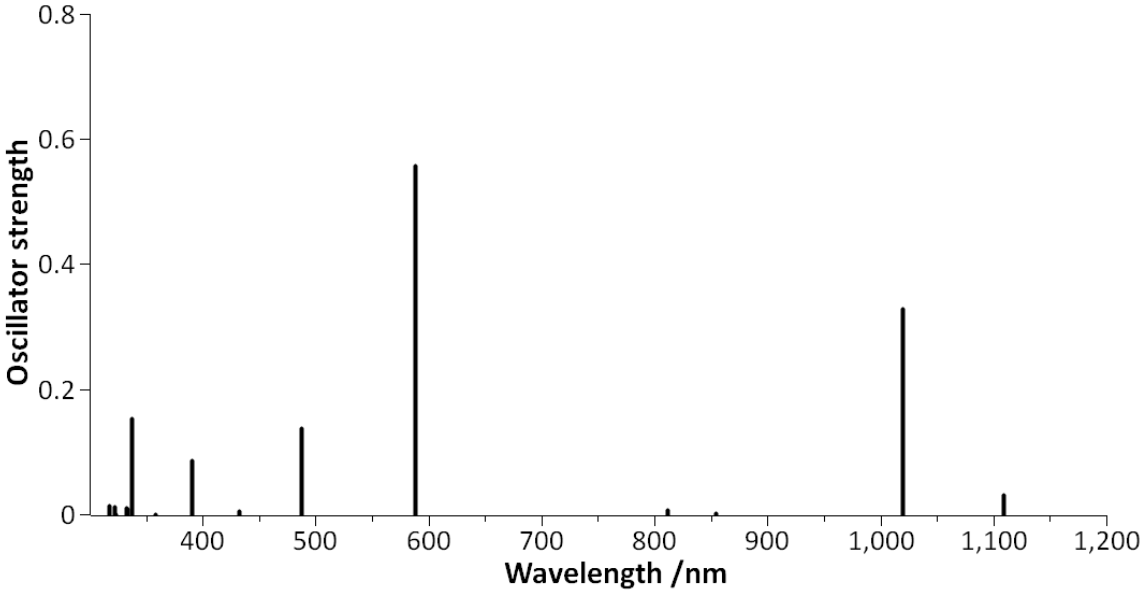

Figure 25. TDDFT Calculated transitions of 3.10.

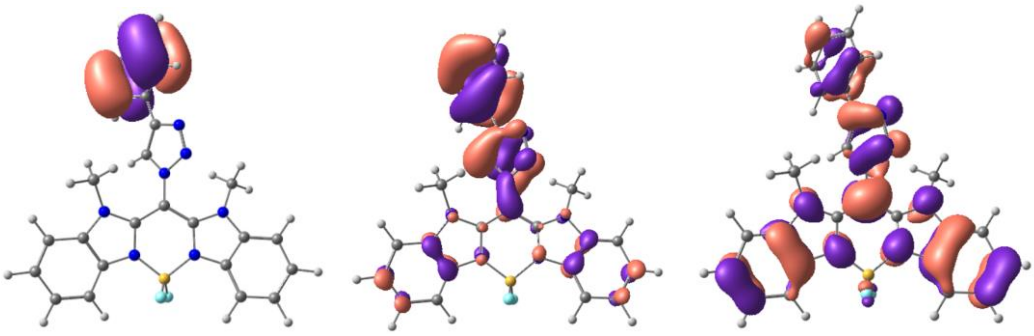

Figure 26. HOMO-1 (left), HOMO (centre), and LUMO (right) of 3.10 using B3LYP. Contour level at 0.03.

Comparing energy levels of the FMOs further shows the effect of mixed FMO contributions in transition energies. As illustrated in Figure 27, despite showing redshift transition wavelengths and a lowering of FMO energies from **3.8** to **3.10**, the HOMO-LUMO gap in fact widens, proving that the extension of the π system through *meso*-substituents principally alters the nature of transitions, matching those conclusions that are based on orbital analyses.

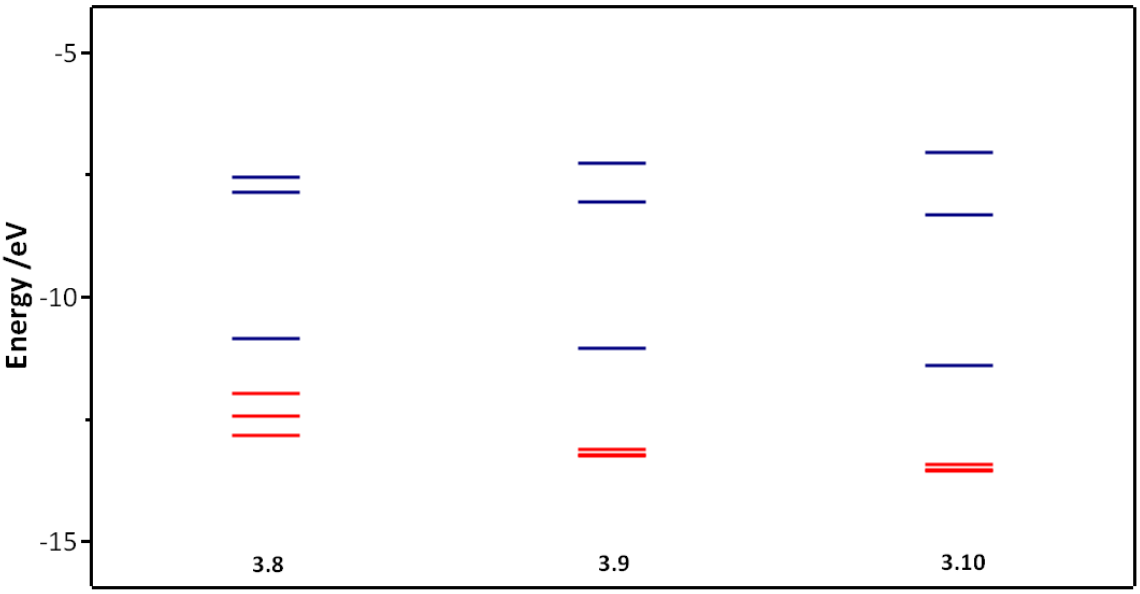

Figure 27. First three occupied (red) and unoccupied (blue) FMOs of 3.8, 3.9, and 3.10.

3.5 Summary

N-substituted bis(benzimidazolyl)methane compound **3.6** was synthesized with good yields following modified literature methods. Full characterizations of **3.6** using NMR spectroscopy indicates the successful synthesis.

Characterizations of crude reaction mixtures showed that difluoroborate chelate **3.7** has been successful, and the boron chelate is highly likely to be fluorescent as expected. Computational studies showed that the boron chelates and derivatives with different meso-substituents show redshifted, intense transitions, and in the case of **3.10**, well in the NIR region at approximately 1100 nm. As predicted, the bis-benzimidazole moiety is sensitive to substitutions and are capable of producing NIR dyes.

3.6 Experimental

3.6.1 Materials and General Procedure

Reagents and solvents were purchased from commercial sources and used without purification if not otherwise noted. Inert experiments were conducted using normal Schlenk line techniques. NMR experiments were conducted at 300 K (unless otherwise noted) on Bruker AV300 (300 MHz) / NEO500 (500 MHz) NMR spectrometers and locked using the deuterium signals of the respective solvents. ^{1}H / ^{13}C NMR spectra were manually calibrated according to literature values of residue solvents[97] (ppm): CD_2Cl_2, 5.32 / 53.84; $CDCl_3$, 7.26 / 77.16.

THF and DIPEA were further purified following reported methods[131].

3.6.2 Synthetic details

1,1-bis(1H-1-methylbenzimidazol-2-yl)ethane (**3.6**)

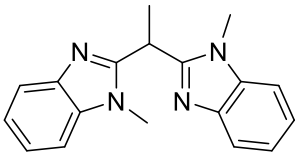

A 250 mL 3-neck round bottom flask was charged with a stir bar, oven dried for 2 h, and cooled to rt under N_2. To the flask, 189 mg **2.6b** (0.720 mmol) and 15 mL dry THF (dried over Na/benzophenone and stored over 4Å molecular sieves) was added. After stirring the mixture for several minutes under N_2, 165.9 mg of NaH (60% dispersion in mineral oil; 4.15 mmol, 5.7 eq.) was added to the slurry. After the rapid gas generation stops, the mixture was stirred for another 30 min under N_2, where 5.8 mL of a 0.25M MeI solution (1.45 mmol, 2.0 eq.) in THF was added dropwise using an oven-dried addition funnel. The mixture was then stirred overnight under N_2 for 19 h and quenched using 20 mL sat. $Na_2SO_{4(aq)}$ solution. After the in vacuo removal of THF, the crude product was extracted with DCM (3×20 mL), dried by Na_2SO_4, filtered, evaporated to an oil, and dried in vacuo. After purified by column chromatography (SiO_2, 1:3 hexanes:EtOAc, R_f≈0.3), the title compound was isolated as a white solid (67.3 mg, 0.232 mmol, 32.2% yield). ^{1}H NMR (CD_2Cl_2, 500 MHz; δ /ppm): 7.70 (d, J=7 Hz, 2H), 7.27 (m, 6H) 4.90 (q, J=7 Hz, 1H), 3.64 (s, 6H), 2.01 (d, J=7 Hz, 3H). ^{13}C{^{1}H} NMR (CD_2Cl_2, 126 MHz; DEPT-135 phase indicated; δ /ppm): 154.0x, 142.7x, 136.9x, 122.8↑, 122.2↑, 119.8↑, 109.6↑, 34.3↑, 30.4↑, 17.4↑.

1,1-bis(1H-1-methylbenzimidazol-2-yl)ethenyl difluoroborate (**3.7**)

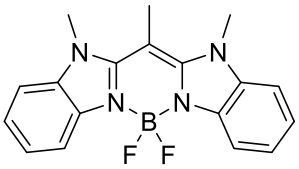

A 100 mL round bottom flask was charged with a stir bar oven dried and cooled under N_2. 29.7 mg (0.102 mmol) 3.6 and 4 mL DCM (stored under molecular sieves) was added to the flask and stirred. To the mixture, 0.11 mL (0.632 mmol, 6.17 eq.) of distilled DIPEA was added using a 1 mL micro-syringe and the resulting colourless mixture was stirred for 30 min, at which point 0.13 mL (1.05 mmol, 10.2 eq.) of $BF_3{\cdot}Et_2O$ was added using a 1 mL micro-syringe. The mixture turns orange upon the addition with considerable amount of fuming. The mixture was then stirred overnight under N_2. The mixture was then washed with saturated $NaHCO_{3(aq)}$ solution (3 × 20 mL) and the organic contents was extracted using DCM (3 × 20 mL). The organic layers was dried over Na_2SO_4, filtered, and evaporated to dryness. The solid was then redissolved in minimal DCM and filtered through a thick layer of neutral, Brockmann level I (deactivated) alumina. The resulting solution was evaporated to dryness, on which the reported crude solid was obtained as a colourless solid. ^{1}H NMR ($CDCl_3$, 500 MHz; δ /ppm): 7.73 (d, *J*=7 Hz, 2H), 7.22 (t, *J*=7 Hz, 2H), 7.17 (t, *J*=7 Hz, 2H), 7.09 (d, *J*=7 Hz, 2H), 3.80 (s, 6H), 2.53 (s, 3H). ^{11}B{^{1}H} NMR (CDCl3, 160.5 MHz; δ /ppm): 2.17 (t, *J*=29.3 Hz). ^{19}F{^{1}H} NMR ($CDCl_3$, 282.5 MHz; δ /ppm): -144.1 (q, *J*=29.3 Hz).

3.6.3 Computational Parameters

All calculations were conducted using ORCA 4.0.1.2 software[103] on Compute Canada clusters, with tight self-consistent field convergence thresholds and tight geometry optimization convergence thresholds. Calculations use B3LYP,[104,105] functional, def2-TZVP[110] basis set, def2/J[111] auxiliary basis set, RIJCOSX[112] approximation, and D3BJ[113] corrections.

Chapter 4 Concluding remarks

The goal of this thesis is to present a viable path to bis-benzimidazole-based NIR dyes, and through experimental and computational methods, this thesis indeed presented NIR-absorbing benzimidazole dyes or those that are predicted to be NIR absorbing and with a clear synthetic pathway towards it.

Reported in Chapter 2, a bis-benzimidazole-based NIR dye **2.14** was isolated and extensively studied. Its exotic connectivity and molecular structure lead to a compelling electronic structure that allows low-energy NIR absorbing transitions, as indicated by experimental and computational evidence presented in that Chapter. Its core chromophore consists of a combination of quinone and benzimidazole moieties, and such combination has no literature precedent. Computational studies on it showed that the core itself is red-absorbing, proving that it could be a feasible platform to a number of otherwise substituted NIR dyes.

Compound **2.14** presents possibilities as a ligand for coordination of metal or non-metal elements, whose preliminary progress was also reported in this thesis. As demonstrated by Scheme 20, **2.14** has three coordination pockets. This feature makes coordination of metal and non-metal elements strategically challenging but opens up opportunities for selective coordination based on their preferred ligand type and coordinating atom, allowing a possible tri-nuclei complex with all different kinds of elements that are structurally and electronically connected.

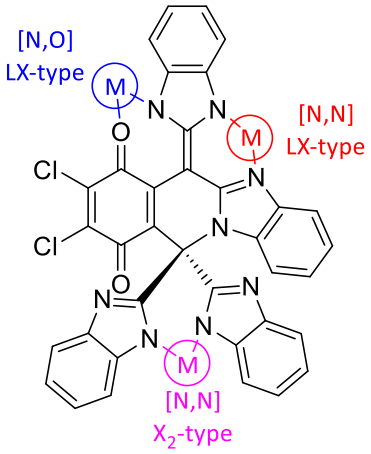

Scheme 20. Possible coordination pockets of 2.14 and its complexes.

There is a feasible synthetic pathway of the core chromophore of **2.14** that exploits the very procedure that surprisingly afforded **2.14**. The intermediate **4.1** can be straightforwardly synthesized based on the literature precedents of benzimidazole reactions reported in this thesis, and from it **4.2** could be synthesized using the **2.14** synthetic procedure. Through multiple steps involving a potentially challenging C-C formation, the CH_2-linked core chromophore could be synthesized. Intermediate **4.2** also can be a precursor to the BF_2-linked derivative and would require reported conditions[132] for making [C,N]-coordinated boron complexes. To bring back the unique chlorinated quinone an electrophilic Cl source would be required to react with the boron-rich intermediate, but such intermediate can also lead to vast number of other derivatives through hydroboration-like reactions. Those synthetic pathways are summarized in Scheme 21.

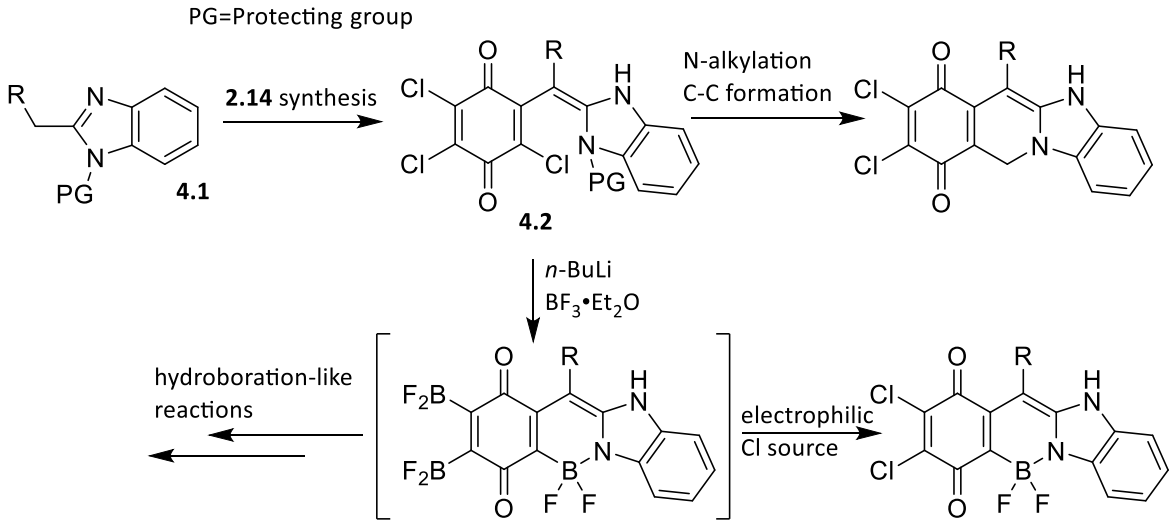

Scheme 21. Proposed synthetic pathway for the core chromophore and its derivatives.

Reported in Chapter 3, the synthesis of an unprecedented N-methyl bis(benzimidazolyl)methane compound **3.6** lead to an attempted boron coordination with promising signs. Although a pure boron chelate **3.7** was not isolated, all NMR evidence points to a successful coordination and the existence of a difluoroborate moiety. Computational studies showed that the oxidized, positively charged species have the capability of absorbing in the NIR. Those complexes would be synthesized through chemical means or studied through in tandem methods, such as spectroelectrochemical experiments and NMR or UV-Vis-NIR monitored flow chemistry.

Instead of a methylene-bridge, an aza-bridged bis-benzimidazole ligand **4.3** should behave similarly to the compound reported in this thesis.[133] Synthesis of such ligand and its boron chelates would enhance the understanding of the bis-benzimidazole system, as demonstrated by the mutualism observed for the development of BODIPY and aza-BODIPY compounds. There is a literature report of a

similar ligand **4.4** and that provides a lead in the synthesis of an aza-bridged bis-benzimidazole ligand.

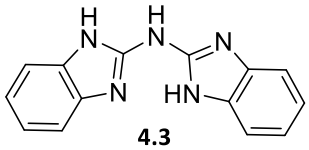

4.3

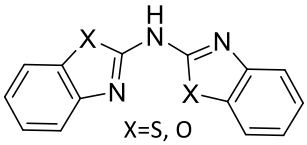

X=S, O

4.4

Through the experimental and computational work on **2.14** and **3.7**, the benzimidazole and bis-benzimidazole systems showed noteworthy potential towards uses as NIR dyes. Those work also extend to the proposed NIR-dyes like **2.18** and **3.10** that contain vibrant chromophores, potentially fluorescent, and may even have unrealized properties that extend the scope of these classes of compounds. Towards bis-benzimidazole NIR absorbing and emitting dyes, this thesis has presented a solid foundation for future work on this field in the years to come.

References

(1) Bruno, T. J.; Svoronos, P. D. N. *CRC Handbook of Fundamental Spectroscopic Correlation Charts*; CRC Press: Boca Raton, 2005. https://doi.org/10.1201/9780849332500.

(2) Ferreira, E. S. B.; Hulme, A. N.; McNab, H.; Quye, A. The Natural Constituents of Historical Textile Dyes. *Chem. Soc. Rev.* **2004**, *33* (6), 329–336. https://doi.org/10.1039/b305697j.

(3) Sharma, R. A.; Gescher, A. J.; Steward, W. P. Curcumin : The Story so Far. *Eur. J. Cancer* **2005**, *41* (13), 1955–1968. https://doi.org/10.1016/j.ejca.2005.05.009.

(4) Chen, X.; Mao, S. S. Titanium Dioxide Nanomaterials: Synthesis, Properties, Modifications and Applications. *Chem. Rev.* **2007**, *107* (7), 2891–2959. https://doi.org/10.1021/cr0500535.

(5) Bafana, A.; Devi, S. S.; Chakrabarti, T. Azo Dyes: Past, Present and the Future. *Environ. Rev.* **2011**, *19* (1), 350–370. https://doi.org/10.1139/a11-018.

(6) Maley, A. M.; Arbiser, J. L. Gentian Violet: A 19th Century Drug Re-Emerges in the 21st Century. *Exp. Dermatol.* **2013**, *22* (12), 775–780. https://doi.org/10.1111/exd.12257.

(7) Penthala, R.; Kumar, R. S.; Kim, H.; Heo, G.; Son, Y.-A. Synthesis, Generic Dyeing of Nindigo Derivatives on Unmodified Polypropylene; First Time Application in Dyeing Technology. *J. Nanosci. Nanotechnol.* **2019**, *19* (11), 7105–7111. https://doi.org/10.1166/jnn.2019.16643.

(8) Scotter, M. The Chemistry and Analysis of Annatto Food Colouring: A Review. *Food Addit. Contam. Part A* **2009**, *26* (8), 1123–1145. https://doi.org/10.1080/02652030902942873.

(9) Kobayashi, Y.; Abe, J. Real-Time Dynamic Hologram of a 3D Object with Fast Photochromic Molecules. *Adv. Opt. Mater.* **2016**, *4* (9), 1354–1357. https://doi.org/10.1002/adom.201600218.

(10) Irimia-Vladu, M.; Gåowacki, E. D.; Troshin, P. A.; Schwabegger, G.; Leonat, L.; Susarova, D. K.; Krystal, O.; Ullah, M.; Kanbur, Y.; Bodea, M. A.; Razumov, V. F.; Sitter, H.; Bauer, S.; Sariciftci, N. S. Indigo - A Natural Pigment for High Performance Ambipolar Organic Field Effect Transistors and Circuits. *Adv. Mater.* **2012**, *24* (3), 375–380. https://doi.org/10.1002/adma.201102619.

(11) Singh, R.; Jain, A.; Panwar, S.; Gupta, D.; Khare, S. K. Antimicrobial Activity of Some Natural Dyes. *Dyes Pigm.* **2005**, *66* (2), 99–102. https://doi.org/10.1016/j.dyepig.2004.09.005.

(12) Housecroft, C. E.; Sharpe, A. G. *Inorganic Chemistry*, 4th ed.; Pearson Education Limited: Harlow, England, 2012.

(13) Kaim, W. Concepts for Metal Complex Chromophores Absorbing in the near Infrared. *Coord. Chem. Rev.* **2011**, *255* (21–22), 2503–2513. https://doi.org/10.1016/j.ccr.2011.01.014.

(14) Ward, M. D. Transition-Metal Sensitised near-Infrared Luminescence from Lanthanides in d-f Heteronuclear Arrays. *Coord. Chem. Rev.* **2007**, *251* (13-14 SPEC. ISS.), 1663–1677. https://doi.org/10.1016/j.ccr.2006.10.005.

(15) Gao, D.; Hu, D.; Liu, X.; Zhang, X.; Yuan, Z.; Sheng, Z.; Zheng, H. Recent Advances in Conjugated Polymer Nanoparticles for NIR-II Imaging and Therapy. *ACS Appl. Polym. Mater.* **2020**, *2* (10), 4241–4257. https://doi.org/10.1021/acsapm.0c00679.

(16) Weissleder, R.; Ntziachristos, V. Shedding Light onto Live Molecular Targets. *Nat. Med.* **2003**, *9* (1), 123–128. https://doi.org/10.1038/nm0103-123.

(17) Frangioni, J. V. In Vivo Near-Infrared Fluorescence Imaging. *Curr. Opin. Chem. Biol.* **2003**, *7* (5), 626–634. https://doi.org/10.1016/j.cbpa.2003.08.007.

(18) Bonnett, R. Photosensitizers of the Porphyrin and Phthalocyanine Series for Photodynamic Therapy. *Chem. Soc. Rev.* **1995**, *24* (1), 19. https://doi.org/10.1039/cs9952400019.

(19) Urbani, M.; Grätzel, M.; Nazeeruddin, M. K.; Torres, T. Meso-Substituted Porphyrins for Dye-Sensitized Solar Cells. *Chem. Rev*. **2014**, *114*(24), 12330–12396. https://doi.org/10.1021/cr5001964.

(20) Yella, A.; Lee, H.-W.; Tsao, H. N.; Yi, C.; Chandiran, A. K.; Nazeeruddin, M. K.; Diau, E. W.-G.; Yeh, C.-Y.; Zakeeruddin, S. M.; Gratzel, M. Porphyrin-Sensitized Solar Cells with Cobalt (II/III)-Based Redox Electrolyte Exceed 12 Percent Efficiency. *Science* **2011**, *334* (6056), 629–634. https://doi.org/10.1126/science.1209688.

(21) Mathew, S.; Yella, A.; Gao, P.; Humphry-Baker, R.; Curchod, B. F. E.; Ashari-Astani, N.; Tavernelli, I.; Rothlisberger, U.; Nazeeruddin, M. K.; Grätzel, M. Dye-Sensitized Solar Cells with 13% Efficiency Achieved through the Molecular Engineering of Porphyrin Sensitizers. *Nat. Chem.* **2014**, *6* (3), 242–247. https://doi.org/10.1038/nchem.1861.

(22) Yao, L.; Zhang, S.; Wang, R.; Li, W.; Shen, F.; Yang, B.; Ma, Y. Highly Efficient Near-Infrared Organic Light-Emitting Diode Based on a Butterfly-Shaped Donor-Acceptor Chromophore with Strong Solid-State Fluorescence and a Large Proportion of Radiative Excitons. *Angew. Chem. Int. Ed.* **2014**, *53* (8), 2119–2123. https://doi.org/10.1002/anie.201308486.

(23) Wang, Y.; Kai, H.; Ishida, M.; Gokulnath, S.; Mori, S.; Murayama, T.; Muranaka, A.; Uchiyama, M.; Yasutake, Y.; Fukatsu, S.; Notsuka, Y.; Yamaoka, Y.; Hanafusa, M.; Yoshizawa, M.; Kim, G.; Kim, D.; Furuta, H. Synthesis of a Black Dye with Absorption Capabilities across the Visible-to-Near-Infrared Region: A MO-Mixing Approach via Heterometal Coordination of Expanded Porphyrinoid. *J. Am. Chem. Soc.* **2020**, *142* (14), 6807–6813. https://doi.org/10.1021/jacs.0c01824.

(24) Sarma, T.; Kim, G.; Sen, S.; Cha, W. Y.; Duan, Z.; Moore, M. D.; Lynch, V. M.; Zhang, Z.; Kim, D.; Sessler, J. L. Proton-Coupled Redox Switching in an Annulated π-Extended Core-Modified Octaphyrin. *J. Am. Chem. Soc.* **2018**, *140* (38), 12111–12119. https://doi.org/10.1021/jacs.8b06938.

(25) Suryani, O.; Higashino, Y.; Mulyana, J. Y.; Kaneko, M.; Hoshi, T.; Shigaki, K.; Kubo, Y. A Near-Infrared Organic Photosensitizer for Use in Dye-Sensitized Photoelectrochemical Water Splitting. *Chem. Commun.* **2017**, *53* (50), 6784–6787. https://doi.org/10.1039/c7cc02730c.

(26) Mishra, A.; Behera, R. K.; Behera, P. K.; Mishra, B. K.; Behera, G. B. Cyanines during the 1990s: A Review. *Chem. Rev.* **2000**, *100* (6), 1973–2011. https://doi.org/10.1021/cr990402t.

(27) Gayton, J.; Autry, S. A.; Meador, W.; Parkin, S. R.; Hill, G. A.; Hammer, N. I.; Delcamp, J. H. Indolizine-Cyanine Dyes: Near Infrared Emissive Cyanine Dyes with Increased Stokes Shifts. *J. Org. Chem.* **2019**, *84* (2), 687–697. https://doi.org/10.1021/acs.joc.8b02521.

(28) Lei, Z.; Sun, C.; Pei, P.; Wang, S.; Li, D.; Zhang, X.; Zhang, F. Stable, Wavelength-Tunable Fluorescent Dyes in the NIR-II Region for In Vivo High-Contrast Bioimaging and Multiplexed Biosensing. *Angew. Chem. Int. Ed.* **2019**, *58* (24), 8166–8171. https://doi.org/10.1002/anie.201904182.

(29) Li, D.; Schreiber, C. L.; Smith, B. D. Sterically Shielded Heptamethine Cyanine Dyes for Bioconjugation and High Performance Near-Infrared Fluorescence Imaging. *Angew. Chem. Int. Ed.* **2020**, *59* (29), 12154–12161. https://doi.org/10.1002/anie.202004449.

(30) Jacquemin, D. New Cyanine Dyes or Not? Theoretical Insights for Model Chains. *J. Phys. Chem. A* **2011**, *115* (11), 2442–2445. https://doi.org/10.1021/jp200940x.

(31) Song, F.; Peng, X.; Lu, E.; Zhang, R.; Chen, X.; Song, B. Syntheses, Spectral Properties and Photostabilities of Novel Water-Soluble near-Infrared Cyanine Dyes. *J. Photochem. Photobiol. A* **2004**, *168* (1–2), 53–57. https://doi.org/10.1016/j.jphotochem.2004.05.012.

(32) Rurack, K.; Spieles, M. Fluorescence Quantum Yields of a Series of Red and Near-Infrared Dyes Emitting at 600-1000 nm. *Anal. Chem.* **2011**, *83* (4), 1232–1242. https://doi.org/10.1021/ac101329h.

(33) Beija, M.; Afonso, C. A. M.; Martinho, J. M. G. Synthesis and Applications of Rhodamine Derivatives as Fluorescent Probes. *Chem. Soc. Rev.* **2009**, *38* (8), 2410–2433. https://doi.org/10.1039/b901612k.

(34) Koide, Y.; Urano, Y.; Hanaoka, K.; Terai, T.; Nagano, T. Development of an Si-Rhodamine-Based Far-Red to Near-Infrared Fluorescence Probe Selective for Hypochlorous Acid and Its Applications for Biological Imaging. *J. Am. Chem. Soc.* **2011**, *133* (15), 5680–5682. https://doi.org/10.1021/ja111470n.

(35) Koide, Y.; Kawaguchi, M.; Urano, Y.; Hanaoka, K.; Komatsu, T.; Abo, M.; Terai, T.; Nagano, T. A Reversible Near-Infrared Fluorescence Probe for Reactive Oxygen Species Based on Te-Rhodamine. *Chem. Commun.* **2012**, *48* (25), 3091–3093. https://doi.org/10.1039/c2cc18011a.

(36) Weissbecker, J.; Loas, A.; Gorun, S. M.; Schlettwein, D. Switching of the Rate-Limiting Step in the Electrochromic Reduction of Fluorinated Phthalocyanine Thin Films by Decreased Intermolecular Coupling. *Electrochim. Acta* **2015**, *157*, 232–244. https://doi.org/10.1016/j.electacta.2015.01.063.

(37) Weil, T.; Vosch, T.; Hofkens, J.; Peneva, K.; Müllen, K. The Rylene Colorant Family-Tailored Nanoemitters for Photonics Research and Applications. *Angew. Chem. Int. Ed.* **2010**, *49* (48), 9068–9093. https://doi.org/10.1002/anie.200902532.

(38) Beverina, L.; Salice, P. Squaraine Compounds: Tailored Design and Synthesis towards a Variety of Material Science Applications. *Eur. J. Org. Chem.* **2010**, No. 7,

1207–1225. https://doi.org/10.1002/ejoc.200901297.

(39) Treibs, A.; Kreuzer, F. -H. Difluorboryl-Komplexe von Di- Und Tripyrrylmethenen. *Justus Liebigs Ann. Chem.* **1968**, *718* (1), 208–223. https://doi.org/10.1002/jlac.19687180119.

(40) Schmitt, A.; Hinkeldey, B.; Wild, M.; Jung, G. Synthesis of the Core Compound of the BODIPY Dye Class: 4,4'-Difluoro-4-Bora-(3a,4a)-Diaza-s-Indacene. *J. Fluoresc.* **2009**, *19* (4), 755–758. https://doi.org/10.1007/s10895-008-0446-7.

(41) Yang, X.; Shi, N.; Bai, L.; Ni, Y.; Li, J.; Si, W.; Li, L.; Shao, J.; Huang, W.; Dong, X. Synthesis, Characterization and Fluorescence Imaging Property of BODIPY-DPP-Based Dyad/Triad. *Dyes Pigm.* **2018**, *157* (March), 396–404. https://doi.org/10.1016/j.dyepig.2018.04.054.

(42) Ni, Y.; Kannadorai, R. K.; Peng, J.; Yu, S. W. K.; Chang, Y. T.; Wu, J. Naphthalene-Fused BODIPY near-Infrared Dye as a Stable Contrast Agent for: In Vivo Photoacoustic Imaging. *Chem. Commun.* **2016**, *52* (77), 11504–11507. https://doi.org/10.1039/c6cc05126j.

(43) Qin, W.; Baruah, M.; Auweraer, M. Van Der; Schryver, F. C. De. Photophysical Properties of Borondipyrromethene Analogues in Solution. *J. Phys. Chem. A* **2005**, *109*, 7371–7384. https://doi.org/10.1021/jp052626n.

(44) Okujima, T.; Tomimori, Y.; Nakamura, J.; Yamada, H.; Uno, H.; Ono, N. Synthesis of π-Expanded BODIPYs and Their Fluorescent Properties in the Visible-near-Infrared Region. *Tetrahedron* **2010**, *66* (34), 6895–6900. https://doi.org/10.1016/j.tet.2010.06.045.

(45) Patra, A.; Patalag, L. J.; Jones, P. G.; Werz, D. B. Extended Benzene-Fused Oligo-BODIPYs: In Three Steps to a Series of Large, Arc-Shaped, Near Infrared Dyes. *Angew. Chem. Int. Ed.* **2020**, *60* (2), 747-752. https://doi.org/10.1002/anie.202012335.

(46) De Jong, F.; Feldt, M.; Feldt, J.; Harvey, J. N. Modelling Absorption and Emission of a: Meso -Aniline-BODIPY Based Dye with Molecular Mechanics. *Phys. Chem. Chem. Phys.* **2018**, *20* (21), 14537–14544. https://doi.org/10.1039/c8cp01877d.

(47) Loudet, A.; Burgess, K. BODIPY Dyes and Their Derivatives: Syntheses and Spectroscopic Properties. *Chem. Rev.* **2007**, *107* (11), 4891–4932. https://doi.org/10.1021/cr078381n.

(48) Wagner, R. W.; Lindsey, J. S. Boron-Dipyrromethene Dyes for Incorporation in Synthetic Multi-Pigment Light-Harvesting Arrays. *Pure Appl. Chem.* **1996**, *68* (7), 1373–1380. https://doi.org/10.1351/pac199668071373.

(49) Li, L.; Han, J.; Nguyen, B.; Burgess, K. Syntheses and Spectral Properties of Functionalized, Water-Soluble BODIPY Derivatives. *J. Org. Chem.* **2008**, *73* (5), 1963–1970. https://doi.org/10.1021/jo702463f.

(50) Nierth, A.; Kobitski, A. Y.; Ulrich Nienhaus, G.; Jäschke, A. Anthracene-Bodipy Dyads as Fluorescent Sensors for Biocatalytic Diels Alder Reactions. *J. Am. Chem. Soc.* **2010**, *132* (8), 2646–2654. https://doi.org/10.1021/ja9084397.

(51) Allik, T. H.; Hermes, R. E.; Sathyamoorthi, G.; Boyer, J. H. Spectroscopy and Laser Performance of New BF2 -Complex Dyes in Solution. In *Proceedings of SPIE 2115, Visible and UV Lasers*; Scheps, R., Ed.; 1994; Vol. 2115, p 240.

https://doi.org/10.1117/12.172742.
(52) McDonnell, S. O.; O'Shea, D. F. Near-Infrared Sensing Properties of Dimethlyamino-Substituted BF2-Azadipyrromethenes. *Org. Lett.* **2006**, *8* (16), 3493–3496. https://doi.org/10.1021/ol061171x.
(53) Loudet, A.; Bandichhor, R.; Wu, L.; Burgess, K. Functionalized BF2 Chelated Azadipyrromethene Dyes. *Tetrahedron* **2008**, *64* (17), 3642–3654. https://doi.org/10.1016/j.tet.2008.01.117.
(54) Gresser, R.; Hummert, M.; Hartmann, H.; Leo, K.; Riede, M. Synthesis and Characterization of Near-Infrared Absorbing Benzannulated Aza-BODIPY Dyes. *Chem. Eur. J.* **2011**, *17* (10), 2939–2947. https://doi.org/10.1002/chem.201002941.
(55) Shimizu, S. Aza-BODIPY Synthesis towards Vis/NIR Functional Chromophores Based on a Schiff Base Forming Reaction Protocol Using Lactams and Heteroaromatic Amines. *Chem. Commun.* **2019**, *55* (60), 8722–8743. https://doi.org/10.1039/c9cc03365c.
(56) Zhao, W.; Carreira, E. M. Conformationally Restricted Aza-Bodipy: A Highly Fluorescent, Stable, Near-Infrared-Absorbing Dye. *Angew. Chem. Int. Ed.* **2005**, *44* (11), 1677–1679. https://doi.org/10.1002/anie.200461868.
(57) Fan, G.; Yang, L.; Chen, Z. Water-Soluble BODIPY and Aza-BODIPY Dyes: Synthetic Progress and Applications. *Front. Chem. Sci. Eng.* **2014**, *8* (4), 405–417. https://doi.org/10.1007/s11705-014-1445-7.
(58) Coşkun, A.; Yılmaz, M. D.; Akkaya, E. U. Bis(2-Pyridyl)-Substituted Boratriazaindacene as an NIR-Emitting Chemosensor for Hg(II). *Org. Lett.* **2007**, *9* (4), 607–609. https://doi.org/10.1021/ol062867t.
(59) Frath, D.; Massue, J.; Ulrich, G.; Ziessel, R. Luminescent Materials: Locking π-Conjugated and Heterocyclic Ligands with Boron(III). *Angew. Chem. Int. Ed.* **2014**, *53* (9), 2290–2310. https://doi.org/10.1002/anie.201305554.
(60) Curiel, D.; Más-Montoya, M.; Usea, L.; Espinosa, A.; Orenes, R. A.; Molina, P. Indolocarbazole-Based Ligands for Ladder-Type Four-Coordinate Boron Complexes. *Org. Lett.* **2012**, *14* (13), 3360–3363. https://doi.org/10.1021/ol301339y.
(61) Nawn, G.; Oakley, S. R.; Majewski, M. B.; McDonald, R.; Patrick, B. O.; Hicks, R. G. Redox-Active, near-Infrared Dyes Based on 'Nindigo' (Indigo-N,N'-Diarylimine) Boron Chelate Complexes. *Chem. Sci.* **2013**, *4* (2), 612–621. https://doi.org/10.1039/C2SC21307A.
(62) Buguis, F. L.; Maar, R. R.; Staroverov, V. N.; Gilroy, J. B. Near-Infrared Boron Difluoride Formazanate Dyes. *Chem. Eur. J.* **2021**, *27* (8), 2854–2860. https://doi.org/10.1002/chem.202004793.
(63) Fischer, G. M.; Isomaki-Krondahl, M.; Gottker-Schnetmann, I.; Daltrozzo, E.; Zumbusch, A. Pyrrolopyrrole Cyanine Dyes: A New Class of near-Infrared Dyes and Fluorophores. *Chem. Eur. J.* **2009**, *15* (19), 4857–4864. https://doi.org/10.1002/chem.200801996.
(64) Li, D.; Zhang, H.; Wang, C.; Huang, S.; Guo, J.; Wang, Y. Construction of Full-Color-Tunable and Strongly Emissive Materials by Functionalizing a Boron-Chelate Four-

Ring-Fused π-Conjugated Core. *J. Mater. Chem.* **2012**, *22* (10), 4319–4328. https://doi.org/10.1039/C1JM14606H.

(65) Lee, J. E.; Choi, G. C.; Rim, B. O.; Kim, S. M.; Park, N. G.; Ha, Y. K.; Kim, Y. S. Theoretical Studies of Boron(III) Complexes for the New Blue Luminescent Material. *Mater. Sci. Eng. C* **2004**, *24* (1–2), 269–273. https://doi.org/10.1016/j.msec.2003.09.012.

(66) Ross, T. W.; Sathyamoorthi, G.; Boyer, J. H. Biimidazol-2-yl-BF2 Complexes. *Heteroat. Chem.* **1993**, *4* (6), 609–612. https://doi.org/10.1002/hc.520040614.

(67) Liu, Q. De; Mudadu, M. S.; Thummel, R.; Tao, Y.; Wang, S. From Blue to Red: Syntheses, Structures, Electronic, and Electroluminescent Properties of Tunable Luminescent N,N Chelate Boron Complexes. *Adv. Funct. Mater.* **2005**, *15* (1), 143–154. https://doi.org/10.1002/adfm.200400081.

(68) Benelhadj, K.; Massue, J.; Retailleau, P.; Ulrich, G.; Ziessel, R. 2-(2'-Hydroxyphenyl)Benzimidazole and 9,10-Phenanthroimidazole Chelates and Borate Complexes: Solution- and Solid-State Emitters. *Org. Lett.* **2013**, *15* (12), 2918–2921. https://doi.org/10.1021/ol400849a.

(69) Nishizeki, M.; Miura, N. Manufacture of Lithographic Plates, Photoimaging Materials Therefor, Radical Generation Therein, Photopolymerization Initiators Therefor. JP 2003206307, 2003.

(70) Ladenburg, A. Derivate von Diaminen. *Chem. Ber.* **1875**, *8*, 677. https://doi.org/10.1002/cber.187500801209.

(71) Phillips, M. A. CCCXVI1.-The Formation of 2-Substituted Benziminazoles. *J. Chem. Soc.* **1928**, 2393–2399. https://doi.org/10.1039/JR9280002393.

(72) Shriner, R. L.; Upson, R. W. Bis-Benzimidazoles from Dibasic Acids. *J. Am. Chem. Soc.* **1941**, *63* (8), 2277–2278. https://doi.org/10.1021/ja01853a506.

(73) Lane, E. S. 460. A Modified Benziminazole Synthesis. *J. Chem. Soc.* **1953**, 2238. https://doi.org/10.1039/jr9530002238.

(74) Vinot, N. Synthèse de Cyanométhyl-2 Benzimidazoles α-Substitués. Leur Ultilisation Possédant d'autres Fonctions. *Bull. Soc. Chim. Fr.* **1966**, No. 12, 3989–3993.

(75) Qian, Y.; Xu, G. 一种蓝紫光转光膜及其制备方法 (Blue Violet Light Conversion Film and Its Preparation Method). CN 108395555 A, 2018.

(76) Kattimani, P. P.; Kamble, R. R.; Meti, G. Y. Expedient Synthesis of Benzimidazoles Using Amides. *RSC Adv.* **2015**, *5* (37), 29447–29455. https://doi.org/10.1039/c5ra00021a.

(77) da Silva Miranda, F.; Menezes, F. G.; Vicente, J.; Bortoluzzi, A. J.; Zucco, C.; Neves, A.; Gonçalves, N. S. Bis-(1H-Benzimidazol-2-yl)-Methanone: New Preparation Method, Crystal Structure, Vibrational Spectroscopy and DFT Calculations. *J. Mol. Struct.* **2009**, *938* (1–3), 1–9. https://doi.org/10.1016/j.molstruc.2009.08.031.

(78) Algul, O.; Duran, N. Activity of Bisbenzimidazoles Derivatives to Staphylococcus Epidermidis. *Asian J. Chem.* **2007**, *19* (4), 3145–3151.

(79) Albers, A.; Demeshko, S.; Dechert, S.; Bill, E.; Bothe, E.; Meyer, F. The Complete Characterization of a Reduced Biomimetic [2 Fe-2 S] Cluster. *Angew. Chem. Int. Ed.*

2011, *50* (39), 9191–9194. https://doi.org/10.1002/anie.201100727.

(80) Efros, L. S.; Khromov-Borisov, N. V.; Davidenkov, L. R.; Nedel, M. M. Imidazole Derivatives. XIV. Oxidation of Benzimidazole and its Methyl Derivatives. *Zh. Obshch. Khim.* **1956**, *26*, 455–458.

(81) Sprecher, C. A.; Zuberbühler, A. D. A Model of Internal Monooxygenase Catalyzed Reactions: Copper-Catalyzed Autoxidation of Bis(1-Methylbenzimidazol-2-yl)Methane. *Angew. Chem. Int. Ed. Engl.* **1977**, *16* (3), 189–189. https://doi.org/10.1002/anie.197701891.

(82) Yao, H. C.; Li, M. M.; Yang, G. S.; Li, Z. J.; Zhu, Y. Ketonization of Methylene of Bis(Benzimidazol-2-Yl)Methane by Molecular Oxygen under the Catalysis of Cobalt(II) Ion. *Inorg. Chim. Acta* **2007**, *360* (14), 3959–3964. https://doi.org/10.1016/j.ica.2007.04.042.

(83) Yang, L.; Wang, F.; Sun, Z.; Kong, X.; Kong, Y. Sensitive and Selective Detection of Phosgene with a Bis-(1: H-Benzimidazol-2-Yl)-Based Turn-on Fluorescent Probe in the Solution and Gas Phase. *Anal. Methods* **2020**, *12* (24), 3123–3129. https://doi.org/10.1039/d0ay00404a.

(84) Pujar, M. A.; Bharamgoudar, T. D.; Sathyanarayana, D. N. Cobalt(II), Nickel(II) and Copper(II) Complexes of Bidentate Bibenzimidazoles. *Transition Met. Chem.* **1988**, *13* (6), 423–425. https://doi.org/10.1007/BF01043702.

(85) Albers, A.; Bayer, T.; Demeshko, S.; Dechert, S.; Meyer, F. A Functional Model for the Rieske Center: Full Characterization of a Biomimetic N-Ligated [2Fe-2S] Cluster in Different Protonation States. *Chem. Eur. J.* **2013**, *19* (31), 10101–10106. https://doi.org/10.1002/chem.201301760.

(86) Essassi, E. M.; Lamkadem, A.; Zniber, R. Recherches en Série Benzodiazepine-1,5: Synthèses des Ditriazolo-[4,3-a; 3,4-d]-Benzodiazepines-1,5. *Bull. Soc. Chim. Belg.* **2010**, *100* (3), 277–286. https://doi.org/10.1002/bscb.19911000313.

(87) Kürti, L.; Czakó, B. *Strategic Applications of Named Reactions in Organic Synthesis*; Academic Press, 2005.

(88) Groves, B. R.; Crawford, S. M.; Lundrigan, T.; Matta, C. F.; Sowlati-Hashjin, S.; Thompson, A. Synthesis and Characterisation of the Unsubstituted Dipyrrin and 4,4-Dichloro-4-Bora-3a,4a-Diaza-s-Indacene: Improved Synthesis and Functionalisation of the Simplest BODIPY Framework. *Chem. Commun.* **2013**, *49* (8), 816–818. https://doi.org/10.1039/c2cc37480c.

(89) Patiny, L.; Borel, A. ChemCalc: A Building Block for Tomorrow's Chemical Infrastructure. *J. Chem. Inf. Model.* **2013**, *53* (5), 1223–1228. https://doi.org/10.1021/ci300563h.

(90) Johnson, R. D. I. NIST Computational Chemistry Comparison and Benchmark Database, NIST Standard Reference Database Number 101 http://cccbdb.nist.gov/. https://doi.org/10.18434/T47C7Z.

(91) Neidlein, R.; Kramer, W.; Leidholdt, R. Zur Verwendbarkeit von 13C-Substituenteninkrementen Bei 1,4-Benzo- und 1,4-Naphthochinonen. *Helv. Chim. Acta* **1983**, *66* (7), 2285–2293. https://doi.org/10.1002/hlca.19830660740.

(92) Mardirossian, N.; Head-Gordon, M. Thirty Years of Density Functional Theory in Computational Chemistry: An Overview and Extensive Assessment of 200 Density

Functionals. *Mol. Phys.* **2017**, *115* (19), 2315–2372. https://doi.org/10.1080/00268976.2017.1333644.

(93) Huynh, M. T.; Anson, C. W.; Cavell, A. C.; Stahl, S. S.; Hammes-Schiffer, S. Quinone 1 e- and 2 e-/2 H+ Reduction Potentials: Identification and Analysis of Deviations from Systematic Scaling Relationships. *J. Am. Chem. Soc.* **2016**, *138* (49), 15903–15910. https://doi.org/10.1021/jacs.6b05797.

(94) Lynch, E. J.; Speelman, A. L.; Curry, B. A.; Murillo, C. S.; Gillmore, J. G. Expanding and Testing a Computational Method for Predicting the Ground State Reduction Potentials of Organic Molecules on the Basis of Empirical Correlation to Experiment. *J. Org. Chem.* **2012**, *77* (15), 6423–6430. https://doi.org/10.1021/jo300853k.

(95) Sakamoto, R.; Kusaka, S.; Kitagawa, Y.; Kishida, M. A.; Hayashi, M.; Takara, Y.; Tsuchiya, M.; Kakinuma, J.; Takeda, T.; Hirata, K.; Ogino, T.; Kawahara, K.; Yagi, T.; Ikehira, S.; Nakamura, T.; Isomura, M.; Toyama, M.; Ichikawa, S.; Okumura, M.; Nishihara, H. Fluorescent Azadipyrrinato Zinc(Ii) Complex: Hybridisation with a Dipyrrinato Ligand. *Dalton Trans.* **2012**, *41* (46), 14035–14037. https://doi.org/10.1039/c2dt32039h.

(96) Zatsikha, Y. V.; Shamova, L. I.; Blesener, T. S.; Kuzmin, I. A.; Germanov, Y. V.; Herbert, D. E.; Nemykin, V. N. Development of a Class of Easily Scalable, Electron-Deficient, Core-Extended Benzo-Fused Azadipyrromethene Derivatives ("MB-DIPY"). *J. Org. Chem.* **2019**, *84* (22), 14540–14557. https://doi.org/10.1021/acs.joc.9b02074.

(97) Fulmer, G. R.; Miller, A. J. M.; Sherden, N. H.; Gottlieb, H. E.; Nudelman, A.; Stoltz, B. M.; Bercaw, J. E.; Goldberg, K. I.; Gan, R.; Apiezon, H. NMR Chemical Shifts of Trace Impurities : Common Laboratory Solvents , Organics , and Gases in Deuterated Solvents Relevant to the Organometallic Chemist. *Organometallics* **2010**, *29* (9), 2176–2179. https://doi.org/10.1021/om100106e.

(98) Bower, V. E.; Bates, R. G. PH Values of the Clark and Lubs Buffer Solutions at 25 C. *J. Res. Natl. Bur. Stand.* **1955**, *55* (4), 197. https://doi.org/10.6028/jres.055.021.

(99) O'Reilly, J. E. Oxidation-Reduction Potential of the Ferro-Ferricyanide System in Buffer Solutions. *Biochim. Biophys. Acta, Bioenerg.* **1973**, *292* (3), 509–515. https://doi.org/10.1016/0005-2728(73)90001-7.

(100) Dolomanov, O. V.; Bourhis, L. J.; Gildea, R. J.; Howard, J. A. K.; Puschmann, H. OLEX2 : A Complete Structure Solution, Refinement and Analysis Program. *J. Appl. Crystallogr.* **2009**, *42* (2), 339–341. https://doi.org/10.1107/S0021889808042726.

(101) Sheldrick, G. M. SHELXT – Integrated Space-Group and Crystal-Structure Determination. *Acta Crystallogr. Sect. A Found. Adv.* **2015**, *71* (1), 3–8. https://doi.org/10.1107/S2053273314026370.

(102) Sheldrick, G. M. Crystal Structure Refinement with SHELXL. *Acta Crystallogr. Sect. C Struct. Chem.* **2015**, *71* (1), 3–8. https://doi.org/10.1107/S2053229614024218.

(103) Neese, F. The ORCA Program System. *Wiley Interdiscip. Rev. Comput. Mol. Sci.* **2012**, *2* (1), 73–78. https://doi.org/10.1002/wcms.81.

(104) Becke, A. D. Density-Functional Thermochemistry. III. The Role of Exact Exchange. *J. Chem. Phys.* **1993**, *98* (7), 5648–5652. https://doi.org/10.1063/1.464913.

(105) Lee, C.; Yang, W.; Parr, R. G. Development of the Colle-Salvetti Correlation-Energy Formula into a Functional of the Electron Density. *Phys. Rev. B* **1988**, *37* (2), 785–789. https://doi.org/10.1103/PhysRevB.37.785.

(106) Yanai, T.; Tew, D. P.; Handy, N. C. A New Hybrid Exchange–Correlation Functional Using the Coulomb-Attenuating Method (CAM-B3LYP). *Chem. Phys. Lett.* **2004**, *393* (1–3), 51–57. https://doi.org/10.1016/j.cplett.2004.06.011.

(107) Perdew, J. P.; Burke, K.; Ernzerhof, M. Generalized Gradient Approximation Made Simple. *Phys. Rev. Lett.* **1996**, *77* (18), 3865–3868. https://doi.org/10.1103/PhysRevLett.77.3865.

(108) Adamo, C.; Barone, V. Toward Reliable Density Functional Methods without Adjustable Parameters: The PBE0 Model. *J. Chem. Phys.* **1999**, *110* (13), 6158–6170. https://doi.org/10.1063/1.478522.

(109) Zhao, Y.; Truhlar, D. G. A New Local Density Functional for Main-Group Thermochemistry, Transition Metal Bonding, Thermochemical Kinetics, and Noncovalent Interactions. *J. Chem. Phys.* **2006**, *125* (19). https://doi.org/10.1063/1.2370993.

(110) Weigend, F.; Ahlrichs, R. Balanced Basis Sets of Split Valence, Triple Zeta Valence and Quadruple Zeta Valence Quality for H to Rn: Design and Assessment of Accuracy. *Phys. Chem. Chem. Phys.* **2005**, *7* (18), 3297–3305. https://doi.org/10.1039/b508541a.

(111) Weigend, F. Accurate Coulomb-Fitting Basis Sets for H to Rn. *Phys. Chem. Chem. Phys.* **2006**, *8* (9), 1057–1065. https://doi.org/10.1039/b515623h.

(112) Neese, F.; Wennmohs, F.; Hansen, A.; Becker, U. Efficient, Approximate and Parallel Hartree-Fock and Hybrid DFT Calculations. A “chain-of-Spheres” Algorithm for the Hartree-Fock Exchange. *Chem. Phys.* **2009**, *356* (1–3), 98–109. https://doi.org/10.1016/j.chemphys.2008.10.036.

(113) Grimme, S.; Antony, J.; Ehrlich, S.; Krieg, H. A Consistent and Accurate Ab Initio Parametrization of Density Functional Dispersion Correction (DFT-D) for the 94 Elements H-Pu. *J. Chem. Phys.* **2010**, *132* (15). https://doi.org/10.1063/1.3382344.

(114) Barone, V.; Cossi, M. Quantum Calculation of Molecular Energies and Energy Gradients in Solution by a Conductor Solvent Model. *J. Phys. Chem. A* **1998**, *102* (11), 1995–2001. https://doi.org/10.1021/jp9716997.

(115) Kuhn, N.; Kuhn, A.; Speis, M.; Bläser, D.; Boese, R. Vinamidin-Chelate Des Bors. *Chem. Ber.* **1990**, *123* (6), 1301–1306. https://doi.org/10.1002/cber.19901230613.

(116) Cappello, D.; Therien, D. A. B.; Staroverov, V. N.; Lagugné-Labarthet, F.; Gilroy, J. B. Optoelectronic, Aggregation, and Redox Properties of Double-Rotor Boron Difluoride Hydrazone Dyes. *Chem. Eur. J.* **2019**, *25* (23), 5994–6006. https://doi.org/10.1002/chem.201900383.

(117) Madhu, S.; Rao, M. R.; Shaikh, M. S.; Ravikanth, M. 3,5-Diformylboron Dipyrromethenes as Fluorescent PH Sensors. *Inorg. Chem.* **2011**, *50* (10), 4392–4400. https://doi.org/10.1021/ic102499h.

(118) Panda, K. N.; Thorat, K. G.; Ravikanth, M. Core-Modified Pentaphyrins(2.1.1.1.1) and Bis(Difluoroborane) Complex: Synthesis, Structure, and Spectral and Redox Properties. *Inorg. Chem.* **2020**, *59* (6), 3585–3595.

https://doi.org/10.1021/acs.inorgchem.9b02905.
(119) Liu, B.; Yu, F.; Tu, M.; Zhu, Z.; Zhang, Y.; Ouyang, Z.; Wang, Z.; Zeng, M. Tracking the Process of a Solvothermal Domino Reaction Leading to a Stable Triheteroarylmethyl Radical: A Combined Crystallographic and Mass-Spectrometric Study. *Angew. Chem. Int. Ed.* **2019**, *58* (12), 3748–3753. https://doi.org/10.1002/anie.201813829.
(120) Dauer, D. R.; Koehne, I.; Herbst-Irmer, R.; Stalke, D. From Bis(imidazol-2-yl)Methanes to Asymmetrically Substituted Bis(Heterocyclo)Methanides in Metal Coordination. *Eur. J. Inorg. Chem.* **2017**, *2017* (13), 1966–1978. https://doi.org/10.1002/ejic.201601470.
(121) Mamalis, P.; Petrow, V.; Sturgeon, B. 331. Some Benziminazolylalanines. *J. Chem. Soc.* **1950**, No. 1600, 1600. https://doi.org/10.1039/jr9500001600.
(122) Quast, H.; Schmitt, E. Notiz Zur Quartärisierung von Heterocyclen. *Chem. Ber.* **1968**, *101* (11), 4012–4014. https://doi.org/10.1002/cber.19681011143.
(123) Dubey, P. K.; Ramanatham, J.; Kumar, R. A Facile Phase-Transfer Catalysed N-Methylation of 2-Substituted Benzimidazoles. *Indian J. Chem. Sect. B* **2000**, *39* (11), 867–871.
(124) Chen, S. H.; Zhao, Q.; Xu, X. W. Preparation and Characterization of a Novel Benzimidazolium Bronsted Acidic Ionic Liquid and Its Application in Esterifications. *J. Chem. Sci.* **2008**, *120* (5), 481–483. https://doi.org/10.1007/s12039-008-0075-3.
(125) Stibrany, R. T.; Schulz, D. N.; Kacker, S.; Patil, A. O.; Baugh, L. S.; Rucker, S. P.; Zushma, S.; Berluche, E.; Sissano, J. A. Polymerization and Copolymerization of Olefins and Acrylates by Bis(Benzimidazole) Copper Catalysts. *Macromolecules* **2003**, *36* (23), 8584–8586. https://doi.org/10.1021/ma034548c.
(126) Bradamante, S.; Antonio, F.; Pagani, G. A. Diheteroarylmethanes. IV. Oxidations and Metal-Promoted Coupling Reactions of Bis(Benzoheteroaryl)methanes. *Gazz. Chim. Ital.* **1996**, *126* (6), 329–337.
(127) Abbotto, A.; Facchetti, A.; Bradamante, S.; Pagani, G. A. 8-Purinyl versus 2-Benzimidazolyl Carbanions: Charge Demands of the Heterocycles and Ligand Properties of the Bis(Heteroaryl)methanes. *J. Org. Chem.* **1998**, *63* (3), 436–444. https://doi.org/10.1021/jo970958l.
(128) Abbotto, A.; Bradamante, S.; Facchetti, A.; Pagani, G. A. Metal Chelation Aptitudes of Bis(o-Azaheteroaryl)Methanes As Tuned by Heterocycle Charge Demands 1. *J. Org. Chem.* **2002**, *67* (16), 5753–5772. https://doi.org/10.1021/jo025696o.
(129) Zhou, Y.; Gong, Y. Asymmetric Copper(II)-Catalysed Nitroaldol (Henry) Reactions Utilizing a Chiral C1-Symmetric Dinitrogen Ligand. *Eur. J. Org. Chem.* **2011**, No. 30, 6092–6099. https://doi.org/10.1002/ejoc.201100857.
(130) Myers, E. L.; Butts, C. P.; Aggarwal, V. K. BF3·OEt2 and TMSOTf: A Synergistic Combination of Lewis Acids. *Chem. Commun.* **2006**, No. 42, 4434–4436. https://doi.org/10.1039/B611333H.
(131) Armarego, W. L. F.; Chai, C. L. L. *Purification of Laboratory Chemicals*, 6th ed.; Elsevier, 2006. https://doi.org/10.1016/C2009-0-26589-5.
(132) Yuan, K.; Yousefalizadeh, G.; Saraci, F.; Peng, T.; Kozin, I.; Stamplecoskie, K. G.;

Wang, S. Impact of Ferrocene Substitution on the Electronic Properties of BODIPY Derivatives and Analogues. *Inorg. Chem.* **2018**, *57* (23), 14698–14704. https://doi.org/10.1021/acs.inorgchem.8b02476.

(133) Kretsch, J.; Koehne, I.; Lõkov, M.; Leito, I.; Stalke, D. Bis(benzoxazol-2-yl)methanes Hounding NacNac: Varieties and Applications in Main Group Metal Coordination. *Eur. J. Inorg. Chem.* **2019**, *2019* (28), 3258–3264. https://doi.org/10.1002/ejic.201900631.

Appendix I Appendix Table of Contents

Appendix II Crystallographic Parameters

Appendix II–1. Crystallography Parameters of 2.13.

Identification Code	**2.13**
Empirical formula	$C_{36}H_{24}B_2Cl_2F_8N_8O_3$
Formula weight	861.15
Temperature /K	296.15
Crystal system	monoclinic
Space group	$P2_1/c$
a /Å	12.6043(4)
b /Å	14.4591(5)
c /Å	21.1238(6)
α /°	90
β /°	100.197(2)
γ /°	90
Volume /Å^3	3788.9(2)
Z	4
ρ_{calc} /g·cm^{-3}	1.510
μ /mm^{-1}	2.333
F(000)	1744.0
Crystal size /mm^3	0.08 × 0.07 × 0.04
Radiation	CuKα (λ = 1.54178 Å)
2Θ range for data collection /°	7.446 to 118.006
Index ranges	-13 ≤ h ≤ 13, -16 ≤ k ≤ 15, -23 ≤ l ≤ 23
Reflections collected	25280
Independent reflections	5419 [R_{int} = 0.1272, R_{sigma} = 0.0873]
Data/restraints/parameters	5419/0/535
Goodness-of-fit on F2	0.990
Final R indexes [I>=2σ (I)]	R_1= 0.0540, wR_2=0.1244
Final R indexes [all data]	R_1=0.0951, wR_2=0.1473
Largest diff. peak | hole /e Å^{-3}	0.61 | -0.43

Appendix II–2. Bond lengths of 2.13.

Atom	Atom	Length/Å	Atom	Atom	Length/Å
Cl1	C2	1.709(4)	C36	C35	1.392(6)
Cl2	C3	1.713(4)	C8	C7	1.413(6)
O1	C1	1.215(5)	C7	C6	1.379(6)
O2	C4	1.234(5)	C7	C15	1.475(6)
F6	B2	1.388(6)	C4	C5	1.429(6)
F7	B2	1.379(6)	C4	C3	1.497(6)
F5	B2	1.370(7)	C6	C5	1.389(6)
F4	B1	1.373(7)	C6	C1	1.508(6)
F2	B1	1.393(7)	C14	C9	1.381(6)
F3	B1	1.368(7)	C14	C13	1.381(6)
F8	B2	1.397(7)	C5	C22	1.534(6)
N2	C8	1.366(5)	C9	C10	1.392(6)
N2	C14	1.419(5)	C21	C20	1.390(6)
N2	C22	1.472(5)	C22	C30	1.527(6)
N8	C36	1.375(5)	C31	C32	1.385(6)
N8	C30	1.324(5)	C2	C1	1.492(6)
N3	C16	1.390(5)	C2	C3	1.317(6)
N3	C15	1.336(5)	C13	C12	1.384(6)
N7	C31	1.388(6)	C24	C29	1.393(6)
N7	C30	1.330(5)	C24	C25	1.397(6)
N6	C23	1.319(5)	C29	C28	1.393(6)
N6	C29	1.380(5)	C10	C11	1.391(7)
N4	C21	1.383(5)	C18	C17	1.382(6)
N4	C15	1.327(6)	C18	C19	1.395(7)
N1	C8	1.340(5)	C11	C12	1.373(6)
N1	C9	1.387(5)	C32	C33	1.374(7)
F1	B1	1.392(8)	C25	C26	1.378(7)
N5	C23	1.358(6)	C20	C19	1.378(7)
N5	C24	1.388(6)	C33	C34	1.392(7)
C16	C21	1.382(6)	C34	C35	1.372(7)
C16	C17	1.382(6)	C26	C27	1.387(7)
C23	C22	1.524(6)	C28	C27	1.371(7)
C36	C31	1.382(6)			

Appendix II–3. Bond angles of 2.13.

Atoms			Angle /°	Atoms			Angle /°
C8	N2	C14	108.4(3)	C30	C22	C5	108.6(3)
C8	N2	C22	125.3(3)	C36	C31	N7	105.9(4)
C14	N2	C22	125.6(3)	C36	C31	C32	122.4(4)
C30	N8	C36	109.1(3)	C32	C31	N7	131.7(4)
C15	N3	C16	109.3(3)	N8	C30	N7	109.2(4)
C30	N7	C31	108.9(3)	N8	C30	C22	128.2(4)
C23	N6	C29	105.2(4)	N7	C30	C22	122.5(4)
C15	N4	C21	110.0(4)	C1	C2	Cl1	116.2(3)
C8	N1	C9	109.2(3)	C3	C2	Cl1	122.7(3)
C23	N5	C24	106.1(4)	C3	C2	C1	121.1(4)
C21	C16	N3	106.3(3)	C14	C13	C12	116.1(4)
C17	C16	N3	131.2(4)	N5	C24	C29	105.8(4)
C17	C16	C21	122.5(4)	N5	C24	C25	132.2(4)
N6	C23	N5	113.3(4)	C29	C24	C25	122.0(4)
N6	C23	C22	124.2(4)	O1	C1	C6	121.2(4)
N5	C23	C22	122.2(4)	O1	C1	C2	121.0(4)
N8	C36	C31	107.0(3)	C2	C1	C6	117.8(3)
N8	C36	C35	131.9(4)	N6	C29	C24	109.7(4)
C31	C36	C35	121.1(4)	N6	C29	C28	129.6(4)
N2	C8	C7	122.0(3)	C28	C29	C24	120.6(4)
N1	C8	N2	108.5(3)	C11	C10	C9	115.8(4)
N1	C8	C7	129.4(4)	C17	C18	C19	121.6(4)
C8	C7	C15	117.4(3)	C4	C3	Cl2	114.5(3)
C6	C7	C8	117.3(4)	C2	C3	Cl2	123.8(3)
C6	C7	C15	125.1(4)	C2	C3	C4	121.7(4)
O2	C4	C5	121.5(4)	C12	C11	C10	122.1(4)
O2	C4	C3	120.2(4)	C33	C32	C31	115.7(4)
C5	C4	C3	118.3(4)	C11	C12	C13	122.0(4)
C7	C6	C5	122.6(4)	C26	C25	C24	116.0(4)
C7	C6	C1	119.0(3)	C18	C17	C16	116.1(4)
C5	C6	C1	118.4(3)	C19	C20	C21	116.3(4)
C9	C14	N2	105.7(3)	C32	C33	C34	122.7(4)
C13	C14	N2	132.0(4)	C20	C19	C18	122.0(4)
C13	C14	C9	122.3(4)	C35	C34	C33	121.1(4)
C4	C5	C22	113.7(3)	C34	C35	C36	116.9(4)
C6	C5	C4	122.2(4)	C25	C26	C27	122.2(4)
C6	C5	C22	122.9(3)	C27	C28	C29	117.3(5)
N1	C9	C10	130.3(4)	C28	C27	C26	121.9(4)
C14	C9	N1	108.2(3)	F6	B2	F8	108.8(4)
C14	C9	C10	121.5(4)	F7	B2	F6	108.9(4)
N4	C21	C20	132.4(4)	F7	B2	F8	109.2(4)
C16	C21	N4	106.2(4)	F5	B2	F6	110.6(4)

C16	C21	C20	121.4(4)	F5	B2	F7	109.7(4)
N3	C15	C7	126.0(4)	F5	B2	F8	109.6(4)
N4	C15	N3	108.2(3)	F4	B1	F2	108.7(5)
N4	C15	C7	125.6(4)	F4	B1	F1	109.7(5)
N2	C22	C23	107.5(3)	F3	B1	F4	110.0(5)
N2	C22	C5	108.2(3)	F3	B1	F2	110.7(5)
N2	C22	C30	107.7(3)	F3	B1	F1	109.9(5)
C23	C22	C5	113.4(3)	F1	B1	F2	107.8(5)
C23	C22	C30	111.2(3)				

Appendix II–4. Solvent mask information for 2.13.

Number	X	Y	Z	Volume	Electron count Content
1	0.212	0.240	0.308	67.9	16.9?
2	0.212	0.260	0.808	67.9	16.5?
3	0.788	0.740	0.192	67.9	17.3?
4	0.788	0.760	0.692	67.9	16.9?

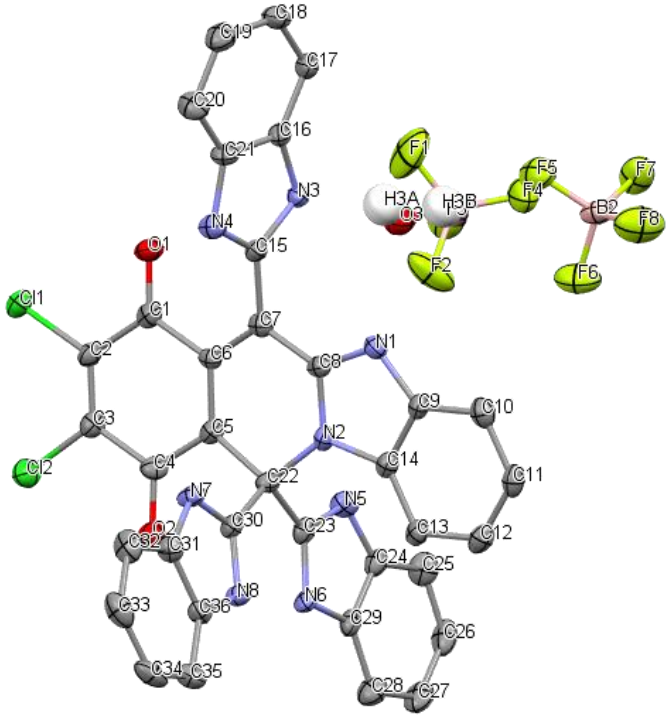

Appendix II–5. ORTEP diagram of crystal structure of 2.13 with labels. Hydrogens, except those on O3, are omitted for clarity. Thermal ellipsoids shown at the 50% probability level.

Appendix III NMR spectra

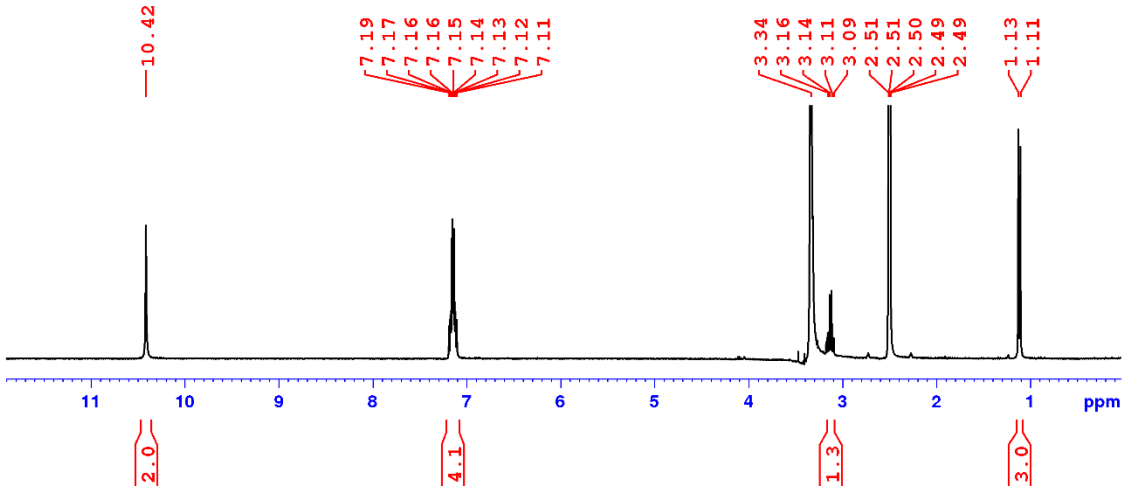

Appendix III–1. ^{1}H NMR spectrum of 2.12b in DMSO-d_6 at 300 MHz.

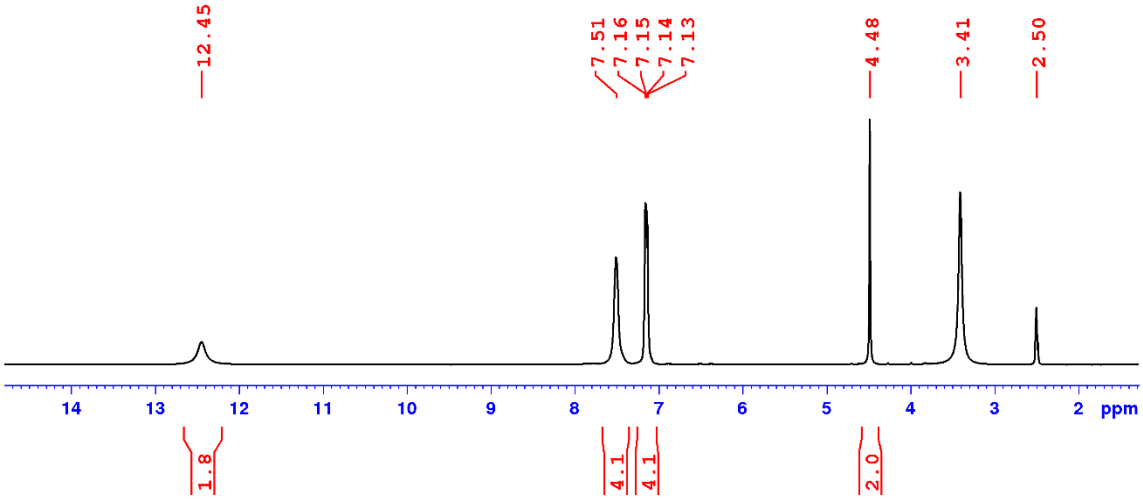

Appendix III–2. ^{1}H NMR spectrum of 2.6a in DMSO-d_6 at 300 MHz.

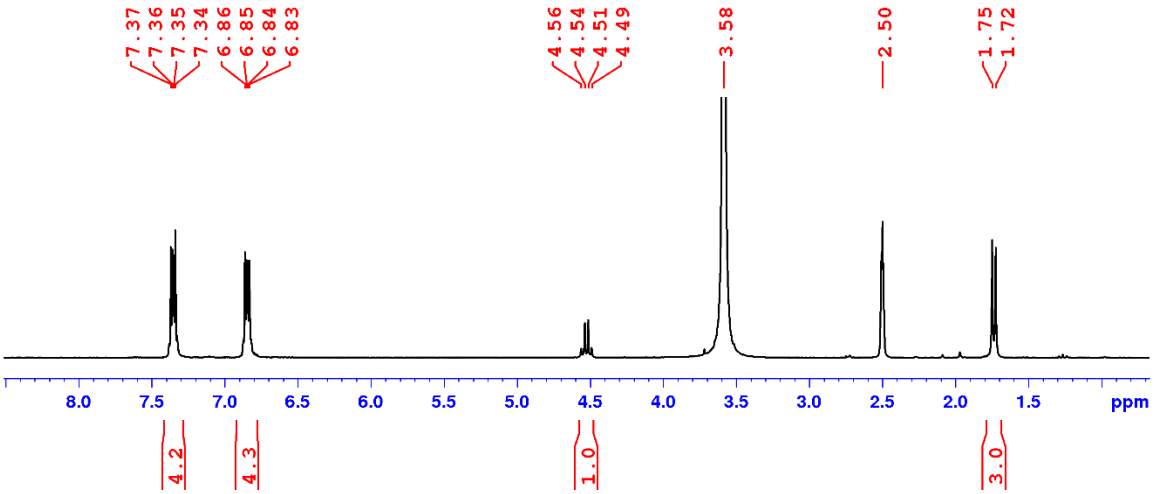

Appendix III–3. ^{1}H NMR spectrum of 2.6b in DMSO-d_6 at 300 MHz.

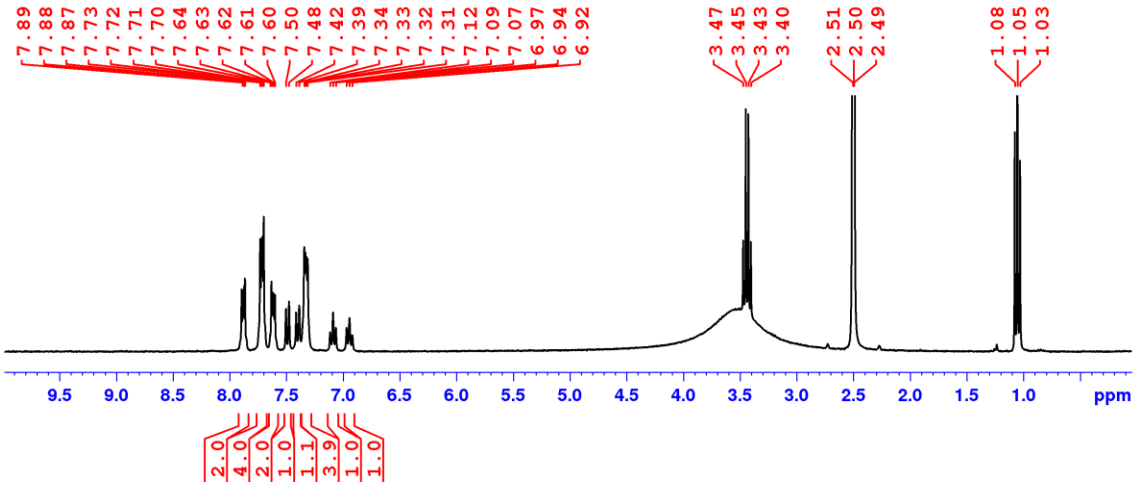

Appendix III–4. ^{1}H NMR spectrum of 2.14 in DMSO-d_6 at 300 MHz.

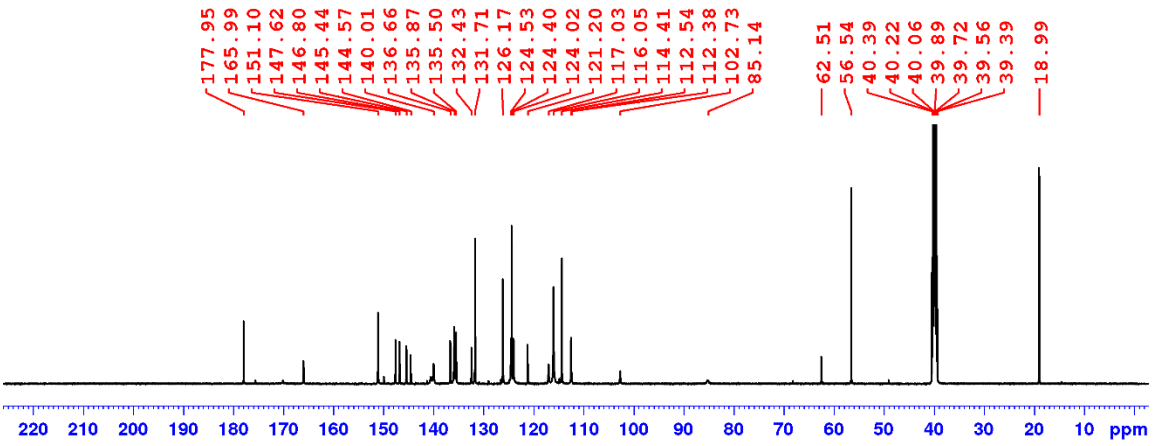

Appendix III–5. ^{13}C NMR spectrum of 2.14 in DMSO-d_6 at 125.8 MHz.

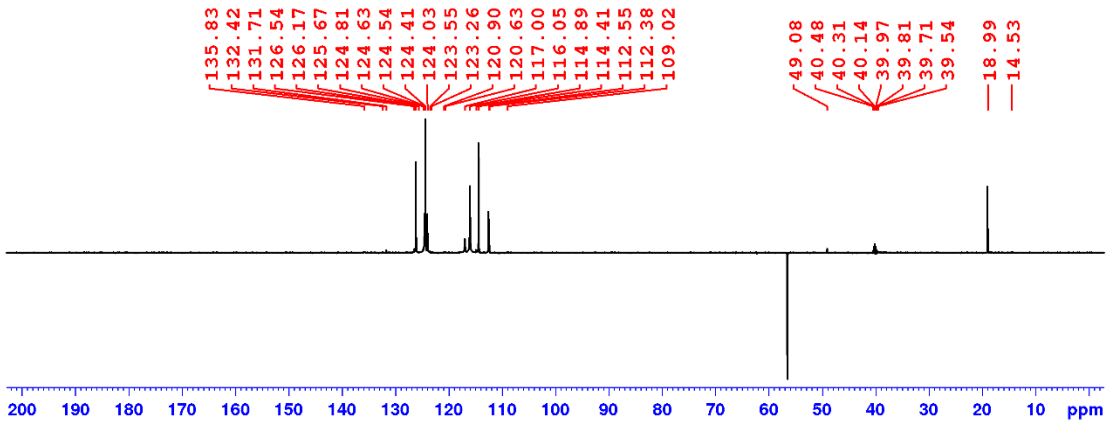

Appendix III–6. DEPT-135 NMR spectrum of 2.14 in DMSO-d_6 at 125.8 MHz.

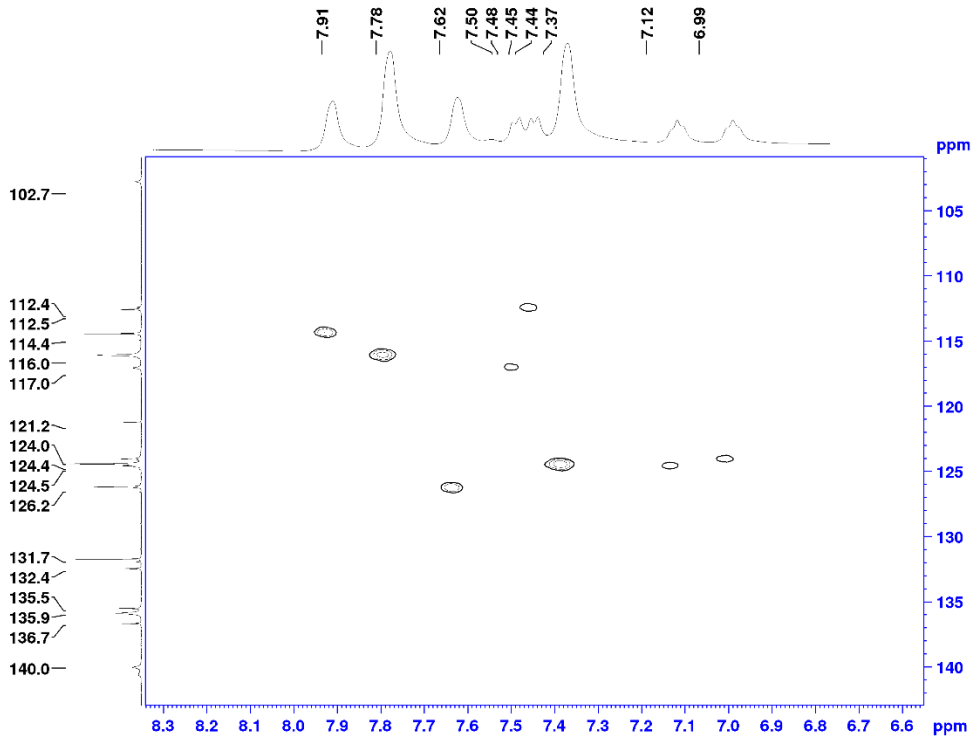

Appendix III–7. $^{1}H–^{13}C$ short-range HSQC spectrum of 2.14 in DMSO- d^{6}.

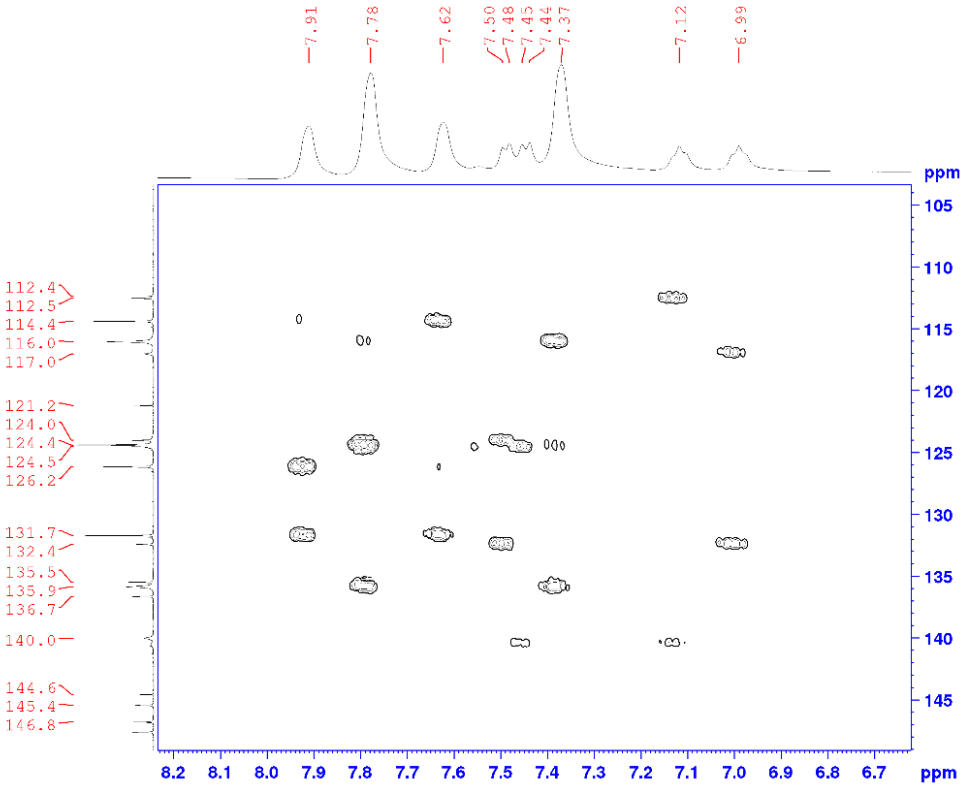

Appendix III–8. $^{1}H–^{13}C$ long-range HMBC spectrum of 2.14 in DMSO-d^{6}.

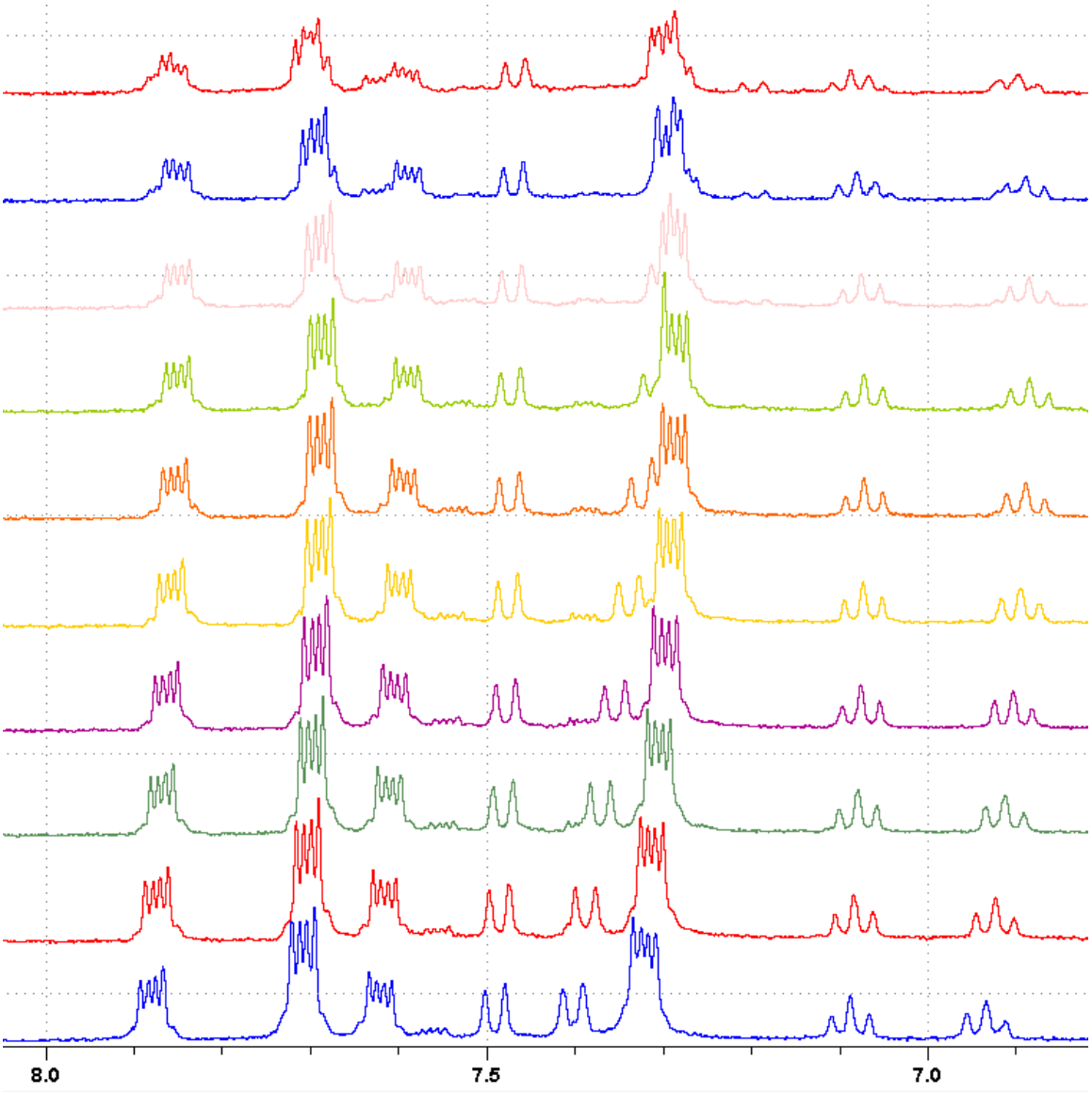

Appendix III–9. NMR spectra of 2.14 in DMSO-d^6 at 360 MHz, acquired at 298K, 310K, 320K, 330K, 340K, 350K, 360K, 370K, and 380K, which is shown as the first spectrum at the top.

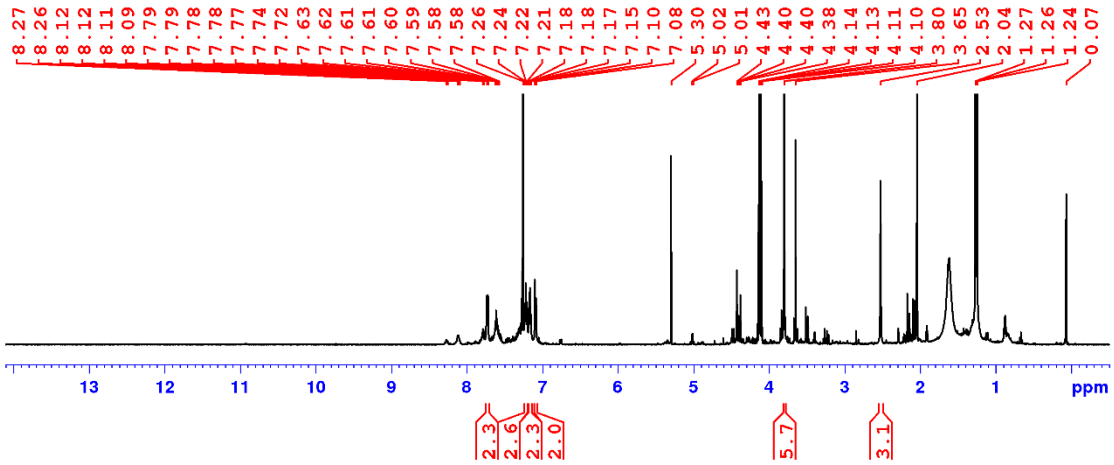

Appendix III–10. ^{1}H NMR spectrum of crude 3.7 in $CDCl_3$ at 500 MHz.

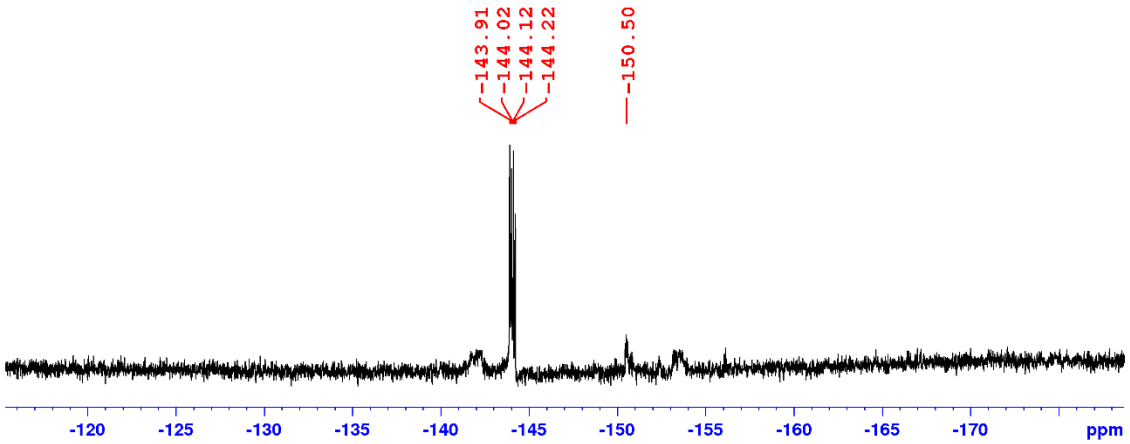

Appendix III–11. ^{19}F{^{1}H} NMR spectrum of crude 3.7 in $CDCl_3$ at 300 MHz.

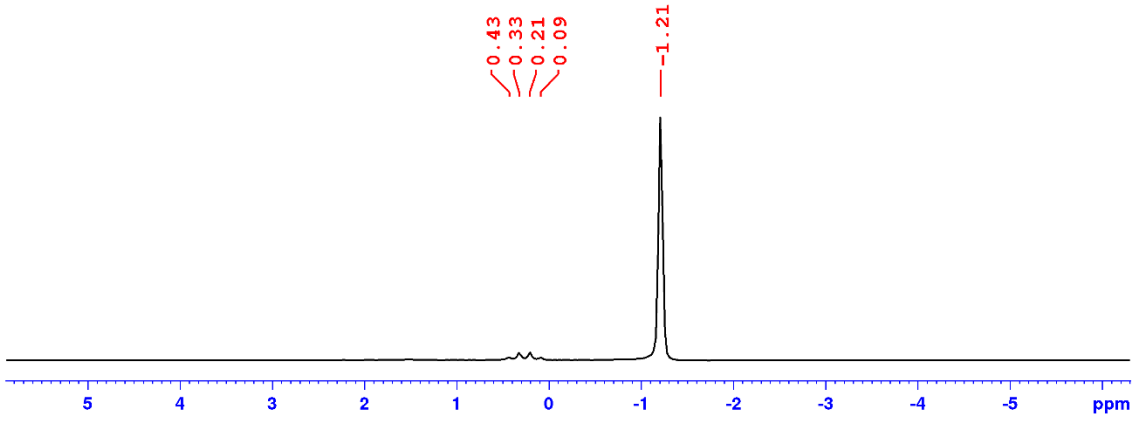

Appendix III–12. ^{19}F{^{1}H} NMR spectrum of $NaBF_4$ in CD_3OD at 300 MHz.

Appendix IV UV-Vis-NIR spectra

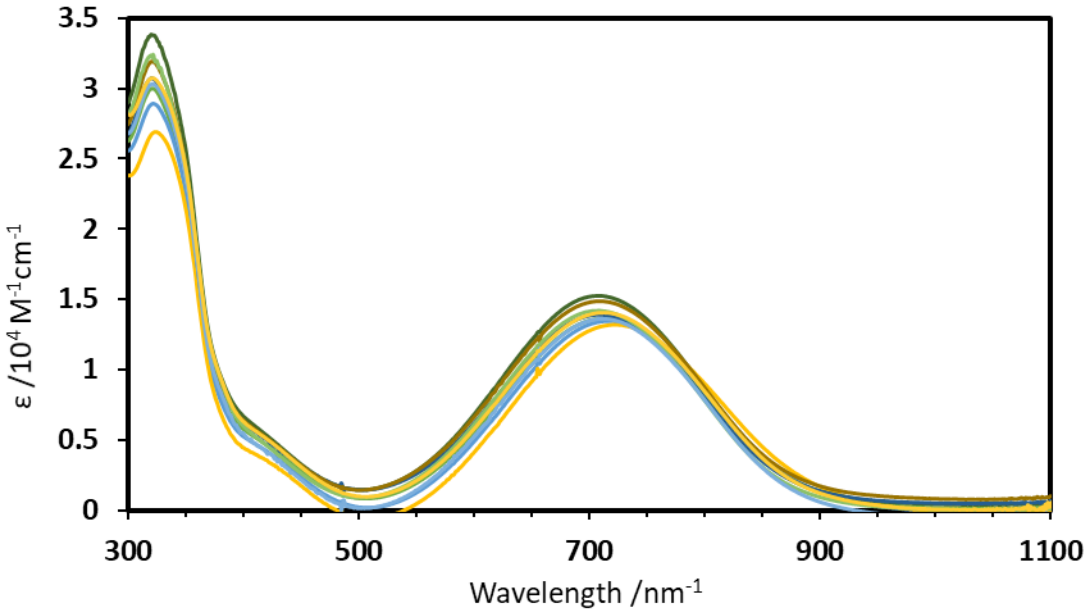

Appendix IV–1. Overlay of all UV-Vis-NIR spectra of 2.14 used in the calculations of its molar extinction coefficients.

Appendix IV–2. Spectral information of UV-Vis-NIR spectra of 2.14.

[] /M	λ_1 /nm	λ_2 /nm
4.73×10^{-5}	321	712
1.89×10^{-5}	322	716
9.47×10^{-6}	324	723
6.11×10^{-5}	320	708
5.09×10^{-5}	321	708
4.07×10^{-5}	321	709
7.43×10^{-5}	320	709
2.23×10^{-5}	321	712
1.49×10^{-5}	321	710

Appendix V Mass Spectra

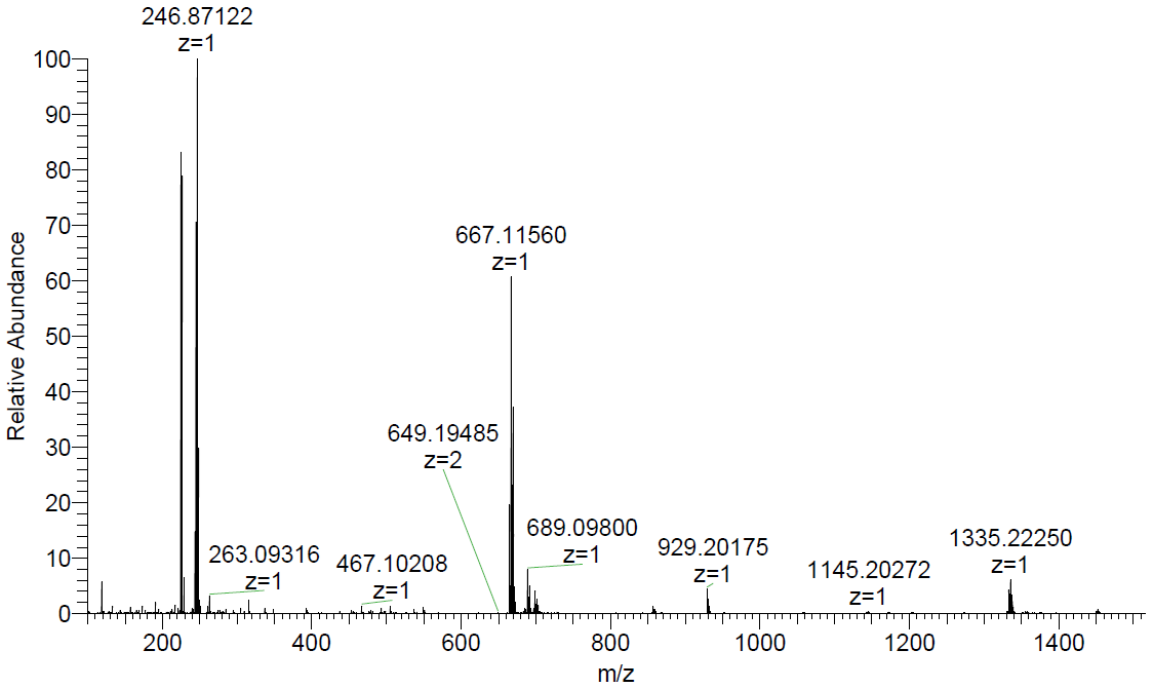

Appendix V–1. HRMS spectrum of 2.14 under positive mode of ESI.

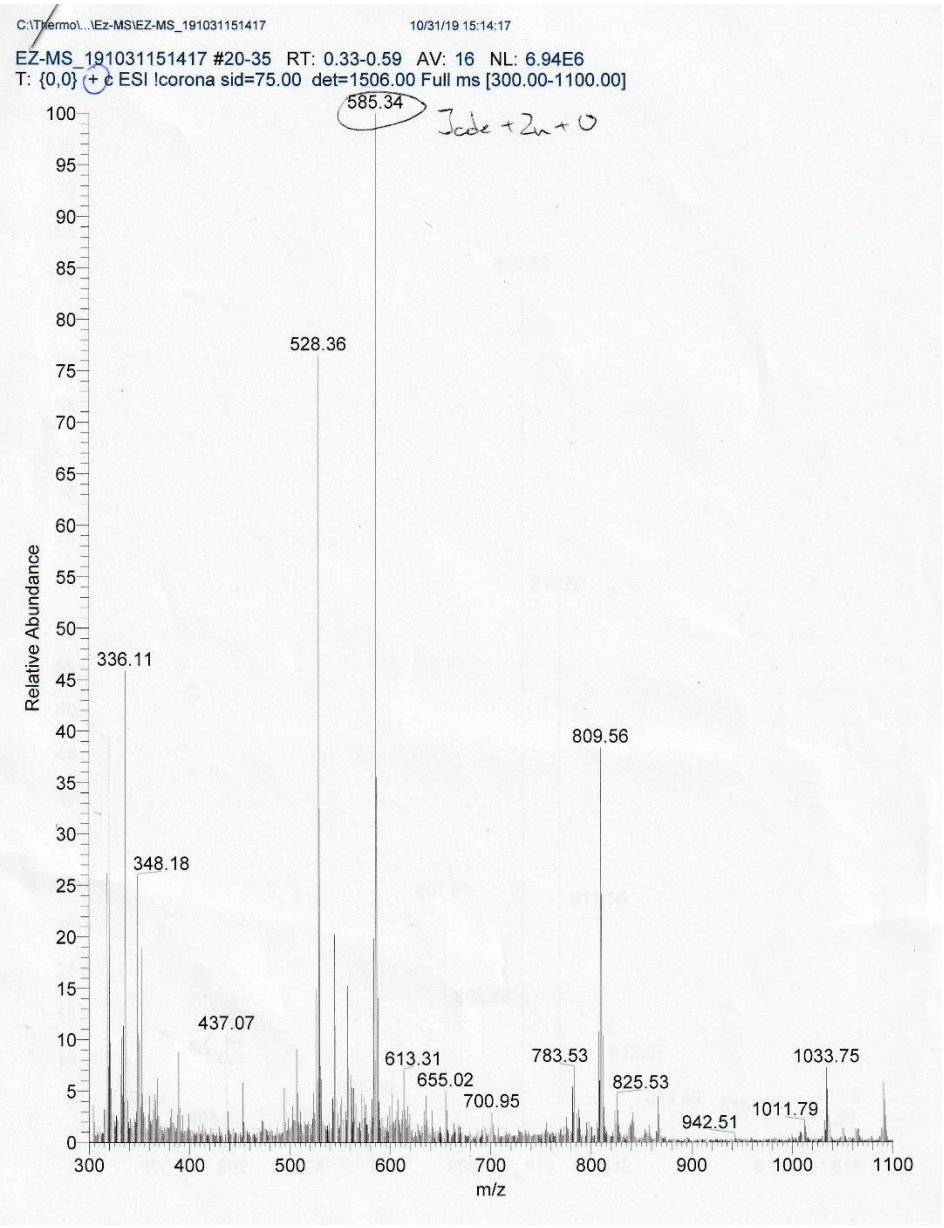

Appendix V–2. Low-resolution mass spectrum of the crude solid from Zn reaction of 2.14.

Appendix VI Computational Parameters

Appendix VI–1. Coordinates of optimized structure for 2.14 in angstroms.

ν_0=0 cm^{-1}

Atom	x	y	z
Cl	12.55694803597846	6.23867371042398	3.94905563358932
Cl	13.43535355735039	6.99003825749474	6.93250168947412
O	9.76718942476256	6.44877019221105	3.58986235741379
O	11.13665854594647	7.53872140330162	8.60527735857848
N	7.09592246770710	7.52506060818695	7.83029422064381
N	8.88743455001267	6.36352697252706	10.53402847467487
H	9.02599866897505	7.23943068060910	11.02318846746649
N	7.44727504933654	7.17984889289286	2.88163814958960
N	8.60358767792510	5.08515822582027	8.72503846215733
N	8.77969282200299	9.12094637651991	10.21489118542625
N	5.56988069227159	7.28320270645824	3.97713079534376
N	5.31948104731620	7.44121178390552	6.49180394162242
N	8.96251512824922	9.95652985740533	8.16104393996416
H	9.06088012009189	9.95112513724825	7.16010014124877
C	6.44466546357160	7.21053341542732	1.93163681399310
C	8.77773468590639	8.84335047368421	8.93710733306267
C	8.95714289976747	5.06259355994638	10.98603434787138
C	6.64938149650835	7.38744479691237	6.53838356563488
C	7.55521324017634	7.21262432633641	5.41863478974316
C	10.78398146938780	7.30300447977194	7.45276068096800
C	8.95080966546311	7.12907924381667	5.75579605088551
C	5.98434831810677	7.65458301135954	8.65415580813165
C	9.39644024362892	7.31871279804076	7.05813598159728
C	4.87823522420654	7.60400299303664	7.78361663640016
C	5.23526992939794	7.28848925449626	2.63950485832824
C	6.91842806947047	7.20684485906223	4.13240658475047
C	8.49130689328820	7.50624937514928	8.27121162917464
C	8.77844625449328	4.26806785138964	9.82882422535390
C	8.67907371648267	6.30604149960997	9.18811056458545
C	11.42995558368007	6.69079144341691	5.16802303765655
C	5.83086997885084	7.80735173140636	10.02821097289442
H	6.67451389535082	7.86346210573333	10.69464622613487
C	9.11315633238558	11.03626129774964	9.01012658039665
C	10.00912323367382	6.74592935127365	4.75102035033409
C	8.99191858211889	10.48984232533054	10.30532665515374
C	3.57858622501598	7.71556617241585	8.27958757160883
H	2.72926574802911	7.67882676723777	7.61054188131067
C	5.25280263766162	7.22279091254893	-0.11514546336003

H	5.23260476905173	7.19554569236004	-1.19666006348113
C	11.80727295271613	6.98706238278357	6.42114458150143
C	3.42305117191457	7.86812058672701	9.64651229944304
H	2.42932476488832	7.95747155879650	10.06581674811770
C	8.79920480457219	2.87635313995019	9.92699545781463
H	8.67188749213670	2.26288306794425	9.04489558745725
C	4.53274879697295	7.91163149956260	10.50489537128759
H	4.37488961813964	8.03628581099509	11.56831993509671
C	9.32544134233088	12.39155009195707	8.79099830713768
H	9.42426920728451	12.80379290939299	7.79507699766928
C	6.47509246900509	7.17517184651180	0.54371605338154
H	7.40760686190786	7.11011790220821	-0.00005457394519
C	4.01383722234796	7.33503424570047	1.97905695530187
H	3.08073377270918	7.39136335243570	2.52199068946942
C	8.98008201771466	2.31814057426604	11.18228392352689
H	8.99910874019927	1.24094147757883	11.29059083598220
C	4.04444904627029	7.30166218431043	0.59033200841669
H	3.11371362781575	7.33381753519217	0.03977245004714
C	9.13793282706309	3.12018200537530	12.32520015026930
H	9.26955075511566	2.64350179915404	13.28809474839403
C	9.13213897140074	4.50546795786439	12.24890135349085
H	9.25972216663136	5.11824802215121	13.13134288402374
C	9.40643844305012	13.19932400319784	9.91658628802150
H	9.57245868078440	14.26182155846547	9.79388202487248
C	9.07911291152233	11.31674692771257	11.42284058111805
H	8.98657603954929	10.90578101135466	12.41914574433941
C	9.28405519372161	12.67079879991624	11.21122008830796
H	9.35689465274099	13.33807133440151	12.05983803274288
H	8.43057401014316	6.94075650123406	2.76604075266556
H	4.99155843595072	7.35244668994230	4.83837889462606

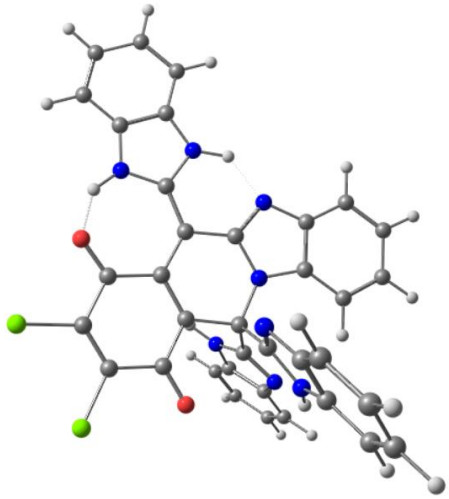

Appendix VI–2. Optimized structure of 2.14.

Appendix VI–3. Coordinates of optimized structure for 2.14t in angstroms.

ν_0=0 cm^{-1}

Atom	x	y	z
Cl	12.49992670102168	6.16819228953493	3.93486078951744
Cl	13.39664348027913	6.85213903771079	6.93250904306407
O	9.68834469130243	6.36734307653512	3.60961696143802
O	11.10525442146311	7.41588275212860	8.62086108434461
N	7.06392741465061	7.41405744765153	7.84009721458128
N	8.89626487098810	6.40441731736850	10.59293082053008
H	9.04379715996731	7.30260055153771	11.03617130940498
N	7.45386083056429	7.44406768437005	2.88578962250603
N	8.55277309362871	5.03433442581024	8.86326393516595
N	8.68902617586275	9.14017559851212	10.16514756434939
N	5.53188391848134	7.40771357040026	3.99853729179546
N	5.31772291485301	7.40158066726740	6.52838607477136
H	4.87481420911612	7.39591670581233	5.58878654916115
N	8.96211321088225	9.86812449464151	8.07946455640338
H	9.11946337270589	9.80457482636937	7.08769035657014
C	6.46340673672665	7.52436247596309	1.93328017178772
C	8.73097507700872	8.79977861190999	8.90263302687370
C	8.96550164115690	5.13083019594642	11.11280652020269
C	6.66486015778231	7.34647244452475	6.54340987479520
C	7.53140982839055	7.23237722321945	5.41783673832265
C	10.74991115327124	7.18537751160697	7.46638366518221
C	8.91554616994723	7.08845118271677	5.76673705663768
C	5.94135613857446	7.51200950747572	8.66658943367050
C	9.36506743564016	7.22018251785396	7.07645675393878
C	4.82729749932399	7.50479970847628	7.81331920902840
C	5.25344895953277	7.52023372591293	2.65666607833978
C	6.86373583760047	7.33478220814117	4.11964496847222
C	8.46379322698680	7.43437140255701	8.28980691917490
C	8.75011804314708	4.27605494339585	10.00633165955952
C	8.65479877106778	6.27716351307202	9.25771047400382
C	11.38393335794881	6.61049325328915	5.16605793402723
C	5.79426693070013	7.61205756622307	10.04361845945918
H	6.64327481028851	7.63763462415949	10.70449907597789
C	9.10981276893331	10.98482183970815	8.87936387645085
C	9.95985042588305	6.67947911875561	4.75574666391226
C	8.92946532596111	10.50784253586231	10.19521444299965
C	3.53138060133798	7.59569185503600	8.30438313542294
H	2.67736695349585	7.58968119833036	7.64152917626973
C	5.27532912448597	7.63500449599179	-0.11127210621662
H	5.25469770541836	7.67245326812060	-1.19284575750897

C	11.76640593280451	6.87673913808141	6.42488635969076
C	3.38622998002093	7.69321216025341	9.68150235531688
H	2.39429559915415	7.76732083374912	10.10681871902275
C	8.76650156754313	2.89173788936974	10.18154265632371
H	8.61375577721072	2.23049225119748	9.33897343938437
C	4.49781360401750	7.70197886269683	10.53229405532241
H	4.34724403470489	7.78608389314240	11.60039450413925
C	9.37228307081404	12.32017849196822	8.59961765467564
H	9.51873516011059	12.67758230952585	7.58863831800955
C	6.49734285309217	7.57609512355948	0.54401206703165
H	7.43001643897478	7.56539721015479	-0.00432844987974
C	4.03315250665408	7.59237265586660	1.98253977908950
H	3.09907010465168	7.59273438746762	2.52853152047856
C	8.97942972642853	2.40343082817745	11.46075967522639
H	8.99802092772809	1.33394256207783	11.62836738138339
C	4.06232340129712	7.64639536806202	0.59801983576835
H	3.13232015270343	7.69538877071339	0.04654675211052
C	9.17136219811211	3.26641357664886	12.55276219521143
H	9.32692980507011	2.84262362617597	13.53652601176750
C	9.17055706433453	4.64473210999009	12.40019959583948
H	9.32704414189395	5.30539107657016	13.24275312236633
C	9.44208361504540	13.17993742764786	9.68590138031368
H	9.64814773820013	14.22883093016036	9.51694726340349
C	9.00480198045707	11.38717143253746	11.27328715557672
H	8.86838188472130	11.03015592903196	12.28523675121164
C	9.26084340837772	12.72123117244493	11.00076735221998
H	9.32856501978791	13.42844951231519	11.81684251694874
H	8.41646915971247	7.17205109651411	2.74114240765975

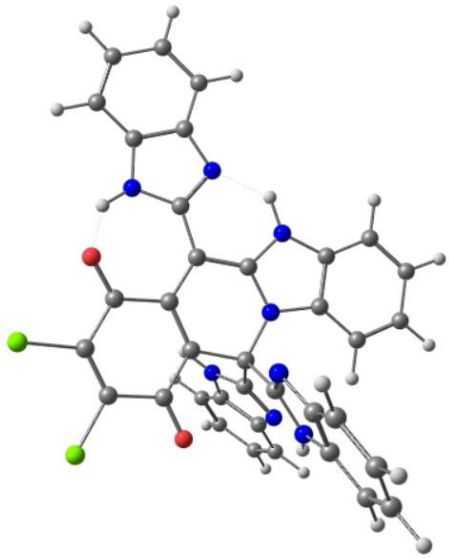

Appendix VI–4. Optimized structure of 2.14t.

Appendix VI–5. Coordinates of optimized structure for 2.16 in angstroms.

ν_0=0 cm^{-1}

Atom	x	y	z
C	-1.91366608014990	-0.41777374648192	0.11362397576516
C	-1.80378363548370	-1.75863376767199	0.10020045589952
C	-0.71045210942758	0.44885786245500	-0.00173106628082
C	0.62481688891452	-0.23219187045059	-0.06870534623669
C	0.69483888320341	-1.60433656446328	-0.09633966377028
C	-0.46722843556732	-2.44125868345597	-0.03633075436601
C	1.76432939119326	0.59592292328195	-0.08695467576874
C	2.98673004104635	-0.03818675676854	-0.06972611059938
N	3.12562031519397	-1.39831007263386	-0.09015282439361
N	4.24844527427186	0.48626244894957	-0.00650641030961
C	5.19357852277280	-0.53210036558334	0.01659332317811
C	4.46944954249495	-1.73647263966954	-0.04197630885059
C	6.57544336766032	-0.52033980529019	0.07482418300910
C	7.22356202828584	-1.75563392533329	0.07257030859961
C	6.50721747480367	-2.95146660439437	0.01338420465137
C	5.11331564722712	-2.96318030144233	-0.04518357997201
H	7.13320477581889	0.40535596980007	0.12289191856379
H	8.30411594576107	-1.78444904845664	0.11929342917337
H	7.04373470077747	-3.89069681766132	0.01382145461763
H	4.55931010519867	-3.88982255349085	-0.09339420935693
C	2.00888375220783	-2.33499985745142	-0.22008888521988
H	2.09490458483234	-3.10375984636783	0.55387341674191
H	2.08542675117438	-2.85911357555981	-1.18123773377814
H	4.43701264043512	1.47085193238235	0.06075209407485
H	1.67242628043444	1.66950290825111	-0.06530243318101
O	-0.80473642881942	1.65701148183117	-0.03874801083461
O	-0.39903333119120	-3.66654890720840	-0.08682898738748
Cl	-3.41609359183273	0.40464130774513	0.26040212817216
Cl	-3.16103016143644	-2.79453834286086	0.23116655795922

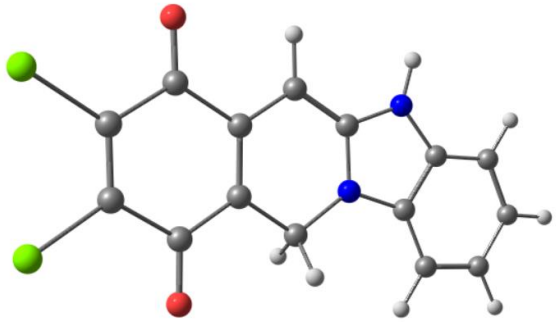

Appendix VI–6. Optimized structure of 2.16.

Appendix VI–7. Coordinates of optimized structure for 2.17 in angstroms.

ν_0=0 cm^{-1}

Atom	x	y	z
C	-2.06656645624936	-0.82240950567699	0.05627446656371
C	-1.82121689799742	-2.10872849903741	-0.23593428232854
C	-0.95811191561780	0.11529520402080	0.37012613377276
C	0.46357161794728	-0.30843125414061	0.10223821433613
C	0.64716107479015	-1.66918349191911	-0.07665066740674
C	-0.41942663969323	-2.61856254861857	-0.23192388043940
C	1.57291954225073	0.61095667946564	0.12237567600484
C	2.84711367221724	-0.01680982373486	0.06604147753713
N	3.04455164317068	-1.35727391487952	-0.00483433932146
N	4.06362740557927	0.57237633897723	0.10283219629116
C	5.05792367227049	-0.38716340140055	0.06606153223716
C	4.40327285386512	-1.62908418007376	-0.00290331995598
C	6.44329015045661	-0.30833390256205	0.08704556626396
C	7.14815375742559	-1.50735546539586	0.04211946590773
C	6.49258939816236	-2.74187733725420	-0.02388251814352
C	5.10395387837975	-2.82544034870663	-0.05018662876551
H	6.95348070219686	0.64358981580486	0.13916657295574
H	8.22988594396878	-1.48436173304388	0.05972744496212
H	7.07808866066686	-3.65086717914807	-0.05481532479036
H	4.59643747286667	-3.77827008591720	-0.10393045129814
C	1.98974075243165	-2.33484173453741	-0.17657696223334
H	2.08578143018021	-3.11445864008960	0.58602403752716
H	2.10959618779234	-2.84124761163802	-1.14117158326027
H	4.06616183302483	1.60870750938976	0.11847614718403
C	1.60553052873415	2.06851275206534	0.11815888807829
O	-1.24737327681812	1.18483715060065	0.87634209987826
O	-0.19046970180648	-3.81500716365347	-0.39784008252101
Cl	-3.65327654931734	-0.16316856059118	0.15404424711597
Cl	-3.04704043899530	-3.24282850256060	-0.59155372277378
N	0.52625472233943	2.91108501729020	0.11174719368970
N	2.74576905427521	2.77179846886825	0.06323259050028
C	0.98415333988490	4.20689820072204	0.08588397850981
C	2.39024879255586	4.10257481576554	0.04563577193434
C	0.32392336175010	5.42843577965918	0.09736845813647
C	1.11683816907418	6.56697601204284	0.06351556177377
C	2.51814629779206	6.48191025352438	0.01935820669331
C	3.17202163139958	5.25867540321750	0.00876558070341
H	-0.39923957884605	2.58903654825924	0.36043233801984
H	-0.75611760692241	5.49093526737003	0.13253051758324
H	0.64447675182019	7.54048411710249	0.07127534672402
H	3.09836663600286	7.39482582649871	-0.00823305261877

H	4.25214203489153	5.19594205033487	-0.02575244622749

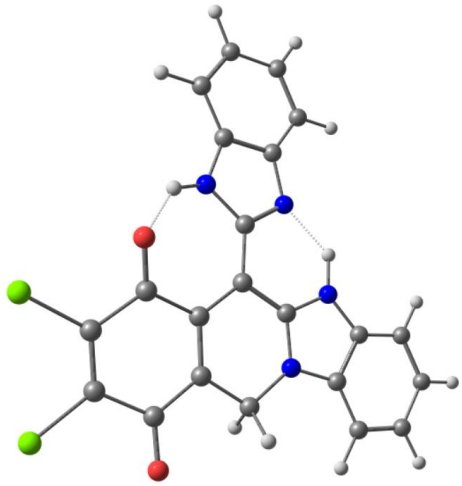

Appendix VI–8. Optimized structure of 2.17.

Appendix VI–9. Coordinates of optimized structure for 2.18 in angstroms.

ν_0=0 cm^{-1}

Atom	x	y	z
C	-1.94921132997322	-0.30288060431455	0.12953874307325
C	-1.95198801657503	-1.65045329581594	0.11666809393967
C	-0.68227385798928	0.46332940804948	-0.02139875860599
C	0.58757915217852	-0.32591790040482	-0.07114545948144
C	0.60244404401455	-1.68922152596525	-0.10661218525298
C	-0.68752836270127	-2.43158799250456	-0.08431955722954
C	1.80288096334792	0.43261575142403	-0.07459269134638
C	3.03858939832450	-0.15827457988985	-0.05208791576360
N	3.18257043262379	-1.53529676432420	-0.04900367336620
N	4.24204541895824	0.49987622710813	-0.01474498983232
C	5.14998828365418	-0.46805160280898	0.00920088095009
C	4.49554284517536	-1.76912863919632	-0.01135715433505
C	6.56959614348120	-0.39444168284015	0.04456338509386
C	7.25758277012721	-1.57091283226135	0.05800828344790
C	6.59205704651433	-2.84459740646708	0.04140234428450
C	5.23025302530183	-2.96975097730523	0.00747193191470
H	7.06458145642388	0.56655273581637	0.05746409605889
H	8.33955176278498	-1.56286552736457	0.08339371535883
H	7.20451193749723	-3.73704085892227	0.05837593539473
H	4.73072418075388	-3.92726592064633	-0.00113931614735
B	1.98169270920011	-2.56761004119923	-0.20930848128681
F	2.08805896433486	-3.49797900422255	0.81054495057434
F	2.11197677265546	-3.12708960845630	-1.47333257703121
H	1.74475235215514	1.51307278175106	-0.07512339988085
O	-0.67795982936213	1.67325691935408	-0.08640238389727

O	-0.72287238937958	-3.63268746709869	-0.22213261593065
Cl	-3.37177168632255	0.63071286212473	0.31290449498236
Cl	-3.37867530580412	-2.57238195741965	0.29363696061454

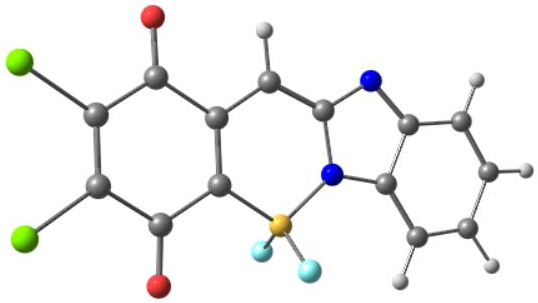

Appendix VI–10. Optimized structure of 2.18.

Appendix VI–11. Coordinates of optimized structure for 2.19 in angstroms.

ν_0=0 cm^{-1}

Atom	x	y	z
C	0.29378494786135	0.37595639223727	-0.00906964050001
C	1.00355928845122	-0.87477897417565	-0.01510023003100
C	0.94105891065372	1.57621878876450	-0.00871785102380
C	2.36260830861304	1.55752383926224	-0.01452283706792
C	2.36671107837416	-0.94100336334597	-0.01660611189456
N	3.23323198210940	2.55469464480532	-0.02401314763961
C	4.46157163721078	1.91776707920142	-0.02247584255707
N	4.38405971739401	0.52833037015755	-0.01684240907176
C	5.65730608402643	2.62144595812819	-0.02086712881965
C	6.92821867287377	1.95956276873326	-0.00097413819231
N	7.08301882339032	0.59201870269641	0.00234710579461
N	8.09940522208611	2.59437077720078	0.01442129092013
C	9.04590481679138	1.61228663693512	0.02803444524900
C	8.42002731411924	0.33159264217684	0.01696362487755
C	10.44658959437568	1.70723594877967	0.04372692625940
C	11.17209300076166	0.53484133945838	0.04291014301906
C	10.53573858565506	-0.72686832927178	0.02711669287637
C	9.15961882225598	-0.85261674320978	0.01502609968194
H	-0.78841430222733	0.34713610068513	-0.00516296687751
H	0.42294996720898	-1.78878211627160	-0.01861108000804
H	0.40700542345118	2.51690536490537	-0.00391180115263
H	2.89370226577023	-1.88595563430495	-0.02116873639178
C	5.66359506507069	4.11111535530071	-0.02576386574023
H	10.92674610047708	2.67639861367976	0.05528573798164
H	12.25356225378965	0.57266287840617	0.05370979664276
H	11.14815648081690	-1.61930318043368	0.02400824765875
H	8.68179423662954	-1.82285932988336	0.00195225697020
C	3.08138047071154	0.28563511947533	-0.01415068309154

H	6.26835423445335	-0.02105251476371	-0.00693886591855
H	4.66729742209667	4.49601917675745	-0.21679944278046
H	6.37706852317350	4.48174530202624	-0.76102719335879
H	6.01584505157472	4.47619738588741	0.94350960418581

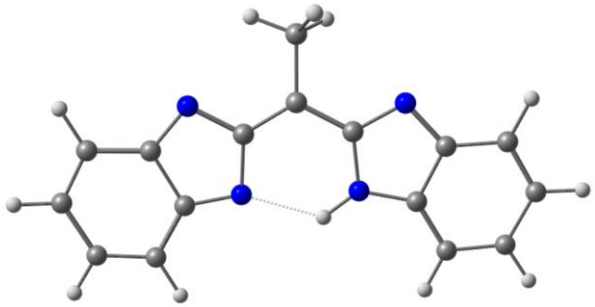

Appendix VI–12. Optimized structure of 2.19.

Appendix VI–13. Coordinates of optimized structure for 3.7 in angstroms.

ν_0=0 cm^{-1}

Atom	x	y	z
C	0.27336573106384	0.38550090297886	1.59628059155111
C	1.09854019159863	-0.44865206135745	2.35394007767651
C	0.80430743178248	1.26496423168229	0.65368418300814
C	2.18175946386272	1.27213538690456	0.50316262012117
C	2.48205220889175	-0.44336556358309	2.19521368796204
N	3.01830875902708	2.01474150199861	-0.33402325499554
C	4.32194142496190	1.63742004021657	-0.08967709310364
N	4.32386743570875	0.67266831706447	0.86638583001946
C	5.47543484324382	2.14260497900290	-0.70881355870932
C	6.64818779530228	1.41799661357529	-0.44114343073437
N	7.87263374768789	1.54880834707148	-1.05983295054103
N	6.74507517987378	0.45102185946877	0.50791456564817
C	8.04406441169089	-0.04233358030112	0.51224742141853
C	8.76159154289791	0.64857325305721	-0.47266791455664
C	8.65309588103421	-1.01905530938719	1.28606971597125
C	9.99357727323120	-1.29317324541664	1.02761874604806
C	10.70096576734427	-0.61489499445230	0.03182064174241
C	10.09197482958736	0.37297411167064	-0.74039806232693
H	-0.79742728757551	0.35617652341905	1.74968392054716
H	0.65224556292163	-1.11399239024149	3.08081594577485
H	0.16327924817730	1.92033662947860	0.07911916776662
H	3.12597046345281	-1.09139993560326	2.77110555950119
C	5.51038079526106	3.52440979027882	-1.32397058281270
C	3.01125501104035	0.42782614085355	1.25451505810471
C	8.13711785787039	2.17897919603940	-2.34009960996214
H	4.74541370596763	4.15300120393666	-0.86880658267113
H	5.36445848869201	3.57306944267570	-2.40759811130914

H	6.46503246241096	4.00373577142857	-1.10302917667907
H	8.69145620481268	3.11279867214272	-2.23068422141293
H	7.20254530003306	2.38014688766641	-2.85202637342937
H	8.72456130689434	1.49306208061581	-2.95190491183519
C	2.54807434580671	2.70318028070330	-1.52257764631797
H	1.56601538605024	2.31069858230584	-1.78187912235192
H	3.22507735743222	2.50156795579174	-2.34995273318221
H	2.46792026639033	3.78102114694097	-1.37644887018789
H	8.09666878210430	-1.54964043101678	2.04449234144744
H	10.49913106466741	-2.04872455533139	1.61404002100303
H	11.73713930080748	-0.86592375693351	-0.15303182260727
H	10.64165712943922	0.90278967631573	-1.50684302487662
B	5.59971602296208	0.01156777575701	1.46215546804599
F	5.48107630750283	-1.37740272181244	1.44692884845926
F	5.83014399808774	0.44919824439511	2.76476864278593

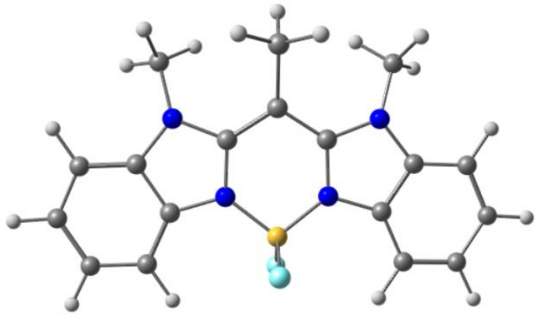

Appendix VI–14. Optimized structure of 3.7.

Appendix VI–15. Coordinates of optimized structure for 3.8 in angstroms.

ν_0=0 cm^{-1}

Atom	x	y	z
C	0.29488393395706	0.39732363309353	1.58541510729742
C	1.14063878246653	-0.46213146165848	2.35697386513959
C	0.78675703530961	1.26444411633253	0.63856271553323
C	2.17586748444177	1.26853404779949	0.47423278560358
C	2.50242015096880	-0.47537241202774	2.20303472403923
N	2.98969460320724	1.99123026157730	-0.34734157292037
C	4.29480889051607	1.59719687240961	-0.11678058031880
N	4.29470886678268	0.61966635343487	0.83014853183034
C	5.47411452750173	2.08636358316657	-0.71527418124963
C	6.65937909950011	1.35888505281555	-0.47961144790620
N	7.88444838651555	1.49075043185695	-1.10387503367396
N	6.76076891227555	0.40173225999750	0.48098845877804
C	8.03479096319240	-0.05020633466363	0.52197336547563
C	8.76077745552410	0.63442384053809	-0.50571160427880
C	8.65101467982747	-1.00061402839717	1.35086082747813

C	9.97463278364804	-1.24993023497785	1.09882722656647
C	10.69324619732460	-0.57699450539733	0.05924286862807
C	10.10838091271871	0.36290140519162	-0.75609665933340
H	-0.77120250081276	0.36342034837765	1.76783003600249
H	0.67728633257630	-1.11835180909074	3.08099713587348
H	0.13185704120225	1.91630186641456	0.07893706098681
H	3.14597157455178	-1.12389335755813	2.77859332557678
C	5.49677536420144	3.37870871798001	-1.47012768603837
C	3.02345962280807	0.40007621267050	1.23735451698784
C	8.21179866204994	2.23181472967751	-2.33058498816760
H	4.73516352059536	4.05491350175706	-1.09459955296055
H	5.32602873282665	3.24619293298312	-2.54276579247519
H	6.45622041792748	3.87217068974656	-1.34334136550795
H	8.54572667472166	3.24139947789042	-2.09563730180482
H	7.35149076627110	2.25673091551696	-2.98996975937705
H	9.00988223728714	1.69864053296239	-2.83887808908133
C	2.47537391575520	2.88786405078180	-1.39185579245007
H	1.44797207931067	2.60547069424818	-1.60018725058312
H	3.05089409427220	2.76484014877387	-2.30302759986095
H	2.50097327838677	3.92337504419704	-1.05547233769519
H	8.10115170195259	-1.50885054664696	2.12896350819219
H	10.50483494257847	-1.97627368877328	1.69952753243158
H	11.73712002662196	-0.82254405082464	-0.08486078179512
H	10.67174343999241	0.87144617895935	-1.52478645128632
B	5.59102433603332	-0.07631568064241	1.44650343794743
F	5.46890555641297	-1.42812633686530	1.35243681713029
F	5.80786751679907	0.38720354637304	2.70593598126620

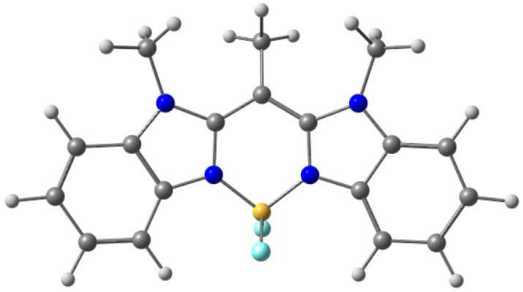

Appendix VI–16. Optimized structure of 3.8.

Appendix VI–17. Coordinates of optimized structure for 3.9 in angstroms.

ν_0=0 cm^{-1}

Atom	x	y	z
C	0.35853876649951	0.65783457891194	1.53181113038353
C	1.12904478872886	-0.46631197248274	1.96095979819103
C	0.90448684688758	1.70430487432373	0.82492604689108
C	2.26701553310800	1.60041335634288	0.52936995974423

C	2.46984369089028	-0.57353665611378	1.69367944098773
N	3.11520110722072	2.42811840072794	-0.15150182558146
C	4.35446188557534	1.82111907479858	-0.19874685355356
N	4.30465406115659	0.67221051851974	0.52329646354687
C	5.51905220108612	2.23584364489305	-0.88687608333150
C	6.71277545353641	1.51910453467234	-0.62991003052122
N	7.94027176360285	1.63345354044642	-1.25187463538791
N	6.80394873859172	0.57608332748546	0.34545159157715
C	8.08429665326190	0.13737947143213	0.41698195163589
C	8.82049987117409	0.81603239576436	-0.60250901886738
C	8.69298365763011	-0.80296856807810	1.26136859306149
C	10.03048807146522	-1.02416971909169	1.05341010459566
C	10.76450398257572	-0.34488692597060	0.03247937400621
C	10.18141153420837	0.57302161728252	-0.80938912320508
H	-0.69615698096175	0.67748843851979	1.77193593548818
H	0.62863366287292	-1.25189179277356	2.51046976321177
H	0.30187052636402	2.53830044895343	0.49625556940744
H	3.06070066798826	-1.41925133146458	2.01342606019311
C	5.48187729028780	3.35157629151334	-1.82698881994406
C	3.03831899037506	0.47764179381856	0.96018782799879
C	8.28130570195498	2.28416775962626	-2.52591574430922
H	8.71834239969300	3.26533001690529	-2.35639452781528
H	7.39327160576440	2.37742925416190	-3.13939207564724
H	8.99782527596383	1.64449307643300	-3.03494752390730
C	2.73823981012411	3.80130633538275	-0.52379647591200
H	2.01657876303817	4.14959979691974	0.21046214228856
H	2.29658670556894	3.82981890055814	-1.51700264760463
H	3.61250571597979	4.44093882900182	-0.49171075934965
H	8.13325201243239	-1.31134174051625	2.03248379651124
H	10.55855971767651	-1.72999825849372	1.67999404400514
H	11.81783236056008	-0.56646302211681	-0.07761445931030
H	10.75311629029139	1.08495933643782	-1.56963055902458
B	5.56116739185479	-0.16338758794229	1.01124975929138
F	5.49361716098708	-1.42318226706127	0.50387054055612
F	5.63412273139553	-0.09809423130733	2.36833329222431
C	6.31117610308808	4.46724734134638	-1.62736532599162
C	4.61802738376634	3.30923179241768	-2.93524477245793
C	4.60976188275646	4.35656930562281	-3.84081372598657
C	5.41698136221114	5.47297317748508	-3.62352428899039
C	6.25392504788646	5.53285150445623	-2.50865625409713
H	6.95792997362163	4.51246649519620	-0.76058171827413
H	3.99806975005785	2.43826278524260	-3.10666062540339
H	3.97733097875343	4.30581403088012	-4.71692328978899
H	5.39096829613225	6.29811806081783	-4.32286418149234

H	6.85991486121567	6.41100235061484	-2.33069121624204

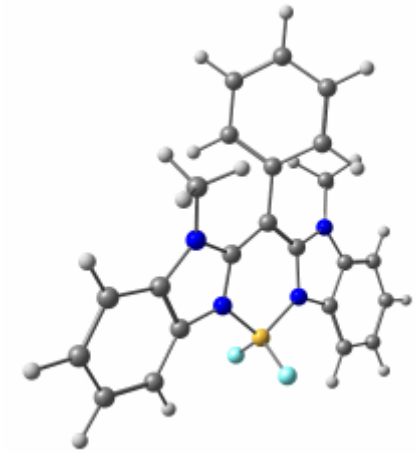

Appendix VI–18. Optimized structure of 3.9.

Appendix VI–19. Coordinates of optimized structure for 3.10 in angstroms.

ν_0=0 cm^{-1}

Atom	x	y	z
C	0.37445610425976	0.62667779704427	1.49185560812973
C	1.23927191807240	-0.40882184263440	1.95224590526500
C	0.82985766976884	1.69579644776176	0.75243011365043
C	2.19500283722656	1.69859671571622	0.45609892852546
C	2.58499103599629	-0.41075123079277	1.67709022322216
N	2.97062828461329	2.58335624678291	-0.24817373285445
C	4.24587236055554	2.07389148412049	-0.30295701408459
N	4.30336912298602	0.93930464119631	0.43750644824869
C	5.38206589530528	2.53367601529662	-1.01866318782507
C	6.62611000034315	1.87589611978319	-0.80626989108601
N	7.79097767616719	1.96707307797603	-1.52957657468792
N	6.80304216931313	1.02337573773795	0.22776769234020
C	8.10650466892296	0.61788072868516	0.23910700713039
C	8.74642369498240	1.21782261451655	-0.87871918187123
C	8.79198417634899	-0.24144863234767	1.10494054411975
C	10.11676630647400	-0.46546629855652	0.81434797710611
C	10.75395205576400	0.13125165007397	-0.30919351460953
C	10.08593734111041	0.97239703785914	-1.17471581600468
H	-0.67790786614830	0.56128076418564	1.73387895930488
H	0.81105798274930	-1.21667371934956	2.52955537497466
H	0.15849972028465	2.46523928623560	0.40038633964724
H	3.24540496961607	-1.19420777509176	2.01817113541676
N	5.25836180561516	3.56819719524324	-1.91218846820100
C	3.05785216530975	0.65772248040207	0.90467991653052
C	7.95996706052442	2.42725717821909	-2.91400003982763

H	8.31701631351335	3.45449259321159	-2.95745529083716
H	7.02057776431844	2.33105091082174	-3.44937092884309
H	8.68864939005180	1.77487896784672	-3.38766917728257
C	2.47361473833596	3.90836040316901	-0.64509638383808
H	1.74260532896695	4.21494336613989	0.09861019233201
H	2.01508172522530	3.87198614811337	-1.62948588162067
H	3.28977956533501	4.62294226787056	-0.63574360785303
H	8.30008968451886	-0.69197652269626	1.95451304436078
H	10.70054607064250	-1.11177903085504	1.45529628695005
H	11.79870893775763	-0.08555635870527	-0.48736837766579
H	10.58719055270817	1.42442425483236	-2.01833842817065
B	5.62459332095752	0.22049210041227	0.93857712953939
F	5.66064212603704	-1.05620143174098	0.46642330202197
F	5.70123888226262	0.32452622806647	2.29289789806800
N	4.21490536616261	3.49940215489026	-2.89777249993889
N	4.39135940688903	4.46438647167391	-3.67175792859688
C	5.48890040102767	5.24655689950601	-3.29565752710272
C	6.03833750938964	4.64538111905302	-2.18023084222663
C	5.84559399551104	6.43526211584027	-4.02122983104226
H	6.85780869124102	4.93148575390219	-1.54616244667322
C	5.08124971458843	6.82221716113997	-5.14293511084330
C	6.94968658148897	7.21837575327689	-3.62809562234514
C	7.27529831273397	8.35591394759852	-4.33568792139202
C	6.51468177878711	8.72762839925830	-5.45105104278534
C	5.41712900478126	7.96319520299500	-5.84631655911973
H	7.54014645334385	6.93920343060653	-2.76488257040424
H	4.83455397997883	8.25869083470458	-6.70813248842829
H	4.24256650556692	6.21416820727072	-5.45057066114676
H	6.78364805616260	9.61461848262982	-6.00928405250866
H	8.11772968575465	8.96171044910404	-4.03139442556694

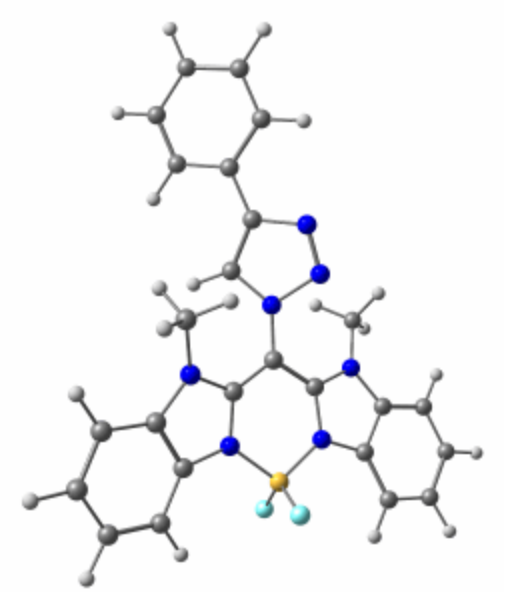

Appendix VI–20. Optimized structure of 3.10.